Investigation into a Magnetic Nanoparticle-Based Molecular Diagnostic Assay

by

Tara Donnelly

2016

Final thesis submitted to the Department of Pure and Applied Chemistry, University of Strathclyde, in part fulfilment of the requirements for the degree of Doctor of Philosophy

This thesis is the result of the author's original research. It has been composed by the author and has not been previously submitted for examination which has led to the award of a degree.

Signed:

Date:

ABSTRACT

The aim of this project was to develop a highly sensitive, closed-tube, multiplexed assay for the detection of DNA using surface enhanced Raman scattering (SERS) analysis. This was achieved through the development of a novel molecular diagnostic assay based on nanoparticle assembly combined with a magnetic manipulation step, consisting of oligonucleotide-functionalised silver nanoparticles and silver-coated magnetic nanoparticles. Hybridisation with target DNA leads to a controlled aggregation of the nanoparticles resulting in strong signal enhancement from a Raman reporter attached to the silver nanoparticle probe. Application of an external magnet allows the hybridised network of nanoparticles to be focussed within the interrogation volume of the laser, thus concentrating the target and removing much of the background matrix.

Sensitive detection of four different 24-base synthetic DNA sequences was demonstrated, using four different Raman reporters. Typically, $\leq$ 20 fmol of target was detected at > 3:1 level of discrimination compared with a blank sample, and the assay was also successfully demonstrated in a duplex format. The rate and extent of hybridisation between target and probes is strongly influenced by the length of target DNA, and an investigation was carried out into the factors affecting this. Increasing the length of probe sequences and using a tail-to-tail orientation, combined with the use of a polymer in the buffer to act as a hybridisation accelerant, resulted in a significant improvement in hybridisation with long target sequences. With these improved conditions, SERS discrimination of > 3:1 compared with blank samples has been demonstrated for just 5 fmol of two different target sequences of $\geq$ 144 bases in length, and the developed assay was also used to successfully detect two different types of PCR-amplified DNA sequence from plasmid DNA. The work presented here represents a step forward in capability within the field of nanoparticle assembly, and moves this technology closer to the point where it can be used in a multiplexed commercial platform.

ACKNOWLEDGEMENTS

I would like to thank my supervisors Prof. Duncan Graham and Prof. Karen Faulds for giving me the opportunity to carry out this interesting project and for the support and assistance that they have provided me with throughout. I would also like to thank Prof. Ewen Smith for all of his help and advice, and for the many hours he spent helping me work through various aspects and challenges of the project. Thanks also to Dr. Graeme McNay from Renishaw Diagnostics Ltd for his encouragement and helpful feedback throughout this period, and to others at RDL who have helped at various stages.

I would like to give particular thanks to several of the Post Docs within the group who helped me enormously throughout my PhD, in particular Dr. David Thompson, Dr. Samuel Mabbott and Dr. Lee Barrett. They gave up their time to help train me on many of the different techniques used and also to give lots of helpful advice throughout the duration of this work. I know I would not have carried this project through to the same level had it not been for their considerable support and helpful suggestions. Particular thanks go to Sam for all the tedious hours spent collecting SEM images for us students.

I would also like to thank everyone else within the Centre for Molecular Nanometrology, past and present, for helping make it such an enjoyable place to work. I have many fond memories and wish everyone well for the rest of their PhD and whatever comes next. Finally, thanks to Barry for putting up with me being a poor student for the last three and a half years, it's over now!

CONTENTS

CHAPTER 1: Introduction

This thesis details the development of a magnetic nanoparticle assembly assay that can be used for the detection of specific deoxyribonucleic acid (DNA) sequences, with the potential for use in molecular diagnostics. The assay consists of oligonucleotide-functionalised silver nanoparticles and silver-coated magnetic nanoparticles, which self-assemble upon hybridisation with a target. Attachment of a dye molecule to the silver nanoparticles allows sensitive detection using surface enhanced (resonance) Raman scattering, SE(R)RS. DNA target sequences specific to several fungal species are the focus of this work. A description of each of the assay components and techniques used is provided here, along with an outline of some of the key research being carried out in the field of DNA detection using nanoparticle assembly and magnetic nanoparticles with SE(R)RS detection.

1.1 Introduction to Deoxyribonucleic Acid (DNA)

DNA (deoxyribonucleic acid) is an essential component of every living organism; its main purpose is the storage and transmission of genetic information. DNA preserves the hereditary information and then transcribes and translates it to allow the synthesis of all the varied proteins of the cell, which are essential for the functioning of an organism. This genetic information is contained within segments of the DNA called genes.

1.1.1 Structure of DNA

DNA exists in a highly ordered state, consisting of a sugar-phosphate ‘backbone’ and a nucleobase attached to each 5-membered sugar ring. The phosphate units are linked to the 5' and 3' carbons of the sugar and the bases are attached to the 1' carbon atom (see Figure 1.1). A nucleotide consists of one phosphate group, one 2'-deoxyribose sugar unit and one nucleobase; an oligonucleotide consists of a short section of

connected nucleotides. Double stranded DNA exists as two parallel strands, with one strand running in the 5'→3' direction and the other in the 3'→5' direction. The two strands are held together through hydrogen bonding between the nucleobases. DNA contains only four different nucleobases: the purines adenine (A) and guanine (G), and the pyrimidines thymine (T) and cytosine (C). Base pairing in DNA is highly specific, with adenine pairing only with thymine, and guanine pairing only with cytosine through hydrogen bonding (see Figure 1.2). The two strands are completely complementary, such that each base on one strand is linked to its corresponding base on the other strand. Within a cell, DNA replication proceeds in the 5' to 3' direction on both strands and DNA sequences are written in the 5' to 3' direction by convention.

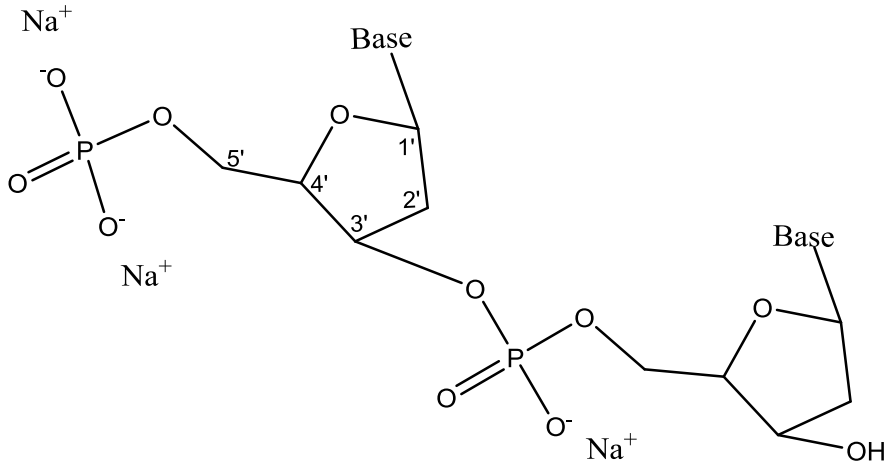

FIGURE 1.1: *Structure of the sugar-phosphate backbone of DNA*

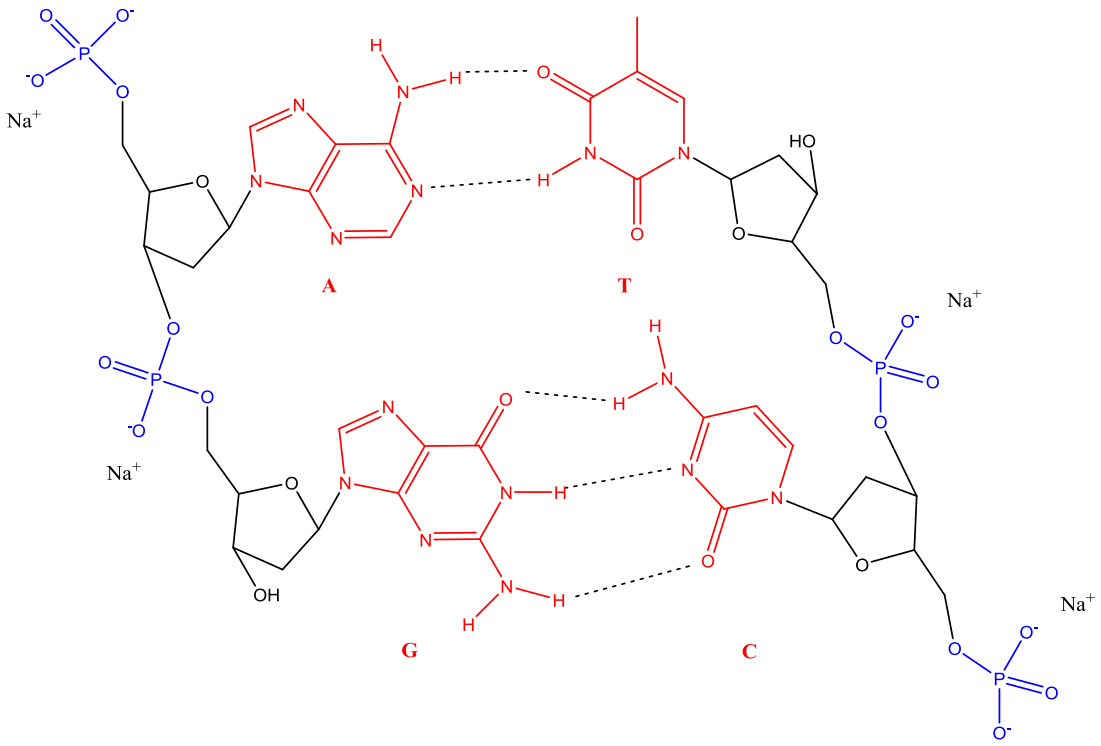

FIGURE 1.2: *Basic primary structure of DNA showing the backbone of phosphate units (blue) and 2'-deoxyribose sugar (black), with one of four nucelobases (red) attached to the sugar. Hydrogen bonding between matching nucleobases is shown by dotted lines.*

The two parallel DNA strands are not straight, but instead coil around in the now familiar double helix format (Figure 1.3). The pitch of the most studied helical form (the B-form) is such that 10 successive nucleotide pairs give rise to one complete turn in 34 Å, and the exterior width of the spiral is around 20 Å.[1] The double helix structure is strong and stable due to the hydrogen bonding between complementary base pairs, as well as aromatic base stacking among the nucleobases. This double helix unwinds and separates during cell replication within an organism, as well as when heated in a laboratory setting, such as during the polymerase chain reaction (PCR) for DNA amplification.

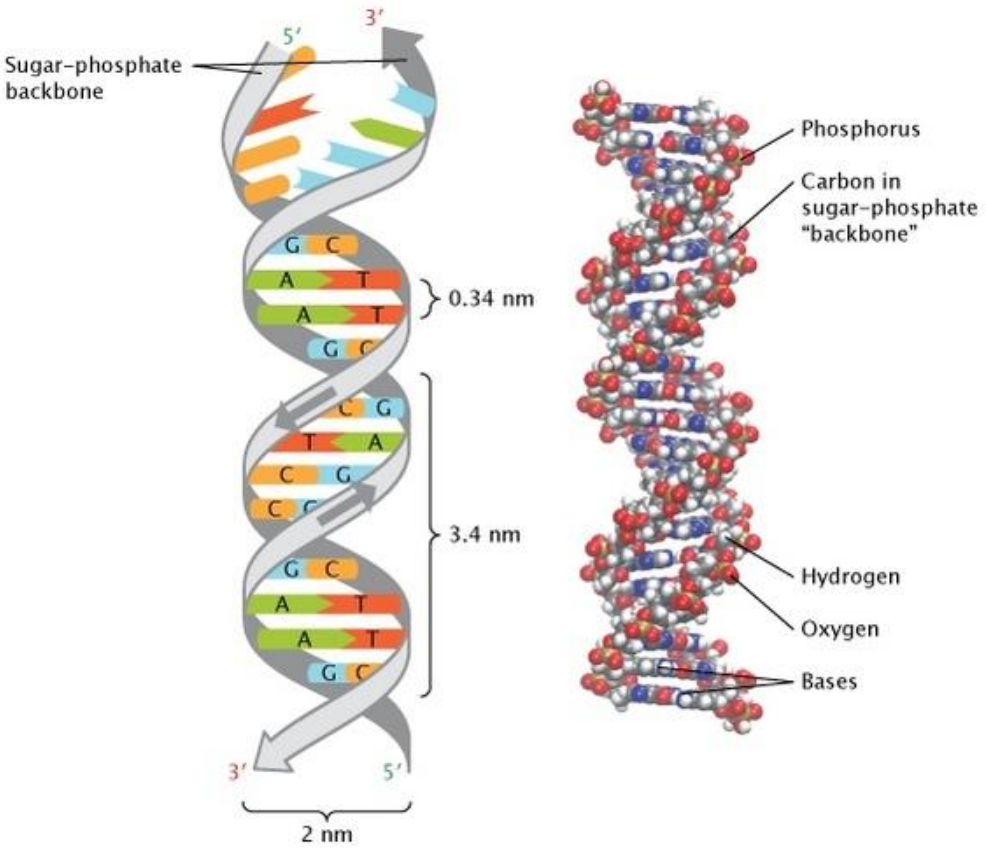

FIGURE 1.3: *Representation of the double helix structure of DNA*[2]

1.1.2 DNA in Cells

While the backbone of DNA consists of long, repeating units of sugar and phosphate molecules that show no variation, the important information with regards to the development and functioning of an organism is encoded within the sequence of bases attached to this backbone. The particular sequence of bases codes for a particular sequence of amino acids, which in turn relates to the formation of a specific protein, therefore changes in the DNA base sequence can directly result in changes to the protein composition. A gene is that segment of the DNA molecule that contains the information necessary to direct the synthesis of one protein, or encodes for a functional ribonucleic acid (RNA).[3]

The entire DNA of a person is held inside every cell in their body in the form of pairs of chromosomes. Human cells contain 46 chromosomes that exist as 22 pairs of homologous chromosomes and the non-homologous chromosomes X and Y, which

determine sex. The DNA from a single human cell has a total length of 2 m, but has a very narrow diameter of approximately 2 nm, which allows it to fold up into a very small volume to fit inside tiny cells, which have a typical diameter of around 10 µm.[1] Due to developments in bioanalytical methods over the last few decades that have allowed fast and efficient sequencing of DNA, it is now possible to determine the complete DNA sequence within a cell. The human genome has been found to consist of approximately 3 x 10^9 base pairs, that code for approximately 100,000 proteins and 20-25,000 genes.[4]

The above description relates to DNA that is part of the human genome. However, other types of DNA can also be present such as viral, bacterial or fungal DNA, which can enter the body through infection. When a person becomes infected by a bacterium, the cells containing the bacterial DNA may be localised at the infected site or may spread throughout the human body. In the case of a viral infection, the viral DNA enters the human cells and uses them as a host to reproduce.

1.1.3 Fungal Infections

Invasive fungal infections have generally received less attention than bacterial and viral infections, yet nonetheless they are responsible for approximately 1.5 million deaths worldwide each year.[5] Over 600 fungal species are reported to cause infection in humans, with effects ranging from minor to fatal.[6] Superficial infections affecting the skin and nails are the most common fungal diseases in humans, such as athlete's foot and scalp ringworm, while mucosal infections of the oral and genital tract are also common, particularly thrush.[5] These infections are generally caused by *Candida* species, which are the second most common cause of fungal infection.[5] Invasive fungal infections are much less common than superficial infections, but have a high mortality rate, with the majority of deaths caused by species from *Cryptococcus*, *Candida*, *Aspergillus* or *Pneumocystis*.[5]

Candida species are the fourth most common cause of hospital-acquired bloodstream infections, with an estimated 400,000 annual cases worldwide and a mortality rate of at least 27%.[5] *Candida albicans* is the most common *Candida* species and, while it is

present in the majority of the population, overgrowth of the fungus can lead to problems in immune-compromised individuals. *Aspergillus fumigatus* and *Aspergillus flavus* are commonly found in the environment, however continuous exposure of the lungs to these species can result in invasive infections in individuals with impaired immune function.[5] *Aspergillus* infections can cause chronic pulmonary aspergillosis, with more than 200,000 cases diagnosed each year and a 50% mortality rate.[5] *A. fumigatus* is also a very common airborne allergen resulting in pulmonary and nasal allergies including asthma.[5]

Current methodologies used for the detection of invasive fungal infections, such as culture-based methods and antigen detection, are said to take too long and suffer from poor specificity and/or sensitivity, which can contribute to missed or delayed diagnosis in patients.[6] As a result, there exists a need for more rapid, robust, cheap and simple diagnostic assays to improve patient treatment and minimise fatalities.[6] Detection of fungal DNA may provide an opportunity to meet some of these criteria for the detection of fungal infections.

1.1.4 DNA Detection in Diagnostics

Detection of specific DNA sequences in biological samples is important for diagnostic purposes, for instance to detect the presence of gene mutations such as single nucleotide polymorphisms (SNPs), or to determine whether a person has been infected by a particular bacterium, virus or fungus. The detection of particular DNA sequences is derived from the specificity of base pairing between complementary strands. Capture probes can be synthesised that consist of a specific sequence of oligonucleotides complementary to the target sequence of interest. When the target is present it hybridises with the probe sequence and a duplex is formed; the presence of a marker molecule will allow detection of this hybridisation event. Initial methods of this type included Southern blot analysis, which involved immobilising a digested genomic DNA sample onto a nitrocellulose or nylon filter.[7] A radioactive or chemically-labelled oligonucleotide strand complementary to the gene of interest was then applied, which would hybridise with the target sequence if present and was

detected via the marker compound.[3] This technique has now largely been superseded by polymerase chain reaction (PCR)-based methods.

The polymerase chain reaction is a very powerful technique that allows the amplification of specific sequences of DNA to produce around a million identical copies of the sequence within just 20 amplification cycles.[8] The PCR process can also be used to introduce a label or marker compound into the amplified DNA, which can subsequently be used to detect the presence of the target sequence. The PCR has become the most widely used technology in the molecular diagnostics of infectious diseases.[9] PCR is frequently used in combination with microarrays to allow very sensitive detection of specific sequences of DNA. Microarrays consist of large numbers of oligonucleotide sequences immobilised as individual spots on a solid substrate, such as a glass slide or nylon membrane. When exposed to a sample consisting of single stranded, labelled DNA fragments, matching sequences will be hybridised and non-matching sequences will be washed away.[9] Subsequent analysis of the label, which is usually fluorescent, provides information on the specific DNA sequences present in the sample. However, while useful for examining multiple sequences of DNA at the same time, microarrays tend to be very expensive which currently limits their use for clinical diagnostics.

Other techniques currently used for the detection of specific sequences of DNA in a clinical setting involve the use of quantitative, real-time PCR. The most common of these is the TaqMan approach, whereby an oligonucleotide probe specific to a target DNA sequence is introduced during PCR.[10] This probe has a fluorophore label attached to the 5'-end and a fluorescence quencher at the 3'-end. When the probe is intact, the fluorophore and quencher are in close proximity and hence no fluorescent signal should be present. However, if the probe hybridises with target DNA then it will be digested by the enzyme Taq polymerase during the normal PCR cycle, thus separating the fluorophore and quencher, and hence a fluorescent signal will be detected. Somewhat similar to this method is the use of either molecular beacons[11] or Scorpion primers[12,13] during the PCR cycle. As with the TaqMan approach, these allow quantitative detection of specific DNA sequences during PCR. Sybr Green is

also used for quantitative PCR, in which the dye intercalates with double stranded DNA (dsDNA) produced during the PCR process, leading to a strong fluorescent signal.[14] However, this is not a sequence specific technique as Sybr Green will intercalate with all dsDNA.

Current methodologies used clinically for the diagnosis of invasive fungal diseases include culturing the organism, PCR-based assays, fungal antigen detection, radiography, and x-ray CT scans.[5] Culture-based methods are insensitive and slow, while the other diagnostic options often suffer from a lack of sensitivity and/or specificity.[5] Better and more rapid diagnostics are therefore believed necessary in order to allow more rapid and appropriate treatment of patients and help reduce mortality rates.[5]

For many of the methods discussed in this section, detection is predominantly by fluorescence, which occurs when a molecule absorbs a high energy photon that excites it both electronically and vibrationally. The system relaxes vibrationally, then after a short period of time (nanoseconds) emits a photon of lower energy/longer wavelength that is measured. The wavelength of the excitation source is therefore close to the absorption maximum of the fluorescent molecule. Fluorescence detection has some inherent limitations, such as a limit in sensitivity of around 10^{-9}-10^{-10} M; this means that PCR-amplification is required for detection of the very low levels of target material typically found in clinical samples. Fluorescence emission also results in broad overlapping resonance bands, which severely limits the multiplexing capabilities of this technique. An alternative detection method that can overcome some of these limitations is to measure the light that is scattered by a molecule, rather than that which is absorbed then emitted, using the technique of Raman spectroscopy.

1.2 Introduction to Raman Spectroscopy and Surface Enhanced Resonance Raman Scattering

In recent years, surface enhanced Raman scattering (SERS) has been widely investigated as an alternative to fluorescence for the detection of specific sequences of DNA due to its high sensitivity and the presence of narrow, distinct spectral bands that make it amenable for the detection of several targets simultaneously.[15,16]

1.2.1 Raman Scattering

When a photon of light interacts with a photostable molecule it may undergo one of three processes: absorption, absorption followed by emission, or scattering. Of the light that is scattered, most has the same frequency as the incident radiation, and the process is termed Rayleigh or elastic scattering. However, a small portion of the light, less than 10^{-7} times the intensity of the incident radiation, undergoes a change in frequency due to an inelastic interaction between the light and the molecule. The energy difference between the incident and the scattered light corresponds to an energy difference between two vibrational energy levels of the molecule. This process is termed Raman or inelastic scattering (see Figure 1.4). The collection of all of the scattered photons from a molecule makes up the Raman spectrum, which acts as a spectroscopic vibrational fingerprint of the molecule providing both structural and chemical information. The Raman process was discovered in 1928 when C.V. Raman examined the light scattered by dense media, and noticed the effect later named after him.[17] Raman scattering results in two series of lines being produced: Stokes, of lower energy than the incident light; and anti-Stokes, of higher energy. At ambient temperature, the population of molecules in the ground vibrational state is always much greater than in excited vibrational states, and so the intensities of the anti-Stokes lines will always be much weaker than those of the Stokes lines.

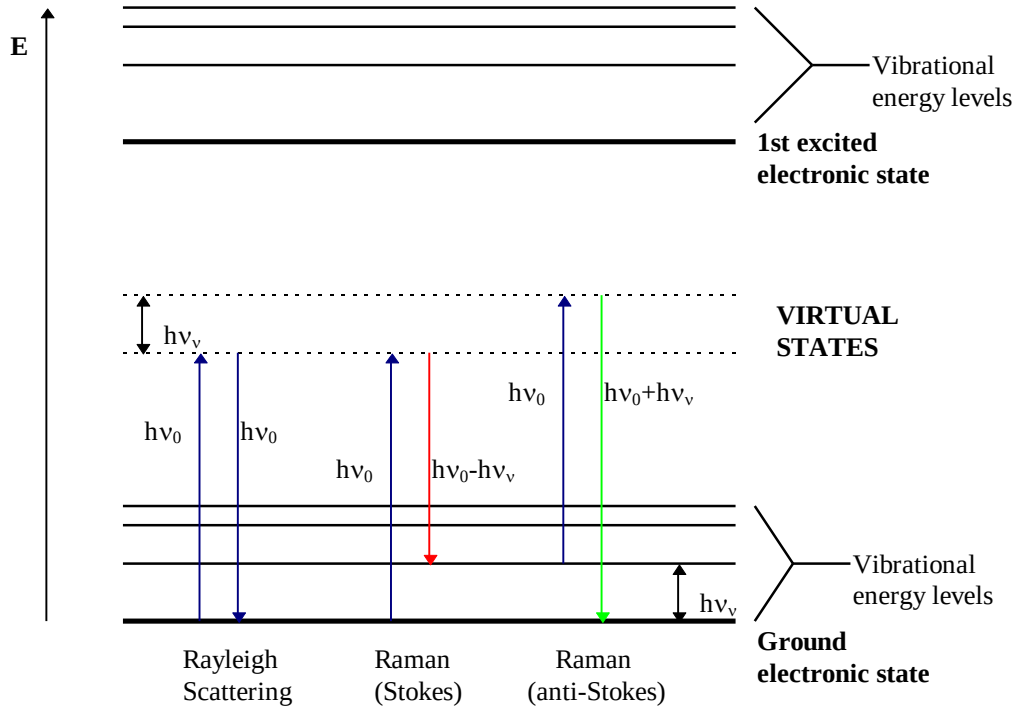

FIGURE 1.4: *Energy transitions involved in Raman scattering (where h = Planck's constant)*

For a polyatomic molecule containing *N* atoms, the molecule has 3*N*-6 normal modes of vibration (or 3*N*-5 for a linear molecule). These normal modes can be a result of bending or stretching motions, or out-of-plane deformations. Each motion is represented as a band on the vibrational Raman spectrum, providing it is a Raman-active vibration. The frequency of the vibrations depends on the masses of the atoms in the molecule, the strength of the bonds between atoms, and the atomic arrangement, thus producing Raman spectra that are unique to a particular molecule.

When a molecule is introduced into an electric field of strength *E*, an electric dipole moment (μ) is induced in the molecule.

$$\mu = \alpha E$$

where the constant α is the polarisability of the molecule, which is a measure of the ease with which the electron cloud around a molecule can be distorted. In the case of electromagnetic radiation, this can be changed to:

$$\mu = \alpha E^0 \cos 2\pi \nu_0 t$$

where E^0 is the amplitude of the electric field, ν_0 is the frequency and t is time. Thus, the electromagnetic radiation induces a varying electric dipole moment which then permits emission of light identical in frequency with that of the incident radiation; this is Rayleigh scattering. However, most molecules are non-isotropic and, therefore, have unequal polarisability along the different axes of the molecule. Raman scattering occurs when a molecular vibration changes the polarisability of the molecule. Thus, the selection rule for a Raman-active vibration is that one or more of the dimensions of the polarisability ellipsoid must change during the vibration. This is in contrast with infrared vibrations, which require a net change in dipole moment during a vibration in order for it to be IR-active. According to the rule of mutual exclusion, in a centrosymmetric molecule a vibrational mode may be either IR active or Raman active but not both. These points are illustrated in Figure 1.5 which shows the four vibrational modes of CO_2.

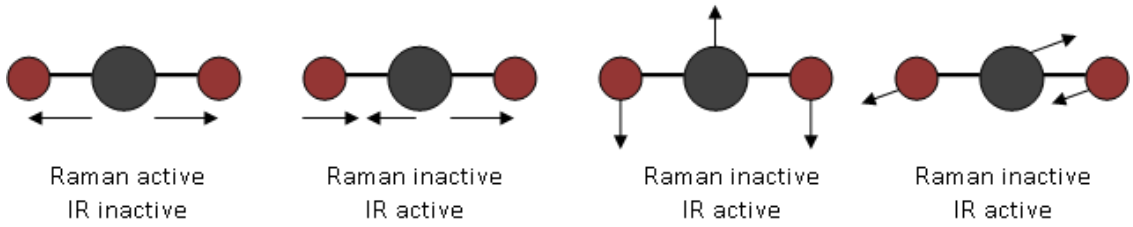

FIGURE 1.5: *Illustration of the four vibrational modes of CO_2, indicating which are IR active and which are Raman active*[a]

Raman measurements can be carried out using a range of excitation frequencies. The intensity of Raman scattering is directly proportional to the fourth power of the excitation frequency, therefore higher frequency lasers (visible or near-UV radiation) give more sensitive Raman spectroscopy. However, problems with sample decomposition or fluorescence can prevent the successful collection of spectra at these higher energies, therefore all these effects must be taken into consideration before deciding upon the correct frequency of radiation to use for a particular analysis. The intensity of Raman scattering also varies widely between analytes since some molecules, such as water, are very weak scatterers while others, for instance

[a] Reproduced in part from the following source: http://www.chemvista.org/ramanIR4.html, accessed 30th April 2015.

molecules containing aromatic rings, give strong scattering.[18] Although Raman scattering in itself is a very weak effect and not suitable for the detection of trace quantities of material, the discovery that a surface enhancement effect allows much more sensitive analysis has greatly expanded the scope and appeal of this method.

1.2.2 Surface Enhanced Raman Scattering (SERS)

SERS was first demonstrated by Fleischmann *et al.*, and reported in 1974, when they observed very intense Raman bands from pyridine adsorbed onto an electrochemically treated silver electrode.[19] It was later discovered that a surface enhancement mechanism was responsible for this increase in intensity of the Raman bands[20, 21] and that it was possible to obtain SERS with a range of substrates and analytes.[22, 23] The SERS effect involves the interaction between a molecule that is adsorbed on the surface of a metal and the surface plasmon of the metal. A plasmon is a wave of valence electrons that oscillates across the surface of a metal, which is created by an excitation source, usually in the visible or near-infrared region. A localised surface plasmon resonance (LSPR) occurs when the metal is confined to nanoscale dimensions, and results in enhancement of the electromagnetic field close to the nanoparticle surface (see Figure 1.6).[24, 25] The resonance frequency of the plasmon is a property of the metal used and the surface roughness features,[18] and is dependent on the dielectric functions of the metal and the surrounding medium.[26]

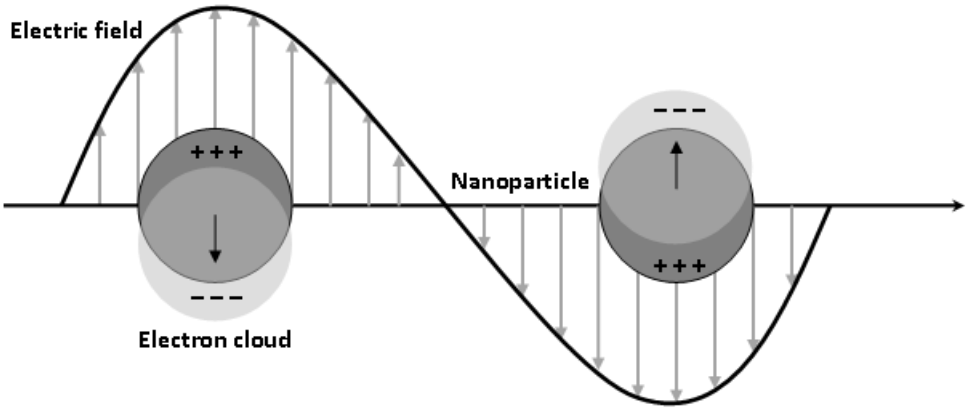

FIGURE 1.6: *Illustration of the localised surface plasmon resonance effect (reproduced from ref[24])*

For SERS measurements, enhancements in the intensity of Raman bands of several orders of magnitude are commonly observed. The degree of enhancement depends on a combination of the excitation frequency, the metal used and its degree of roughness, with the largest enhancements obtained when the analyte is adsorbed directly onto the metal surface.[18] Single molecule SERS was reported in 1997 and highlights the high sensitivity that is possible using this technique.[27, 28]

It is commonly accepted that two mechanisms are involved in the SERS enhancement process, namely the electromagnetic mechanism and the charge transfer mechanism:

• The Electromagnetic Mechanism: The electrons at smooth metal surfaces are tightly bound and so provide no enhancement effect. However, if the surface of the metal is roughened the surface plasmons are no longer tightly bound to the metal and become localised in the depressions in the metal surface. The electric field on a rough surface becomes greatly enhanced if the incident photon energy is in resonance with a normal mode of the free electrons in the metal. Only certain metals such as silver, gold or copper have the resonant frequency of their surface electron waves in the visible region and thus give a large SERS effect. A molecule adsorbed on a roughened surface of one of these metals will be bathed in the surface plasmons and will experience an enhanced electric field from the metal in addition to the

electric field from the incident light. As a result, the molecule will scatter light with an enhanced intensity compared to an isolated molecule.

• The Charge Transfer Mechanism: This involves the transfer of charge between the adsorbed molecule and the metal surface through a bond. The enhancement mechanism requires new electronic transitions between the adsorbed molecule and the metal surface, made possible when the molecule is chemically bonded to the surface. This mechanism is dependent on the nature of the molecules involved.

Only polarisation changes in the molecule which are perpendicular to the surface will be observed. For example, if a planar molecule such as pyridine is lying flat very little scattering is obtained, whereas if it is perpendicular to the surface considerable scattering is obtained. At less than monolayer coverage the molecule lies flat but as more molecules are added they have to stack up for all the molecules to fit, at which concentration the signals become very intense. Therefore, the technique gives orientational information and, since it gives information on the vibrations of the molecule, it can also give information on bonding to the surface [29].

1.2.3 Surface Enhanced Resonance Raman Scattering (SERRS)

The resonance Raman effect occurs when the energy of the incident photons coincides with the energy of an electronic transition in a molecular species, i.e. when the frequency of the laser excitation line lies close to an absorption maximum of the molecule (see Figure 1.7). This results in an enhancement in the intensity of certain Raman bands of a few orders of magnitude.

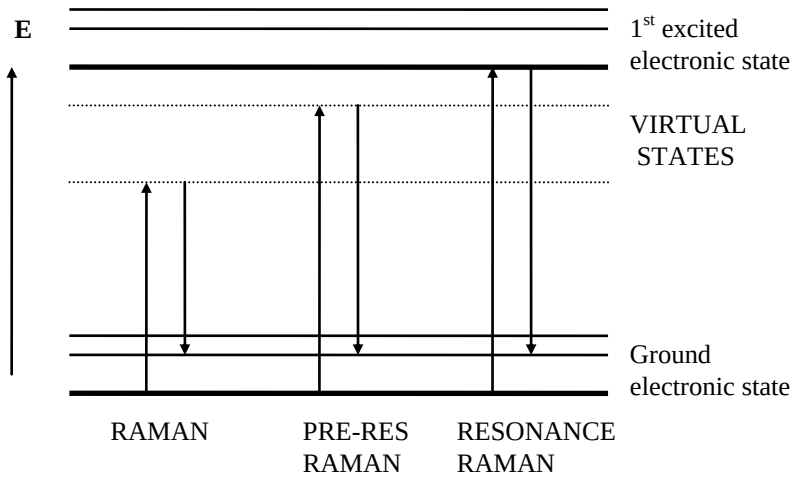

FIGURE 1.7: *Comparison of the energy transitions involved in normal Raman and resonance Raman scattering*

The measurement of resonance Raman scattering using visible lasers requires the presence of a chromophore in the molecule being analysed. However, problems can arise due to self-absorption of the Raman scattered light by the sample, or photodecomposition of the sample due to absorption of the incident radiation. Fluorescence can also be a problem as this effect competes with the resonance Raman effect since the excitation band must be close to the absorption maximum of the molecule. This can lead to significant background emission from the molecule, and may totally swamp the resonance Raman signal depending on the nature of the interaction of the light with the molecule.

SERRS can be thought of as a combination of SERS and resonance Raman scattering, and can result in very intense scattering from the combination of the two enhancement effects. In order for SERRS to work, the molecule to be studied must contain an appropriate chromophore situated in close proximity to a suitably roughened metal surface, and the excitation frequency must be close to the molecular resonance frequency of the chromophore. If the analyte of interest does not contain a chromophore and/or is not a good Raman scatterer, a dye may be used as a label or marker compound to allow intense SERRS spectra to be obtained. An additional advantage of SERRS is that fluorescence is often quenched, therefore many more

molecules can be studied than with resonance Raman scattering. In order for SERRS to be achieved, an enhancing surface is required. While a number of possibilities exist as to the creation of such surfaces, the focus of this report is on the use of metal nanoparticles for this purpose.

1.3 Introduction to Nanoparticles

Nanoparticles are generally considered to be particles with at least one dimension in the range 1-100 nm. They are of interest because certain of their properties, in particular their interaction with light, differ from the bulk material and properties such as size, shape and colour can be tuned to suit a particular application. The use of metal nanostructures is an essential component of SERS and the optical properties of the nanoparticles are central to plasmonics.

In order to be suitable for plasmonics, and hence SERS applications, a nanoparticle must be able to support a strong surface plasmon at the desired resonance wavelength. This ability is dependent on the metal's dielectric function, which is a measure of the interaction between its electrons and the light.[30] The dielectric function includes both a real (ε_r) and an imaginary (ε_i) part, both of which vary with excitation wavelength. The strength of the surface plasmon is directly proportional to the quality factor (Q), described as:

$$Q = \omega(d\varepsilon_r / d\omega) / 2(\varepsilon_i)^2$$

where ω is the excitation frequency.[30] Compared to a range of metals that can be used for plasmonics applications, Ag has the largest quality factor across most of the spectrum from 300 to 1200 nm as a result of its intrinsic dielectric functions. Au is only suitable for wavelengths above 500 nm, while Cu is only suitable above 600 nm.[30]

1.3.1 Nanoparticle Synthesis

A wide range of methods have been developed for the synthesis of silver nanoparticles with controlled size and shape, including spheres, cubes, wires, and branched and hollow structures.[30] The most common method used to create metal nanoparticles involves chemical reduction of dilute solutions of metal salts to form suspensions of colloidal particles in solution; these are easy to prepare and provide reproducible, fresh surfaces for each analysis. The reaction generally involves the reduction of the metal ions to form the neutral metal atoms (e.g. $Au^{3+} \rightarrow Au^{0}$ or $Ag^{+} \rightarrow Ag^{0}$), and is a three stage process: nucleation, whereby the initial reduction of metal ions to atoms takes place to form polydisperse nuclei; growth, where more gold/silver particles are added to the existing nuclei and these become larger and more monodispersed; and coagulation, where the nanoparticles can be made larger still by grouping multiple nuclei into particles. Excess coagulation will cause the colloid to be unstable, therefore a capping agent must be added to stop it.

The method of citrate reduction to create silver colloid was first reported by Lee and Meisel in 1982, and involves the sodium citrate reduction of boiling silver nitrate in aqueous solution, with the citrate ions acting as both a reducing agent and a stabiliser.[31] The method remains in wide use today due to its simplicity, however single reactions are known to produce silver nanoparticles with a wide range of shapes and sizes.[30] The surface of citrate-reduced silver nanoparticles consists of a layer of citrate with pendant negatively charged groups. As a result, positively charged molecules readily adhere to the surface while negatively charged molecules and some neutral species do not.[32] One alternative method for the synthesis of silver nanoparticles involves the reduction of silver nitrate using hydroxylamine hydrochloride at alkaline pH.[33] This method is fast, simple, and can be carried out at room temperature, and the SERS enhancement possible from these nanoparticle surfaces was found to be comparable to that when using citrate-reduced nanoparticles.[33]

Control of the size of a nanoparticle is important when considering its interaction with light. When the radius (R) of a nanoparticle is much smaller than the

wavelength of light, the scattering cross section is directly proportional to R^6 and the absorption cross section is directly proportional to R^3. Larger nanoparticles therefore scatter light more efficiently than smaller nanoparticles,[30] and the preferred surface roughness for SERS is said to be approximately 50 nm.[18]

1.3.2 Creation of Hot Spots in Nanoparticles

Individual nanoparticles do not give very large Raman signal enhancements. In order to obtain a rough surface suitable for SERS, the nanoparticles must first be aggregated resulting in small clusters dispersed throughout the medium. The electric field intensity is very high in the interstices of the aggregates (also termed 'hot-spots') due to the coupling of the surface plasmons, resulting in the large enhancement of the Raman bands. This is illustrated in Figure 1.8, which shows the electromagnetic (EM) enhancement at regions around and between two 90 nm AuNPs separated by a distance of 0.25 nm.[34] In a study by Khan *et al.* on the analysis of SERRS-active sites, it was found that the percentage of dimers that were SERRS-active was significantly greater than the percentage of active single silver nanoparticles. Furthermore, as the number of particles in the aggregate increased, the relative SERRS activity also increased.[35] A further study by McMahon *et al.* investigated the electromagnetic enhancements at different nanoparticle separations, using 90 nm gold nanoparticles. They found that, as the edge-to-edge distance decreased from 1 to 0.5 nm, the enhancement increased from 10^8 to 10^{10}, and when this was reduced to 0 nm (i.e. the nanoparticle edges were touching), an enhancement of 10^{14} was obtained.[34] A further study by the same group highlighted that achieving sub-nanometre separation between nanoparticles was crucial in order to achieve maximum SERS enhancement.[36]

In order to obtain reproducible spectra, the aggregation step must be carefully controlled, and the aggregates formed must remain stable for a period of time significantly longer than that required to take the spectrum. Aggregation can be performed in several ways by the addition of a suitable aggregating agent, such as sodium chloride, nitric acid, poly-L-lysine or spermine hydrochloride. Each of these induces aggregation in a different way, and the choice of agent will depend on the

analyte being studied and the particular assay conditions. It is often difficult to obtain consistent aggregation within samples as a range of cluster sizes is generally formed. An alternative method that allows a more controlled aggregation is to use linker molecules between the nanoparticles, which can be either chemical or biological. The use of DNA linkers as a way to bring about controlled nanoparticle assembly is described in the next section.

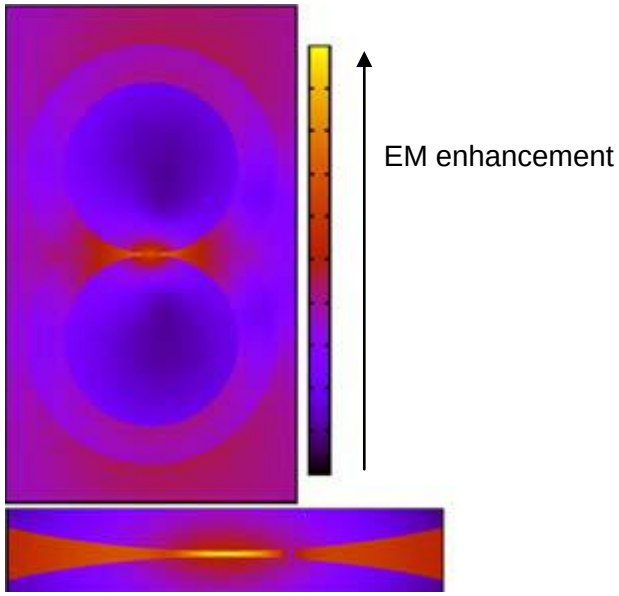

FIGURE 1.8:[34] *EM enhancement at λ=785 nm for two 90 nm AuNPs separated by 0.25 nm (taken from ref[34] with permission).*

1.4 DNA Detection Using Nanoparticles

Gold and silver nanoparticles can be functionalised by attaching specific oligonucleotide sequences or antibodies to their surface, producing nanoparticle probes that are specific to particular DNA sequences or proteins of interest. This, combined with the optical properties of these nanoparticles as a result of their surface plasmon resonance, makes them ideal candidates for use in biosensors.

1.4.1 Nanoparticle Assembly through DNA Hybridisation

A common method that has been investigated for detecting specific short sequences of DNA using nanoparticles is the nanoparticle assembly approach, also referred to as a DNA sandwich assay. This incorporates two sets of nanoparticles, each of which is functionalised with a different, short oligonucleotide sequence that is complementary to a section of the target DNA. When the nanoparticle probes and target are mixed, sequence-specific hybridisation occurs according to the Watson-Crick base pairing rules (see Figure 1.9). This causes a controlled and directed aggregation of the nanoparticles, which results in a change in their surface plasmon resonance frequency. This may result in a colour change that is visible by eye if the concentration is high enough, or more often is observed using spectrometric detection, such as by measuring the change in the extinction spectrum by ultraviolet-visible (UV-Vis) spectroscopy. The hybridisation of probes and target in the assembly is reversible and the oligonucleotide sequences, and hence the nanoparticles, can be separated again by application of heat. Another aspect of this technique is that no external aggregating agent needs to be added to the sample mixture as this is provided through the hybridisation event.

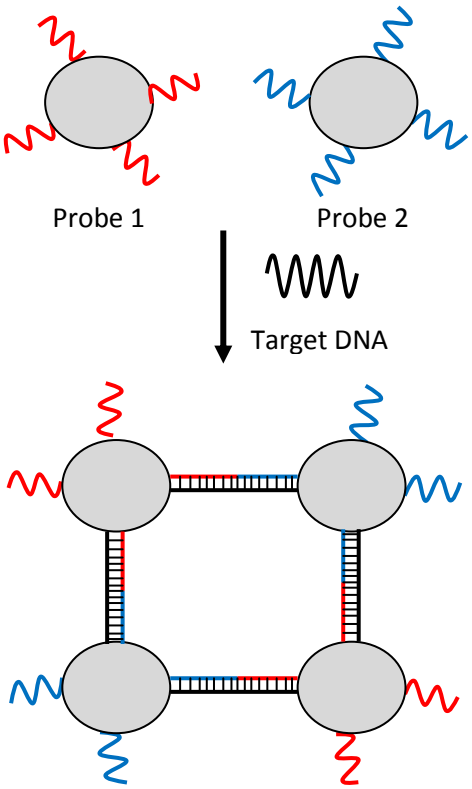

FIGURE 1.9: *Simplified schematic representation of nanoparticle assembly through DNA hybridisation*

1.4.2 Non-SE(R)RS Detection of Nanoparticle Assembly

The first use of the nanoparticle assembly approach for detection of DNA sequences was described in 1996 by Mirkin *et al.*, who investigated changes in the colour and extinction spectra of oligonucleotide-functionalised 13 nm gold nanoparticles in the presence of a synthetic target DNA sequence,[37] and by Alivisatos *et al.*, who described the DNA-directed assembly of 1.4 nm gold nanoparticles.[38] Following this initial proof-of principle, work continued within the Mirkin group to extensively investigate and develop this colorimetric detection technique further using gold nanoparticle probes,[39] and later using silver nanoparticles.[40] The technique was often used in combination with melting transition analysis to provide sufficient selectivity to discriminate single bases mismatches from the target,[41] and the factors affecting the optical, melting and hybridisation properties of the nanoparticle assemblies were investigated,[42-44] along with determination of the factors affecting the extent of oligonucleotide-loading on the nanoparticles.[45, 46] The multiplexing capability of the

technique was explored using different sized Au nanoparticles with scattered light detection,[47] and also using a combination of Au nanoparticles with Ag-core/Au-shell nanoparticles to allow a two colour-change colorimetric detection method.[48] This assay was further developed into a commercial system incorporating silver-amplified gold nanoprobes in a micro-array format with a light scattering detection technique, and has been applied to the detection of bacterial and human genomic DNA without target amplification.[49, 50, 51]

The work of the Alivisatos group in this field continued down a different route, focussing on the use of DNA to initiate the controlled assembly of functionalised nanoparticles, rather than on the detection of target DNA as such. By controlling the conditions to allow formation of dimers and trimers, rather than clusters of nanoparticles, they have used the approach to develop 'molecular rulers' in which distances between single pairs of silver or gold nanoparticles are monitored based on the distance dependence of their plasmon coupling.[52, 53] More recently, this approach has also been applied to larger nanoparticle assemblies in a 3-dimensional arrangement.[54]

Graham and co-workers reported the first use of oligonucleotide-functionalised silver nanoparticles in a nanoparticle assembly assay for target DNA detection, in which single base mismatches were differentiated by utilising differences in the melting profiles.[55] Further studies were aimed at improving the stability of the oligonucleotide-silver nanoparticle conjugates by using disulfide-modified oligonucleotide probes[56, 57] and investigating the hybridisation behaviour of the conjugates using fluorescence-based measurements.[58] The group also reported on the first mixed-metal nanostructures using a combination of oligonucleotide-functionalised gold and silver nanoparticles, with their multi-wavelength detection capabilities investigated using extinction spectroscopy.[59]

The nanoparticle assembly approach, with detection by UV-Vis spectroscopy, has recently been used in an assay for the detection of *Chlamydia trachomatis* using PCR-amplified DNA from a 30 mL sample of human urine.[60] The assay employed

gold nanorods (~ 45.0 x 13.5 nm) conjugated with two different 12-base oligonucleotide sequences to produce two capture probes. When applied to a synthetic target DNA sequence, differences in extinction profiles allowed discrimination of a single-base mismatched target from a perfectly complementary target. When applied to a real sample (200 base-pair PCR product) the assay could discriminate between target DNA and other PCR-amplified non-target DNA sequences within the concentration range of 0.25-20 nM of amplified target.[60]

1.4.3 Detection of Nanoparticle Assembly by SE(R)RS

The use of metal nanoparticles in combination with SE(R)RS for the detection of biological molecules such as DNA and proteins has been widely investigated.[15, 61] Advances that have been made using DNA-directed nanoparticle assembly of oligonucleotide-functionalised nanoparticles for the detection of specific short sequences of DNA are detailed here.

The technique was first exploited by Graham *et al.*[62] and then Nie *et al.*[63] to allow the use of SERS for DNA detection, with both groups separately demonstrating the novel combination of DNA-directed nanoparticle assembly with SERS analysis in solution using functionalised AgNPs and AuNPs, respectively. This work highlighted how a biological recognition event can result in a change from a 'SERS off' to 'SERS on' state, using a Raman active reporter molecule as a marker for the presence of target DNA. Compared to gold, silver provides a better ratio of scattering to absorption from photons interacting with its surface, therefore is expected to give a stronger SERS enhancement.[18]

In the initial study by Graham and co-workers, two batches of silver nanoparticles were functionalised by addition of a SERRS-active azo-dye and a 12-base oligonucleotide sequence to their surface.[62] Although a background spectrum was observed without target being present, significant enhancement of the Raman spectral peaks of the dye was obtained upon addition of the 24-base target sequence, with clear discrimination compared with a non-complementary sequence at a target concentration of 1.25 nM.[62] Further work was aimed at improving various aspects of

the assay, such as ease of probe preparation and versatility,[64, 65] the use of mixed metal nanoparticles to improve stability while maintaining high sensitivity[66] and investigation of the assay for single base mismatch discrimination.[67] An interesting study was also carried out correlating the plasmonic response with the SERS output for silver nanoparticle assemblies with controlled interparticle distances.[68] To date, all published work by this group has involved the detection of short (generally 24-base) single stranded synthetic oligonucleotide sequences and has not been applied to clinical samples.

In the assay developed by Nie and co-workers, based on gold nanoparticle-oligonucleotide conjugates, an enhanced SERRS intensity ratio of 200-300 was reported for a target concentration of 25 nM compared to a 23-base length single base mismatch sequence.[63] Zhang *et al.* described an aqueous-based sandwich assay that used silver nanoparticles conjugated with a range of oligonucleotide sequences and Raman reporter molecules in a multiplexed system.[69] A successful triplex assay was demonstrated for 30-base synthetic target oligonucleotide sequences at 10 nM concentration. This assay employed triple cyclic-disulfide modified oligonucleotides rather than the more commonly used monothiol-capped sequences in an effort to produce more stable conjugates.[69]

Other groups have also investigated and developed nanoparticle assembly assays with SE(R)RS analysis where the substrate is a solid surface, rather than an aqueous colloid. Hu *et al*. developed a three-probe system: the capture probe consisted of a 15-base oligonucleotide sequence complementary to a section of the target sequence, attached to a gold electrode surface; the two detection probes consisted of complementary 17-base dye-labelled oligonucleotide sequences conjugated to gold nanoparticles in aqueous solution, one of these sequences was complementary to a section of the target sequence.[70] The assay involved a 60 minute exposure of the capture probe to target DNA and then multiple 30 minute exposures to each of the detection probes in turn, with wash steps in between. The system was designed to allow the nanoparticles in the detection probes to be pulled close together to increase the electromagnetic field enhancement and hence maximise the Raman signal

intensity, irrespective of the size of the target oligonucleotide sequence. This assay allowed detection of a 33-base synthetic oligonucleotide sequence at a concentration of 10 fM.[70]

Mirkin and co-workers have also investigated DNA microarrays with SERS detection with the aim of maximising sensitivity and multiplexing potential compared to fluorescence-based detection methods.[71,72] These methods used a dye-labelled gold nanoparticle as the detection probe with the capture oligonucleotide sequence attached directly to a glass surface, rather than to a second nanoparticle. Subsequent deposition of silver onto the bound Au nanoparticles provided the SERS enhancement. A detection limit of 20 fM and discrimination between 6 different 30-base synthetic oligonucleotide targets was reported.[71]

In summary, the controlled assembly of nanoparticles through DNA hybridisation, coupled with SE(R)RS analysis, is a relatively new approach that has been studied by a number of research groups to expand knowledge on its functioning and capabilities. The potential of this approach to allow highly sensitive and selective detection of oligonucleotides has been clearly demonstrated, particularly when used in a microarray format. However, expansion of the assays to allow the detection of long target sequences, or double stranded DNA target from a clinical sample, has so far not been realised.

1.5 Introduction to Magnetic Nanoparticles

Magnetic nanoparticles (MNPs) are of interest due to certain properties that differ from the bulk material. When the size of a magnetic particle reduces below a critical level, generally a few tens of nanometres depending on the material, each nanoparticle becomes a single magnetic domain and shows superparamagnetic behaviour, i.e. each particle is uniformly magnetised with all the spins aligned in the same direction.[73] Above the blocking temperature, the direction of magnetisation of these nanoparticles is constantly fluctuating, resulting in a net magnetisation of zero.

Each individual nanoparticle has a large constant magnetic moment and behaves like a giant paramagnetic atom except that, rather than each individual atom being independently influenced by an external magnetic field, the magnetic moment of the entire nanoparticle will align with the field. This results in a very fast response to applied magnetic fields but with negligible residual magnetism once the external field is removed.[73]

Magnetic nanoparticles have been widely researched within the last two decades to investigate their potential for use in therapeutics and diagnostics, as well as non-biological applications such as magnetic storage media and magnetic inks for jet printing.[74] For *in vivo* applications, synthesised MNPs are bound to specific drugs, proteins or nucleotides which can then be directed to the appropriate organ, tissue or tumour using an external magnetic field. Careful control of particle size, surface chemistry, biocompatibility and non-toxicity are all important aspects that must be managed.[74] In a similar manner to silver and gold nanoparticles, suitably coated magnetic nanoparticles can also be functionalised by the addition of an oligonucleotide sequence to their surface, producing magnetic nanoparticle probes that are specific to particular DNA sequences of interest. Their magnetic properties allow the target material to be easily collected and removed from the sample matrix, and these features have been used in the development of several DNA extraction assays.

In recent years, diagnostic assays have been investigated that use MNPs alongside Ag or Au nanoparticles, all of which can be functionalised with oligonucleotide sequences or antibodies. These assays combine the optical properties of the noble metal nanoparticles with the magnetic collection capabilities of the MNPs, thus giving the potential for very low limits of detection when used alongside sensitive detection techniques such as SE(R)RS. This was demonstrated by Jun *et al.* who used nanoparticles consisting of a magnetic core with a silica coating and Ag nanoparticles embedded on the surface. Using an external magnetic field to induce aggregation of the nanoparticles, the peak intensity of an attached Raman active

material increased approximately 1000-fold compared to the solution of loosely dispersed nanoparticles.[75]

1.5.1 Synthesis of Magnetic Nanoparticles

Magnetic nanoparticles are generally made in the form of a colloid, where the nanoparticles are suspended in a liquid and are stabilised by electric charges on their surface. The most commonly synthesised MNPs are composed of iron oxides, either magnetite (Fe_3O_4) or maghemite (γ-Fe_2O_3). Maghemite is composed of Fe^{3+} cations only while magnetite contains both Fe^{3+} and Fe^{2+} ions ($Fe^{2+}Fe_2^{3+}O_4$). Both adopt a cubic spinel structure and have similar magnetisation values.[76] Magnetite is not very stable and is transformed into maghemite in the presence of oxygen,[74] and care must be taken to eliminate oxygen from the reaction mixture if only magnetite is to be produced.

The simplest method for the synthesis of MNPs that are miscible in water involves the co-precipitation of iron salts in aqueous solutions. Different experimental parameters can be varied to control the size, shape and composition of the MNPs, such as the ratio of Fe^{2+}/Fe^{3+}, the type of salts used, pH and temperature. This technique does tend to result in MNPs with a fairly wide size range, however by carefully controlling the nucleation and growth steps, it is possible to get more monodispersed MNPs.[73, 74]

The thermal decomposition method can be used to synthesise monodispersed MNPs in non-aqueous media. This method involves the thermal decomposition of organometallic compounds such as metal acetylacetonates or metal cupferronates in high-boiling organic solvents containing stabilising surfactants such as fatty acids or oleic acid.[73] A further possible technique for MNP synthesis is the microemulsion or reverse micellar method, where surfactant molecules are used to stabilise the microdroplets formed within an immiscible liquid. However, this method is said to produce particles with a wide range of shapes and sizes, and in lower yield than the thermal decomposition or co-precipitation methods.[73]

1.5.2 Coated Magnetic Nanoparticles

With both magnetite and maghemite nanoparticles, the surface iron atoms coordinate with water in aqueous solutions, which readily dissociates to leave the iron oxide surface hydroxyl functionalized. Around the isoelectric point the iron oxide nanoparticles become unstable in water. These MNPs therefore need to be coated in order to induce stability, as well as to extend their range of properties and enable them to be functionalised, thus allowing their use in a wide range of applications.[74] It is important however that the application of a coating does not adversely affect the magnetic properties of the iron oxide core to any great extent. This can be determined by measuring the saturation magnetisation of the nanoparticle before and after coating. Saturation magnetisation is the point at which further application of an external magnetising field causes no further increase in the magnetisation of the material, i.e. it is the maximum possible magnetisation of a material.

MNPs are commonly synthesised with an inert silica coating on their surface. This improves their stability and prevents particle aggregation due to the resulting shielding of the magnetic dipole interaction, as well as an enhancement of the coulomb repulsion of the MNPs due to the negative charge of the silica layer.[74] These nanoparticles can then be functionalised using standard silica chemistry techniques. Lee *et al.* prepared magnetite nanoparticles with a silica shell using a reverse-micellar procedure.[77] The MNPs were synthesised first, then the silica shell was formed by adding tetraethyl orthosilicate (TEOS) and 3-aminopropyl-triethoxysilane. Using this technique, MNPs with a core diameter of 5-7 nm were typically obtained. The particle size was easily controlled by adjusting the ratio of the concentration of polar solvent:surfactant and the thickness of the silica shell was controlled by varying the amount of TEOS added.[77]

MNPs are also commonly coated with a layer of silver or gold, thus combining the magnetic properties of the iron oxide core with the plasmonic properties of the noble metal shell within a single nanoparticle. Du and Jing prepared Ag-coated magnetite nanoparticles with a diameter of 50 ± 20 nm and a Ag shell thickness of 5 nm.[78] The magnetite nanoparticles were first synthesised using a co-precipitation method, and

then were coated with 3-aminopropyltrimethoxysilane and then with silver through reduction of silver nitrate, using hydroxylamine hydrochloride. The saturation magnetisation of the Ag-coated MNPs was found to be a little lower than that of the uncoated MNPs, although both types of nanoparticle were paramagnetic and could be magnetically separated from solution.[79] The core/shell MNPs were used as active SERS substrates for the determination of environmental pollutants.

Kumar *et al.* also used the co-precipitation method for the synthesis of Fe_3O_4, which was then fully oxidised to γ-Fe_2O_3 by heating in dilute nitric acid.[80] The MNPs were subsequently coated with either Ag or Au through hydrazine reduction. This study found that a 20% Au coating on γ-Fe_2O_3 did not alter the magnetic behaviour of the MNPs, whereas a 10% Ag coating reduced the saturation magnetisation by 50%, although the nanoparticles were still super-paramagnetic at room temperature.[80] Robinson *et al.* also found that the saturation magnetisation of their synthesised Fe_3O_4 nanoparticles was virtually unchanged following coating with a gold shell.[81]

1.5.3 Use of Magnetic Nanoparticles for Diagnostics

DNA-functionalised MNPs have been incorporated into molecular diagnostic assays as a means of separating target DNA from the sample matrix. They can be used in a single probe system to extract target DNA from a biological medium, or they can be incorporated within a dual DNA-probe sandwich assay alongside Au or AgNPs, combining target separation with the plasmonic properties of the NP, as outlined in the following examples.

i) Non-SERRS detection

MNPs conjugated with an oligonucleotide sequence can be used in a single probe system to allow specific sequences of DNA to be extracted from a biological medium, thus acting as a purification and concentration step. In one such example, carboxyl-coated MNPs were functionalised with a 5'-amino-oligonucleotide sequence and used to isolate messenger RNA from breast cancer cells, and also to extract the supercoiled form of plasmid DNA from agarose gel.[82]

Magnetic nanoparticles are also commonly used in a two-probe system alongside Ag or Au nanoparticles. Mirkin and co-workers prepared 200-300 nm diameter particles consisting of a silica core, coated with iron oxide nanoparticles and encased in a layer of gold. These were conjugated with two different oligonucleotide sequences and used in a sandwich assay with analysis by extinction spectroscopy for the detection of synthetic target oligonucleotides.[83] Other research by this group has utilised magnetic microparticles as a means of extracting target DNA from a sample, which was subsequently released and used in a silver-amplified, gold nanoprobe sandwich complex,[84] and in the development of the 'bio-bar-code assay', which is a DNA amplification method. In this latter assay, oligonucleotide-functionalised gold nanoparticles were used for signal amplification and the magnetic microparticles were used for separation of the target from the sample matrix.[85] The bio-bar-code assay has also been use for protein detection,[86] and a commercial system has been developed based on this.

Zhou *et al.* developed a 2-probe sandwich assay consisting of gold-coated Fe_3O_4 nanoparticles and gold nanoparticles, each conjugated to a different oligonucleotide sequence that was complementary to a section of the target DNA.[87] The synthetic target oligonucleotide was first captured by an overnight hybridisation with the gold-coated MNPs, then separated and hybridised with the gold nanoparticles in a second overnight step. The hybridised complex was precipitated via a 12 hour magnetic collection. Detection was by extinction spectroscopy of the supernatant and was based on the change in the size of the peak at ~ 520 nm following magnetic collection of the precipitate, due to unhybridised gold nanoparticles. A detection limit as low as 0.1 fM was reported using this lengthy process.[87]

ii) SE(R)RS Detection

Liang and co-workers were the first to report the use of MNP conjugates in a sandwich assay, along with a Raman-active dye and detection by SERRS.[88] The capture probe consisted of a 15-base oligonucleotide sequence conjugated to amino-group functionalised silica-coated MNPs, while the detection probe incorporated SiO_2–coated AgNPs conjugated with Rhodamine B isothiocyanate dye and an 18-

base oligonucleotide sequence. Both probes were hybridised with a 33-base synthetic target sequence in a sandwich assay format, then separated using an external magnet and analysed using 633 nm laser excitation, with detection based on the dye intensity.[88] Following addition of the target, this assay required two separate mixing stages, each lasting several hours, followed by phosphate buffered saline (PBS) washes and magnetic separation, resulting in quite a lengthy procedure. A limit of detection was not presented by the authors, however the experiments used a rather high target DNA concentration of 600 nM.[88]

More recently, Zhang *et al.* developed an assay that used silica-coated MNPs conjugated with a 26-base oligonucleotide sequence to form the capture probe, while the detection probe consisted of a gold nanoparticle functionalised with a Raman reporter molecule (5,5'-dithiobis(succinimidy-2-nitrobenzoate)) and a different 24-base oligonucleotide sequence.[89] Both probes were hybridised with a 53-base synthetic target oligonucleotide sequence for one hour at room temperature. The nanoparticle assemblies were then precipitated out of solution using a small external magnet and SERS analysis carried out on the magnetic plug using 785 nm laser excitation. A large increase in SERS intensity was observed when the sample was concentrated by magnetic pull-down, with the assay sensitivity reported to be 10 pM of synthetic target DNA.[89]

This same group also developed a single nanoparticle-probe assay for DNA detection with SERS analysis and used it to demonstrate the simultaneous detection of two different target DNA sequences.[90] The capture probe consisted of a gold-coated MNP conjugated with a 25 or 26 base oligonucleotide sequence specific to either the West Nile virus or the Rift Valley Fever virus. The reporter probes consisted of a 25 or 26 base oligonucleotide sequence attached to a Raman-active dye molecule. Hybridisation occurred in the presence of a complementary 53-base target DNA sequence and, with application of an external magnet, the reporter probes were collected and interrogated by a 785 nm laser. The limit of detection of this assay was rather more modest that the previously described assay at 20-100 nM for the individual synthetic targets, with sensitivity reduced further for duplex detections.[90]

Guven *et al.* developed a magnetic nanoparticle-based sandwich assay using Au@MNP-oligonucleotide conjugates as the capture probe and gold nanorod-DTNB[b]-oligonucleotide conjugates as the reporter probe.[91] Upon mixing of both probes with the 32-base target, a sandwich complex was formed that could be magnetically separated and collected, resuspended in PBS and spotted onto TLC paper, then analysed using 785 nm laser excitation. The LOD for the assay was reported to be 11 nM, although discrimination in signal intensity of > 2:1 compared with a non-complementary sequence was only achieved for target concentrations greater than 100 nM.[91] The authors also reported successful application of the assay to the detection of PCR-amplified sequences from a real sample of maize for the purpose of detecting genetically modified organisms.[91]

In a slightly different approach, Strelau *et al.* used streptavidin-modified magnetic beads of several hundred nanometres in diameter for target separation.[92] The beads were incubated with a biotin-labelled target DNA sequence then hybridised with a dye-labelled, short synthetic oligonucleotide sequence. The hybridised complex was then applied to a solid substrate comprised of AgNPs formed upon a glass surface and the dye detected by SERS; this assay therefore uses a SERS active surface rather than SERS active nanoparticles per se.[92] The assay was applied to both synthetic 30-base target oligonucleotide sequences as well as biotin-labelled PCR product, and the multiplexing capability of the assay was demonstrated by simultaneously detecting 3 different PCR products labelled with 3 different dyes.[92] This article represented a proof of principle and further data would be needed to confirm the sensitivity and robustness of the assay.

Li and co-workers reported a successful sandwich assay utilising oligonucleotide functionalised polyacrylic acid-coated magnetic nanoparticles and dye-labelled polymer/AgNP/silica composite nanospheres as the two probes, with both types of nanoparticle measuring a few hundred nanometres in diameter. Following a 4 hour incubation with target at room temperature, the nanoparticle assemblies were

[b] DTNB = 5,5-Dithiobis(2-nitrobenzoic acid), a Raman active molecule

magnetically collected and washed with PBS before analysis using 632.8 nm laser excitation.[93] This assay allowed 10 pM detection of a 30-base synthetic target sequence, and was shown to successfully detect and differentiate up to three different synthetic targets in one sample.[93]

The assays developed to date have generally used polymer,[93] silica[88, 89] or Au-coated MNPs,[90, 91] although Lin *et al.* recently described an assay that incorporated a very thin Ag shell around the MNP core.[94] AuNPs are generally more stable than Ag, however AgNPs give a better ratio of scattering to absorption, thereby typically giving stronger SERS enhancements.[95] The summary of literature results outlined here also highlights that the use of a magnetic-based nanoparticle assembly assay can offer improved levels of detection compared with a purely suspension-based assay with no magnetic collection, as detailed in Section 1.4.3. The use of micro-arrays is an exception to this and indeed, as shown in the example of the work by Strelau *et al.*,[92] the combination of magnetic collection combined with a micro-array detection platform offers perhaps the best detection capability. MNPs can be considered as somewhat similar to a microarray as they allow the sample to be concentrated within a defined area, although with the advantage that hybridisations are carried out in solution and therefore are likely to have better hybridisation kinetics. MNPs also offer a much large surface area than a solid chip therefore can capture more target sequences, and the target hybrids can be easily separated from the reaction mixture by an external magnet and concentrated into a small spot, which is ideal for SERS sampling and allows strong signal amplification.[93]

1.6 Aims of the Project

The aim of this project is to develop a highly sensitive, closed-tube, multiplexed assay for the detection of DNA with SERS as the detection technique, using nanoparticle assembly to switch on an enhancement of a Raman marker through DNA hybridisation, combined with a magnetic manipulation step to move the nanoparticle aggregate into the interrogation volume. This will simultaneously

remove the target from the bulk of solution and concentrate it into a very small volume, which should improve both the signal to noise ratio and the assay sensitivity compared to current nanoparticle assembly approaches in solution. The assay should be designed in a closed tube format that does not require any sample manipulation or separation steps once the sample has been added to the testing vessel, and should be capable of detecting several different disease states in one single test. This will be important in order to capitalise on one of the key benefits that SE(R)RS-based detection methods offer over fluorescence.

This project is sponsored by an industry partner, Renishaw Diagnostics Limited (RDL). Ultimately, in the long term, the intention is for the assay to progress on from the research domain to be usable in a clinical diagnostics setting if it is found to be good enough. It is important, therefore, that the developed assay is stable, robust and reliable, as well as highly sensitive and selective, and all of these issues will need to be addressed throughout the assay's development. The assay also needs to be capable of detecting clinically relevant targets, in particular PCR-amplified sections of target DNA specific to several fungal species.

To achieve this assay to the end user level of acceptability, the following specific objectives have been set: synthesis of the necessary functionalised nanoparticles; evaluation of the assay performance with ideal targets; and testing of the assay with realistic clinical targets. It should be noted that the purpose of the assay is to detect specific sequences of DNA related to particular fungal infections, and not to detect single-base mismatches as would be required for the detection of single nucleotide polymorphisms.

CHAPTER 2: Development of a Silver and Magnetic Nanoparticle Assay for Sensitive DNA Detection by SERS

Sections of the text and some figures used throughout this chapter have previously been published[96] and are reproduced by permission of The Royal Society of Chemistry.

2.1 Introduction to the Assay

This chapter describes the development of a novel multi-target molecular diagnostic assay combining positive target recognition with magnetic capture to allow sample concentration and clean-up, with highly sensitive detection provided by SERS. The assay is based on nanoparticle assembly and incorporates two probes, with the DNA sequence on each probe complementary to a section of the target DNA (see Scheme 2.1). Probe 1 consists of a AgNP conjugated to a 12-base DNA sequence and a Raman reporter; probe 2 consists of a Ag-coated MNP (Ag@MNP) conjugated to a different 12-base DNA sequence. In the presence of a 24-base target sequence, hybridisation between the probes and target leads to a controlled aggregation of the nanoparticles. This places the Raman reporter in areas of high electric field intensity, giving rise to a strong enhancement of the Raman signal; hence the reporter molecule acts as a marker for the presence of target DNA. Using a simple flow cell, the hybridised nanoparticle network is concentrated using a small magnet and the immobilised plug washed to remove interfering background material, followed by direct laser interrogation of the magnetic plug (see Scheme 2.2).

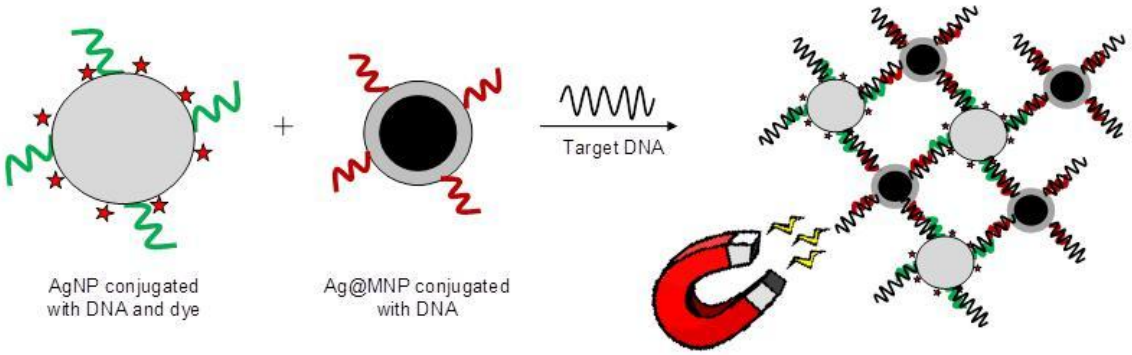

SCHEME 2.1: *Simplified schematic representation of the developed nanoparticle assembly assay showing controlled assembly of DNA-conjugated silver nanoparticles (AgNPs) and silver-coated magnetic nanoparticles (Ag@MNPs) in the presence of target DNA (not to scale)*

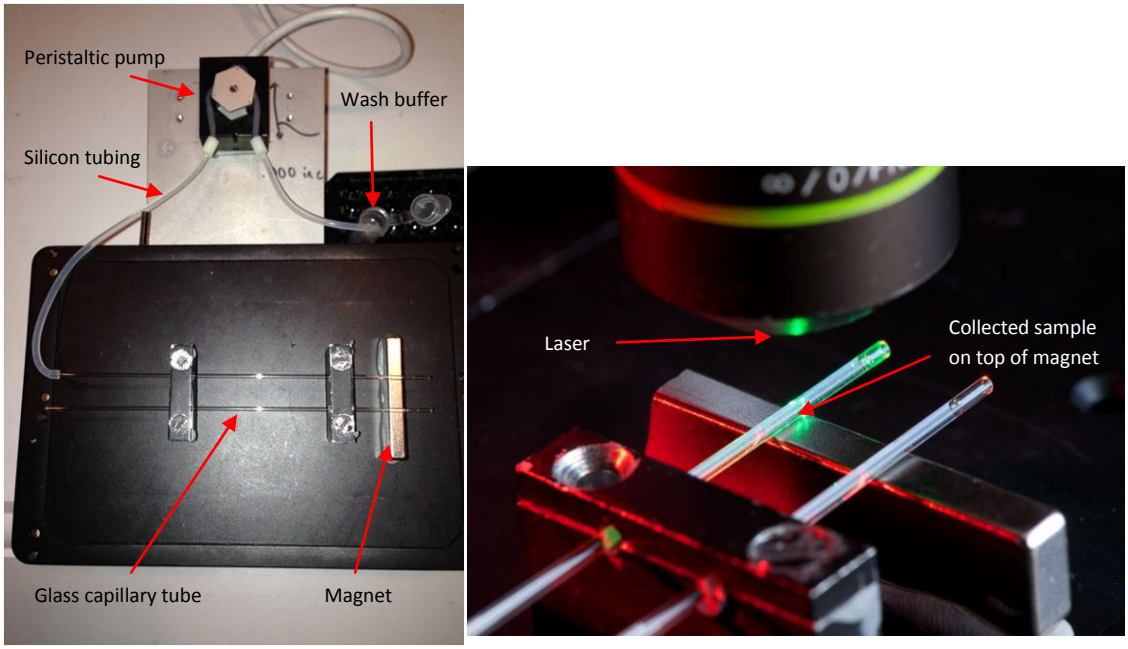

SCHEME 2.2: *Photographs showing the setup used to allow collection of magnetic nanoparticles within a simple flow cell (left) and analysis of the magnetic plug using a fixed laser (right)*

By conjugating the Raman reporter to the AgNP probe only, and combining with the wash step to remove any non-hybridised AgNP probe, there should be no reporter present within the immobilised magnetic network unless target DNA is present. This should result in much lower background reporter levels when compared to solution-

based systems in which the reporter-labelled probes remain in suspension throughout SERS analysis (see Scheme 2.3 for an illustration of this process). This assay therefore uses a Raman-active compound to act as a label to indicate the presence or absence of the target DNA. While direct SERS detection of DNA on nanoparticle surfaces is possible, the similar structure of different oligonucleotide sequences means that it is difficult to differentiate between their spectra, therefore dye labelling is often used instead to allow easier differentiation of sequences.[71]

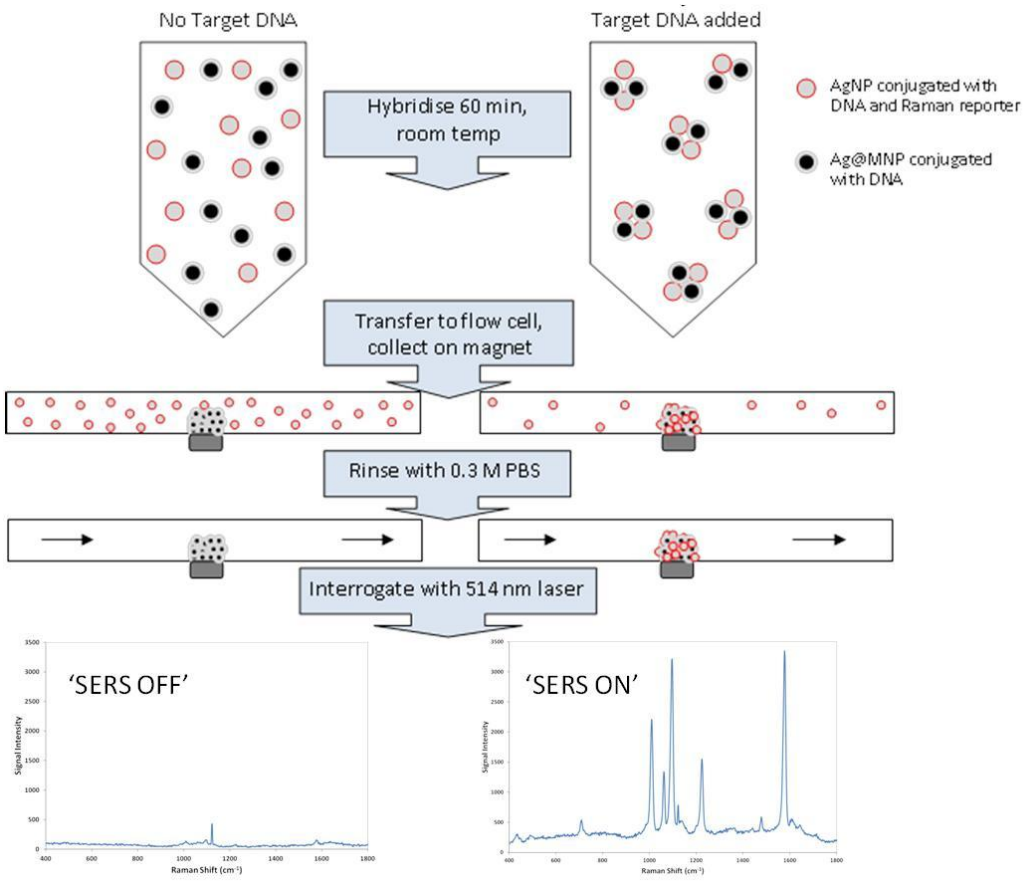

SCHEME 2.3: *Flow diagram illustrating the concept of the developed magnetic nanoparticle assembly assay, showing the differences at each step between a sample containing target DNA and a sample with no target DNA*

2.2 Synthesis of Nanoparticles and Conjugates

2.2.1 Oligonucleotide Sequences used in Assay Development

The assay was originally developed using model probe and target oligonucleotide sequences in which the target sequence related to a region of the *Chlamydia trachomatis* ompA gene.[97] Subsequently, to fit in with the requirements of the industrial sponsor, the focus of the work shifted and the sequences were altered to allow the detection of fungal targets, specifically of the *Candida* and *Aspergillus* species. Chapter 1 has explained the importance of developing a reliable and sensitive assay for the detection of these fungal species in clinical samples, ideally in a multiplexed format. The specific sequences used throughout the development of the assay are set out in Table 2.1. All targets used throughout this chapter are synthetic, single-stranded 24-base sequences that are exactly complementary to the two corresponding 12-mer probe sequences.

The 5'-thiol modification (HS-) on the probe sequences is used to anchor the oligonucleotides onto the silver surface of the nanoparticles, while the three hexaethylene glycol (HEG) units act as a 'spacer' group between the nanoparticle and the oligonucleotide sequence in order to prevent steric crowding and increase hybridisation efficiency.[55, 57, 98] The orientation of the nanoparticles in the hybridised assembly is controlled by the position of the thiol modification relative to the oligonucleotide sequence. By having the thiol group at the 5' end for both probes, the result is a 'head-to-tail' orientation of the nanoparticles (see Figure 2.1). Tail-to-tail orientations are also reported to give good SERRS enhancement,[64] and further details of these are provided in Chapters 3 and 4. However, 3'-thiol modifications have been reported to produce less stable conjugates with silver nanoparticles,[55] hence the use of a 5'-thiol modification for both probes in the initial development of the assay.

TABLE 2.1: *Details of 12-base probe and 24-base target sequences used during assay development*

Sequence Name	**Sequence Details (all shown in 5' → 3' direction)**
Model (CLY)*	P1: HS-$(HEG)_3$-CCTTAGTCCCTG P2: HS-$(HEG)_3$-CAATAGAGGCAT Target: CAGGGACTAAGGATGCCTCTATTG
Candida krusei† (KRU)	P1: HS-$(HEG)_3$-GGCGAACCAGGA P2: HS-$(HEG)_3$-CGATTACTTTGA Target: TCAAAGTAATCGTCCTGGTTCGCC
Candida albicans† (ALB)	P1: HS-$(HEG)_3$-TGGGTCTTGTAA P2: HS-$(HEG)_3$-TTGGAATGAGTA Target: TACTCATTCCAATTACAAGACCCA
Aspergillus fumigatus† (FUM)	P1: HS-$(HEG)_3$-CCCTCGGAATGT P2: HS-$(HEG)_3$-ATCACCTCTCGG Target: CCGAGAGGTGATACATTCCGAGGG
Non-complementary* (Non-Comp)	CGAGTTGACGTTAAGATCCGTATT
* Sequences synthesised in-house † Sequences purchased externally P1/P2 = Probe 1/Probe 2 HS- = thiol modification HEG = hexaethylene glycol	

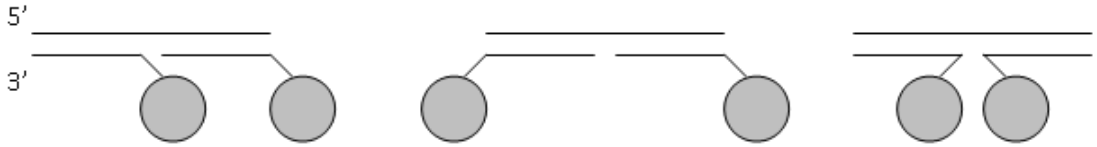

FIGURE 2.1: *Schematic representation showing nanoparticles in a head-to-tail (left), tail-to-tail (middle) and head-to-head (right) orientation*

2.2.2 Nanoparticles used in Assay Development

The silver nanoparticles used throughout this work were prepared using either a citrate-reduction or a hydroxylamine-reduction method. The citrate reduction method was used throughout the first half of the project as it was capable of producing stable, relatively monodispersed nanoparticles that could be readily functionalised with

oligonucleotides, although the quality of colloid produced using this method was often unpredictable. The hydroxylamine reduction method was later adopted due to its simplicity and reduced batch-to-batch variation, which resulted in more consistently monodisperse nanoparticles with no loss in functionalisation capability. Characterisation data for typical batches of each are shown in Figures 2.2 and 2.3, with calculated concentrations of 608 pM and 321 pM for the citrate-reduced and hydroxylamine-reduced batches, respectively. From the SEM images, using ImageJ software, the diameter of the citrate-reduced AgNPs was calculated as 39 ± 9 nm excluding rods (n = 110), and 48 ± 10 nm (n = 107) for the hydroxylamine-reduced AgNPs.

The frequency and shape of the main extinction peak are a result of the interaction of the surface plasmon with light, and relate indirectly to the size and shape of the nanoparticles. The maximum extinction wavelength (λ_{max}) gives an indication of the average particle size, with higher λ_{max} values indicating larger nanoparticles.[99] This is because, as its size is increased, the charge separation on the nanoparticle during the dipole oscillation increases, leading to a lower frequency for the collective oscillations of the electrons and hence a red-shift for the dipole resonance peak.[30] The width of the peak gives an indication of the particle size distribution, with broader peaks indicating more polydisperse nanoparticles.[99]

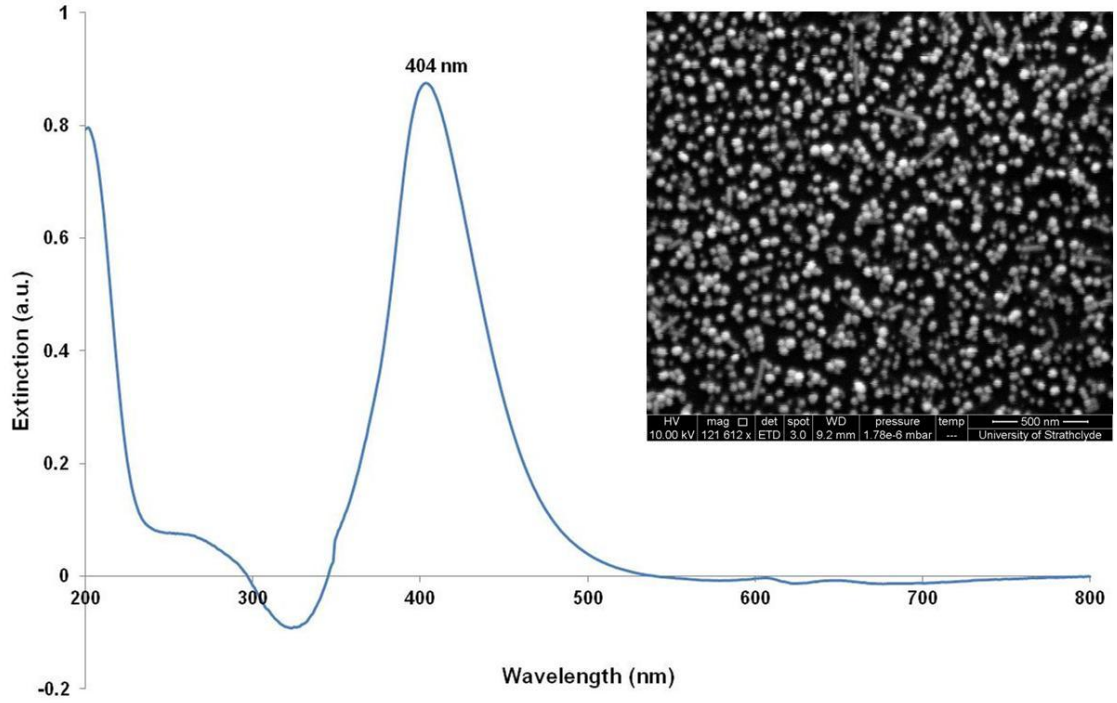

FIGURE 2.2: *Extinction spectrum of citrate-reduced AgNPs and (inset) an SEM image of the same batch of nanoparticles (scale bar is 500 nm).*

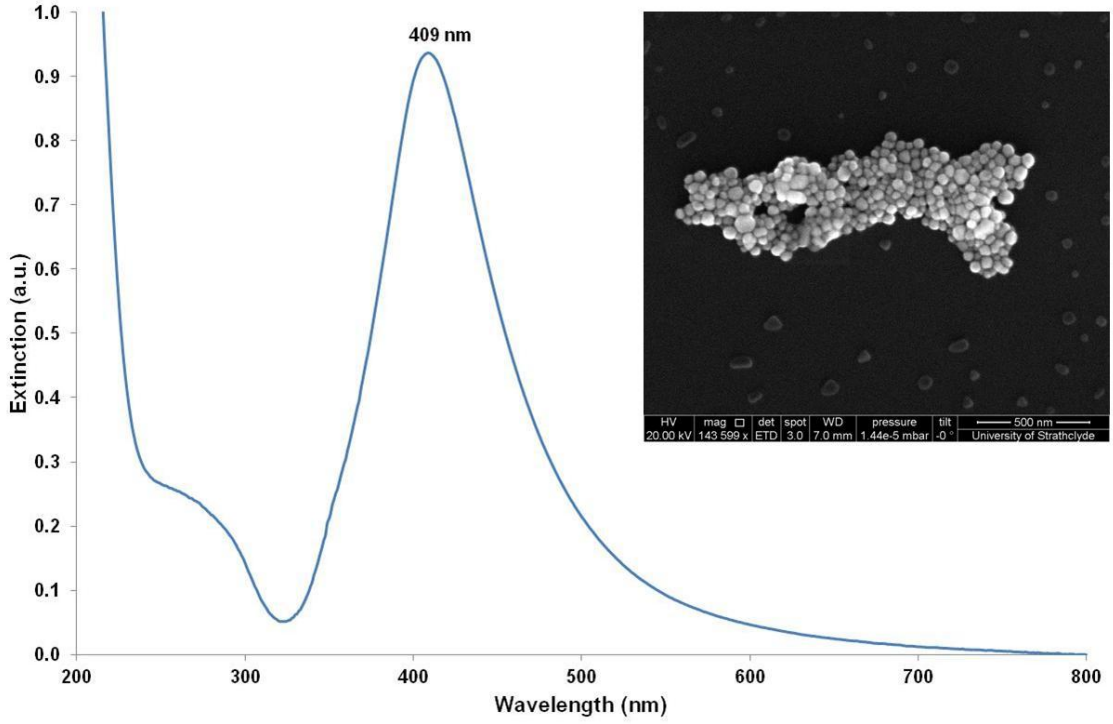

FIGURE 2.3: *Extinction spectrum of hydroxylamine-reduced AgNPs and (inset) an SEM image of the same batch of nanoparticles (scale bar is 500 nm)*

Magnetic nanoparticles in the form of maghemite (γ-Fe_2O_3) were prepared using a co-precipitation method by combining Fe(II) and Fe(III) salts in heated aqueous NaOH to produce magnetite (Fe_3O_4), with subsequent oxidation to maghemite.[80] The MNPs were then coated in silver to allow them to be linked directly with thiol-terminated oligonucleotides, to ensure stability of the MNP-oligonucleotide conjugates in buffers and salt solutions, and to benefit from the strong Raman enhancement provided by the Ag coating.

Throughout the first half of the project, MNPs were coated with Ag using a hydrazine reduction method, which involved successive additions of silver nitrate, sodium citrate and hydrazine hydrate to the maghemite nanoparticles.[80] The resultant Ag@MNPs were readily conjugated with oligonucleotides and provided strong SERS enhancement of a Raman reporter when utilised within the assay. However, as a result of problems with assay stability due to potential nanoparticle interactions, further methods for coating the MNPs with Ag were investigated. The selected method, modified from that used by Mandal *et al.*[100] used a milder glucose-reduction process that allowed a good level of silver coverage on the MNPs and improved stability of the Ag@MNPs before and after conjugation with oligonucleotides. Conjugates prepared from glucose-reduced Ag@MNPs gave better SERS discrimination between target and blank samples compared with hydrazine-reduced Ag@MNPs due to a lower level of dye interference in blank samples, which was likely due to a reduced level of interaction between the AgNPs and Ag@MNPs. Storing the prepared Ag@MNPs in a low concentration of sodium citrate was also found to improve their stability over time, with the nanoparticles remaining stable for a period of several months when stored at room temperature. Characterisation data for a typical batch of glucose-reduced Ag@MNPs is shown in Figure 2.4, with a calculated average diameter of 30 ± 10 nm (n = 107).

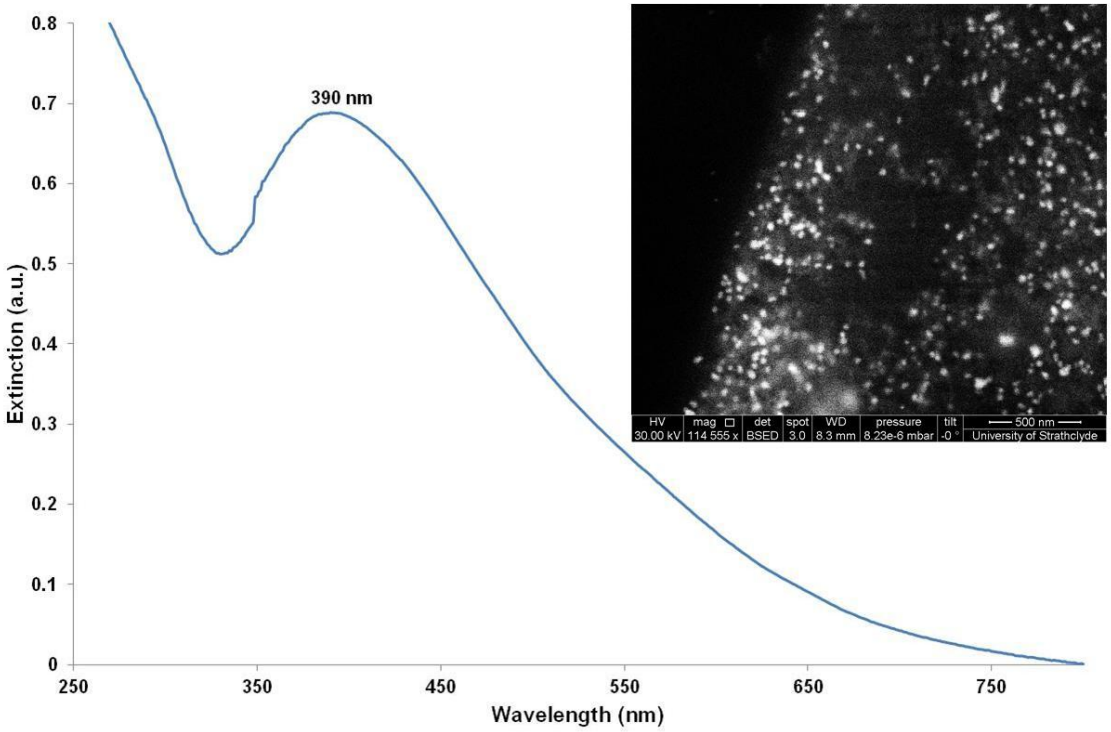

FIGURE 2.4: *Extinction spectrum of glucose-reduced Ag@MNPs and (inset) an SEM image of the same batch of nanoparticles (scale bar is 500 nm)*

2.2.3 Nanoparticle Conjugation within the Assay

When preparing nanoparticle-oligonucleotide conjugates, it is important to ensure that they are stable in high salt concentrations as typically found in hybridisation buffers. Addition of salt during the conjugation process is also required to prevent intra-strand repulsion between neighbouring oligonucleotides, due to the negatively charged phosphate backbone of DNA, and thus allow a higher level of oligonucleotide loading onto the nanoparticle surface.[46] However, NaCl is a very effective aggregating agent for silver nanoparticles, and will cause them to aggregate irreversibly if they do not contain a sufficient protective layer of oligonucleotides attached to their surface. Initial conjugation of nanoparticles was therefore carried out using an established salt-ageing method, during which phosphate buffer and NaCl were added to the nanoparticles and thiolated oligonucleotides in a slow and controlled manner over a period of several days, which allowed the oligonucleotide sequences sufficient time to attach and 'protect' the nanoparticle before the next increase in ion concentration, and so on. This method has been reported for the

successful synthesis of oligonucleotide-functionalised gold[46] and silver[55] nanoparticles. However, in addition to the time involved to make these conjugates, the procedure was often found to be unreliable, with the nanoparticles frequently aggregating irreversibly during one of the aliquot additions resulting in a waste of expensive oligonucleotide. For these reasons, a different conjugation process was adopted midway through this project, based on a method published by Zhang *et al.* that involved lowering the pH to allow rapid attachment of the oligonucleotides to the nanoparticle surface, before pH-readjustment and addition of buffers.[101] With some minor modifications from the published method, this technique was found to be much more reliable than the salt-ageing method and allowed conjugate preparation within a few hours, rather than several days.

The same procedure was used to conjugate both the AgNPs and Ag@MNPs, with the exception that a low concentration of polyacrylic acid (PAA) was added to the Ag@MNPs following conjugation. This was found to improve their stability in hybridisation buffer, as evidenced from extinction spectra and dynamic light scattering (DLS) sizing measurements. The use of PAA to improve the stability of uncoated iron oxide MNPs was described by Hajdu *et al.*, who determined that there was H-bonding between the iron oxide surface and the PAA.[102] The observed improvement in stability with Ag@MNPs in this study therefore suggests that there may not be complete coverage of Ag around the MNP core, but rather some uncoated maghemite remains that is available to bind with the PAA. The use of PAA was not found to affect the level of hybridisation between probes and target, or to cause any interference in the SERS signal.

The number of oligonucleotides attached to a AgNP following conjugation was calculated using an established method.[46] This involved using a probe sequence with a fluorescent dye attached, and then detaching this from the nanoparticle following conjugation and measuring the amount of fluorescence in solution. By comparing this level to control samples, the number of oligonucleotide strands per nanoparticle could be determined. The dye used was Cy3 and the probe sequence was as follows: HS-Cy3-$(HEG)_3$-TCTCAACTCGTA, i.e. a thiolated 12-mer probe with $(HEG)_3$

spacer, as with the probes detailed in Table 2.1 and used throughout this chapter. Conjugation was carried out using hydroxylamine-reduced AgNPs and the fast, low-pH conjugation method, resulting in a conjugate with a nanoparticle concentration of 378 pM; full details are provided in the Experimental section. Based on the calibration graph of control samples (Figure 2.5) and the measured fluorescence signal intensity of the samples of detached probe sequence (7,680 ± 672), the number of oligonucleotide strands per 48 nm AgNP was calculated as approximately 1,300 ± 200. This compares well with the value calculated by Hurst *et al.* of 1,200 DNA strands per 50 nm AuNP.[46]

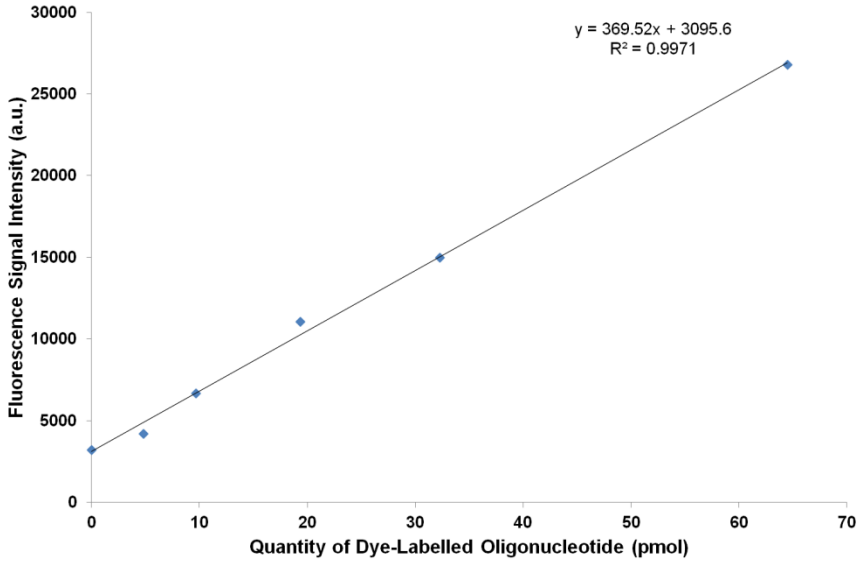

FIGURE 2.5: *Change in fluorescence signal intensity with concentration of dye-labelled oligonucleotide sequence in a range of control samples, showing line of best fit (black line) through the data points (blue diamonds)*

2.2.4 Raman Reporters used in Assay Development

A Raman reporter molecule must possess a number of characteristics for successful use in a nanoparticle assembly assay. It must exhibit a strong and distinctive SERS signal, attach strongly to the nanoparticle to minimise leaching from the surface, and be stable in all buffers used during storage and hybridisation. There should be minimal fluorescence background, and ideally the Raman spectrum should possess unique peaks that would allow multiplexing with other reporters. Additionally, the

reporter must not cause aggregation of the nanoparticles in the concentration at which it is used. A range of Raman reporters was investigated throughout this research; the SERS spectra and structures of those found to give the best results are shown in Figures 2.6-2.9, with the extinction spectra of the four reporters shown in Figure 2.10. The SERS spectra were all collected using 514 nm laser excitation (1 x 1 second accumulation) on salt-aggregated hydroxylamine-reduced AgNPs.

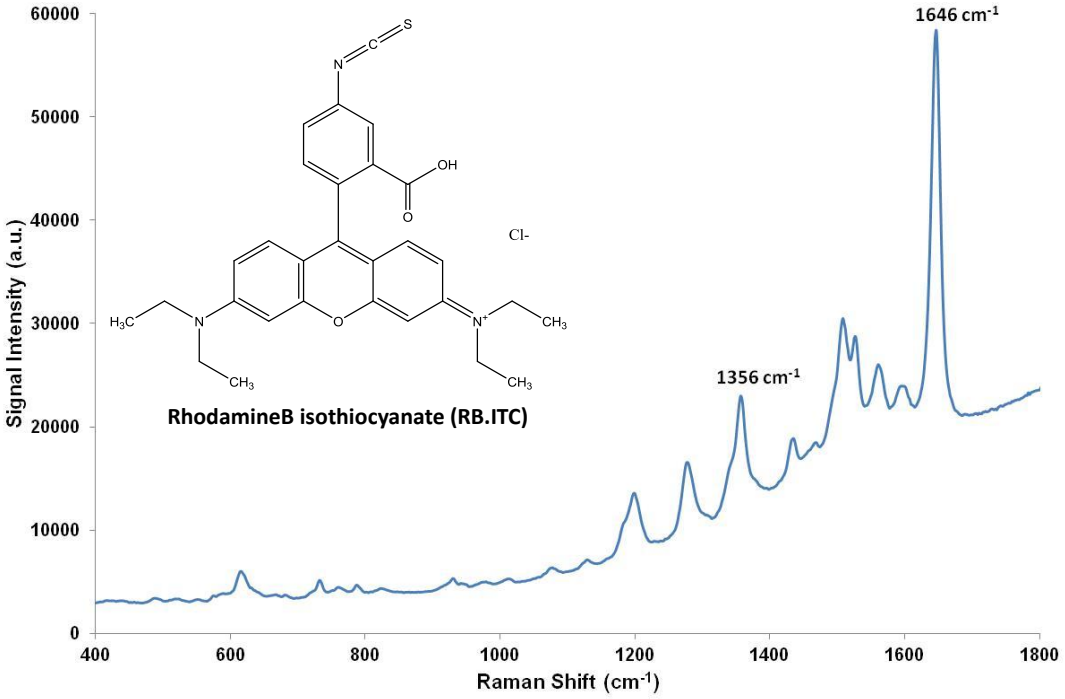

FIGURE 2.6: *Structure (inset) and uncorrected SERS spectrum for 1x10^{-7} M RB.ITC. The peaks at 1356 cm^{-1} and 1646 cm^{-1} relate to the xanthene ring C-C stretching vibrations.*[103]

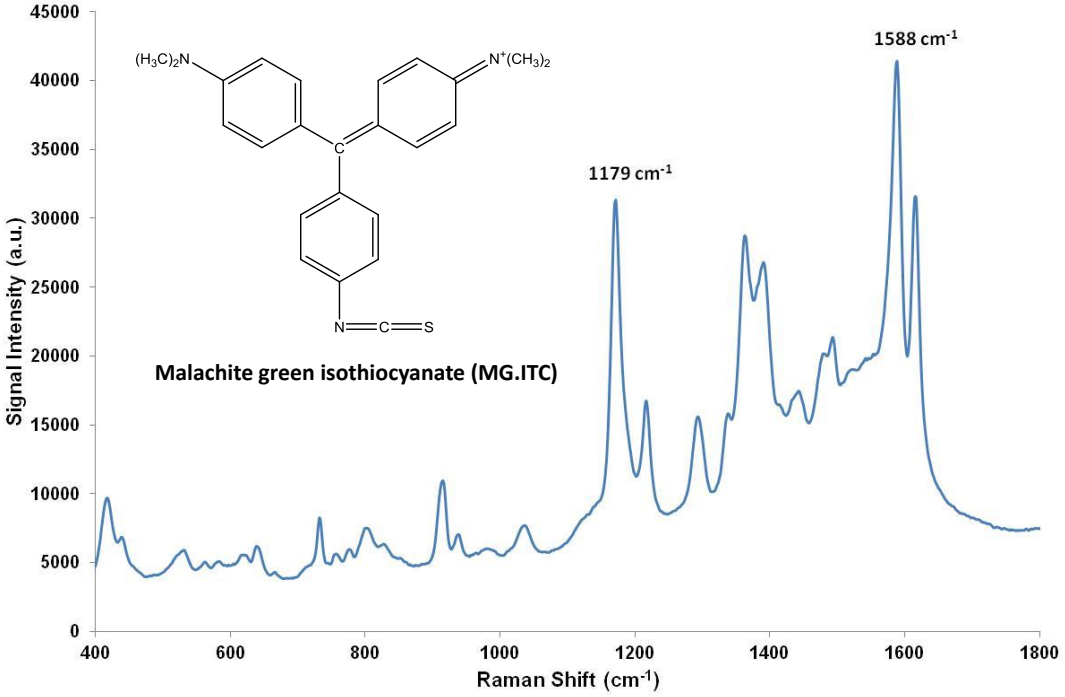

FIGURE 2.7: *Structure (inset) and uncorrected SERS spectrum for 1x10^{-7} M MG.ITC. The peak at 1179 cm^{-1} relates to the ring C-H in-plane bending and at 1588 cm^{-1} to the phenyl N-C and ring C-C stretching modes.*[104]

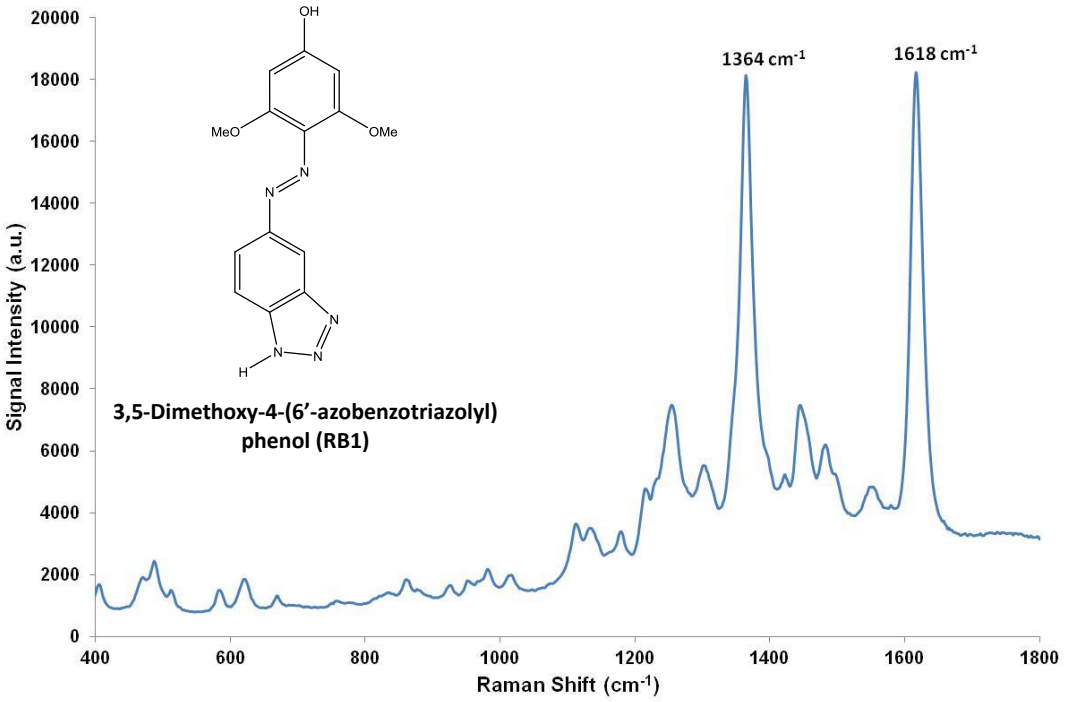

FIGURE 2.8: *Structure (inset) and uncorrected SERS spectrum for 1x10^{-8} M RB1. The peak at 1364 cm^{-1} relates to the azo stretch and at 1618 cm^{-1} to a modified quadrant stretch of the aromatic ring system.*[105]

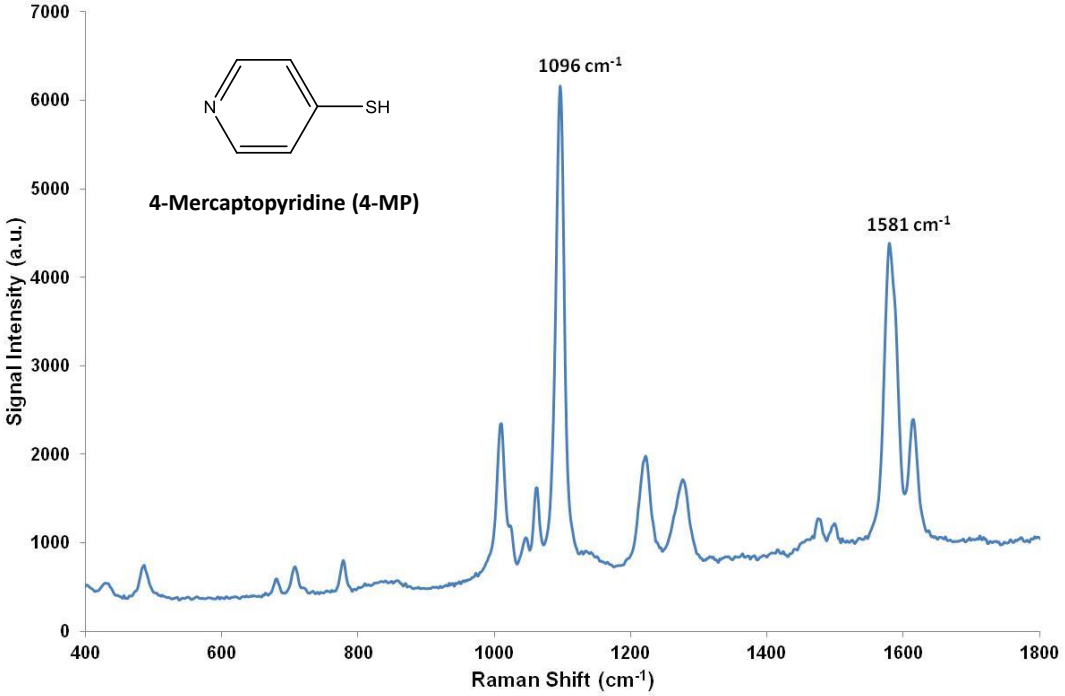

FIGURE 2.9: *Structure (inset) and uncorrected SERS spectrum for 1x10^{-6} M 4-MP.The peak at 1096 cm^{-1} relates to the in-plane ring-breathing mode coupled to the C-S stretching mode and at 1581 cm^{-1} to the pyridine ring C=C stretching mode.*[106]

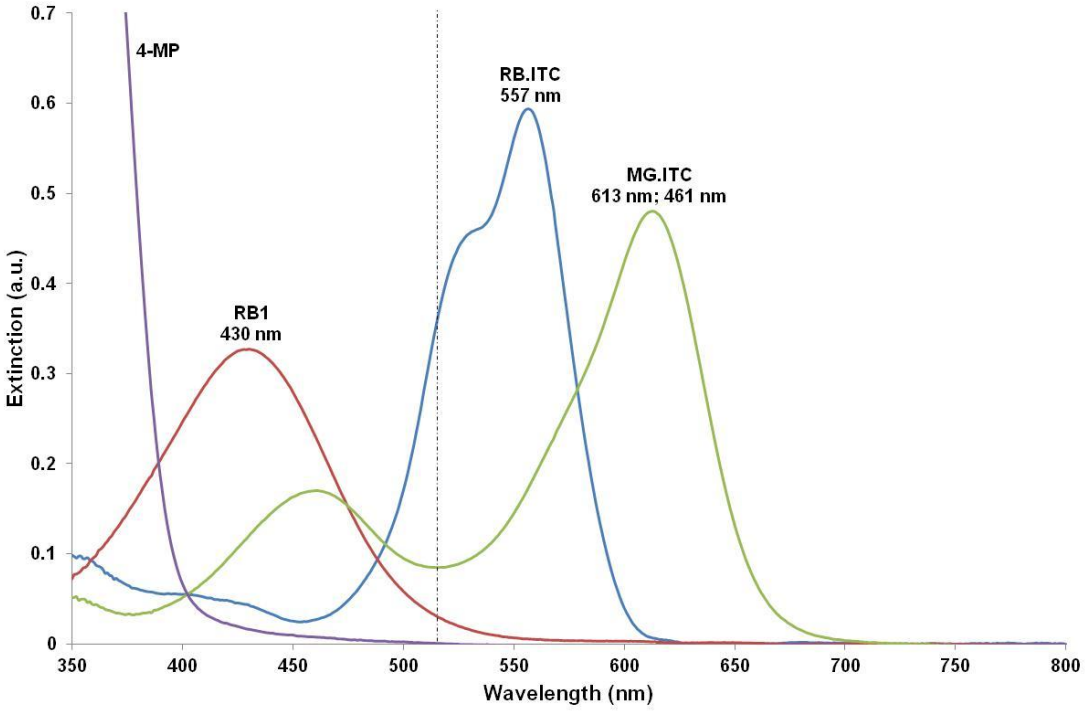

FIGURE 2.10: *Extinction spectra of aqueous dilutions of the four Raman reporters; 1 mM 4-MP, 10 µM RB1, 1 µM RB.ITC and 10 µM MG.ITC. Black dashed line represents excitation wavelength of laser used (514 nm)*

Initial work on the assay used the commercial dye RB.ITC as the Raman label, attaching through the isothiocyanate group to produce a strong Ag-S bond with the nanoparticles.[107] RB.ITC has a maximum absorption at 557 nm, which is almost in resonance with the 514 nm laser used throughout this work, and very sensitive detection of this dye was achieved as expected. However due to ongoing problems with fluorescence, which would limit the potential for multiplexing, other Raman reporters were investigated. Attachment of a fluorescent dye to a AgNP surface should result in fluorescence quenching,[18] and the presence of the high fluorescence background may therefore suggest that not all of the dye was attached to the nanoparticle surface or may have leached from the surface, although other researchers have also reported on measurable fluorescence levels from Ag-bound RB.ITC.[108]

RB1 has been used as a marker for DNA detection,[105] and attaches covalently to the AgNP surface through the benzotriazole group.[109] This dye was synthesised within our group, and was detected at very low levels within the assay. No fluorescent background was observed with this dye due to the laser excitation wavelength being off-resonance to the absorption maxima of the dye. MG.ITC, another commercial dye that attaches to the AgNP surface through the isothiocyanate group,[107] was also found to give strong SERS enhancement with no observed fluorescent background. 4-MP, while non-resonant, was of interest due to its small size which may have allowed better attachment to the conjugated NP surface. 4-MP attaches covalently to the surface through a Ag-S bond.[106]

It is important to select the appropriate concentration of dye to use since excess dye can lead to high background signals and reduce the level of discrimination between target and blank samples. On the other hand, if too little dye is used then weak signals can result even at high target concentrations. Different concentrations are required depending on the particular dye and a workable compromise needs to be reached, particularly when used in a multiplexed platform.

2.3 Nanoparticle Assembly Using Functionalised Probes

So far, this chapter has described the development of the various components of the nanoparticle assembly assay. From this point onwards the implementation of the assay as a whole, incorporating all of these constituent parts, will be described. The functioning and stability of the assay were primarily assessed using extinction spectroscopy and SERS measurements.

The data presented here relates to each of the four different 24-base synthetic target sequences and their corresponding probes, as shown in Table 2.1. All of these conjugates were prepared using the fast, low-pH method with the probe 1 sequence conjugated to citrate-reduced AgNPs and the probe 2 sequence to glucose-reduced Ag@MNPs. The conjugates are as follows:

- Probes specific for *C. krusei* target, using 4-mercaptopyridine as a reporter (probes designated KRU-P1-MP and KRU-P2).
- Probes specific for *C. albicans* target, using malachite green isothiocyanate as a reporter (ALB-P1-MG and ALB-P2).
- Probes specific for the model sequence, using RhodamineB isothiocyanate as a reporter (CLY-P1-RhB and CLY-P2).
- Probes specific for *A. fumigatus* sequence, using RB1 as reporter (FUM-P1-RB1 and FUM-P2).

The particular probe/target combinations used in each experiment are as detailed in the text and figure captions.

2.3.1 Extinction Spectra Measurements of Nanoparticle Assembly

i) Reaction Kinetics Measurement

Reaction kinetic studies were carried out using extinction spectroscopy to determine the extent of aggregation within a sample following addition of either target or non-complementary DNA to the two probes. For the data shown in Figure 2.11, samples were prepared by combining 10 pM of each conjugate (KRU-P1-MP and KRU-P2) with 5 nM KRU target/non-comp sequence in 0.3 M PBS, with spectra collected

every 10 min for 100 min at room temperature. In the presence of target DNA there was a reduction in absorbance of the main peak and the appearance of a second peak at a longer wavelength (Figure 2.11, top); this was due to individual nanoparticles being brought into close proximity resulting in a change in surface plasmon resonance (SPR), indicating successful DNA-mediated nanoparticle assembly. Previous studies have also shown this effect in a AgNP-AgNP sandwich assay.[55] In contrast, addition of a non-complementary sequence caused no SPR changes (Figure 2.11, bottom), indicating that no hybridisation or non-specific aggregation occurred, and highlighting the stability of both probes in the hybridisation buffer. Similar results to those shown were achieved with each of the different probe sequences as detailed in Table 2.1. Any change in the SPR peak height or width for the non-complementary sample was evidence of instability of either one or both of the probes within the hybridisation buffer, and these issues were addressed and resolved throughout the assay development stage.

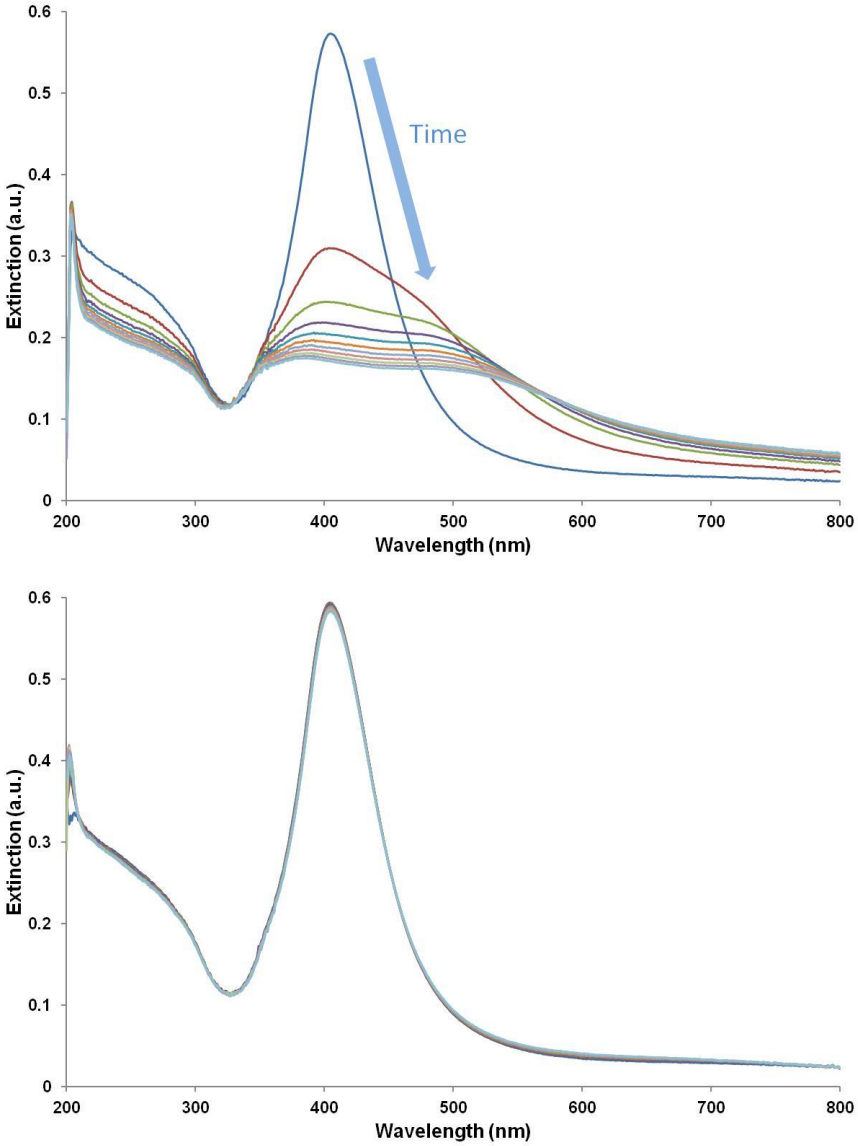

FIGURE 2.11: *Changes in extinction spectra for samples of 10 pM KRU-P1 and 10 pM KRU-P2 conjugates with 5 nM KRU target (top) or non-complementary sequence (bottom) in 0.3 M PBS, showing spectra collected every 10 min for 100 min at room temperature.*

Changes in the rate and extent of hybridisation in the presence of target DNA occur for a number of reasons, including the concentration and length of the target sequence,[110] temperature, and hybridisation buffer.[42] Figure 2.12 compares the nanoparticle assembly rates for samples of FUM-P1-RB1 and FUM-P2 conjugates (5 pM of each) with different concentrations of FUM target sequence in 0.3 M PBS at room temperature. The rate is measured as the ratio of the extinction value of the nanoparticle assemblies with that of the individual nanoparticles (i.e.

extinction$_{520}$/extinction$_{405}$ for these conjugates) at set periods of time following addition of target to the probes. These results show an increase in the rate and extent of nanoparticle assembly with increasing target concentration over the range 500 pM to 20 nM, with a drop in assembly rate at the higher target concentration of 50 nM. This reduction in nanoparticle assembly rate with very high target concentrations was also observed with other probe-target combinations (data not shown) and may be due to slower diffusion of the nanoparticle probes within the matrix when there is a large excess of target DNA present.

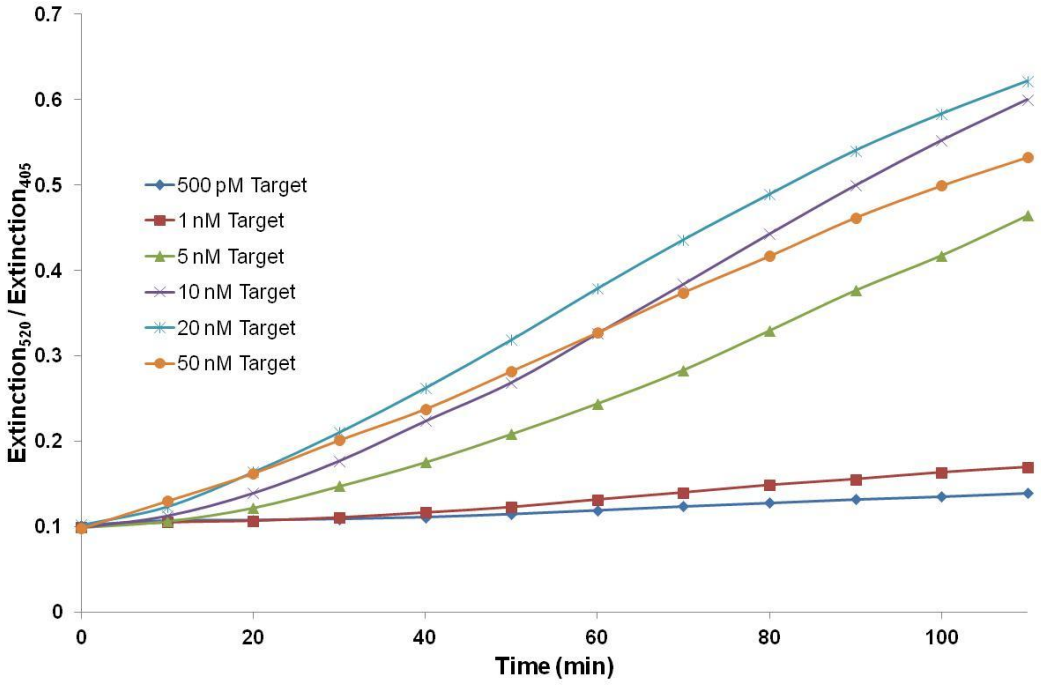

FIGURE 2.12: *Changes in nanoparticle assembly over a 110 min period following addition of different concentrations of target sequence to a mixture of 5 pM FUM-P1-RB1 and FUM-P2 conjugates in 0.3 M PBS buffer. Results are for single samples.*

Higher salt concentrations in the hybridisation buffer allow faster hybridisation by providing more charge screening between the probe and target oligonucleotides.[42] This is illustrated in Fig 2.13 (top) for hybridisation of FUM conjugates with 2 nM target sequence in various concentrations of PBS buffer. However, increased salt concentrations also increase the instability of the nanoparticles (Fig 2.13, bottom),

therefore 0.3 M PBS was used as the hybridisation buffer for all of the experiments within this chapter. Further details of the effects of hybridisation buffer, target length, and probe length and orientation on the nanoparticle assembly process are provided in Chapter 3.

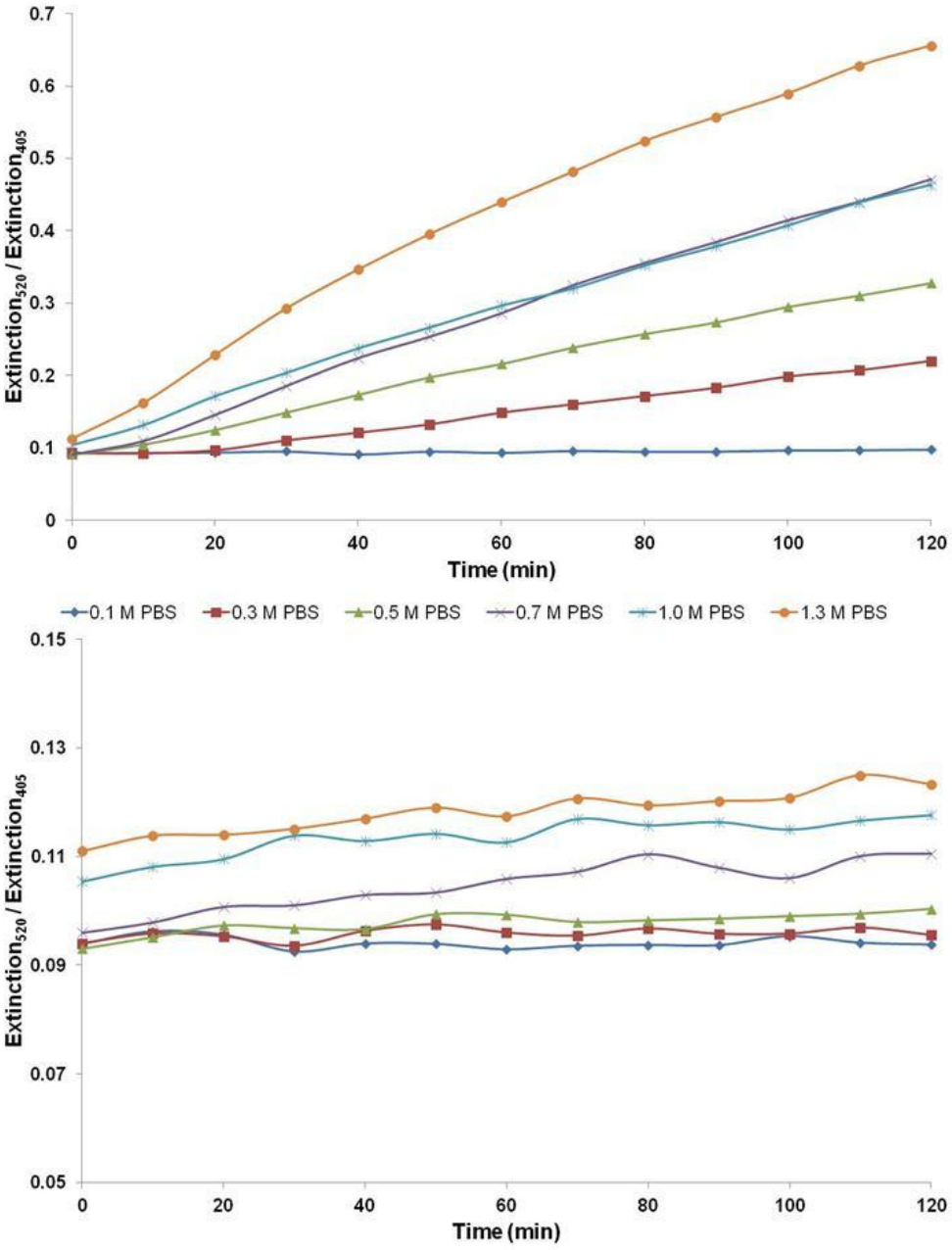

FIGURE 2.13: *Changes in nanoparticle assembly over a 2 h period following addition of 2 nM target sequence (top) or 10 nM non-comp sequence (bottom) to a mixture of 5 pM FUM-P1-RB1 and FUM-P2 conjugates in various concentrations of PBS buffer. Results are for single samples.*

ii) Melting Transition Measurements

The melting temperature (T_m) of a DNA duplex is defined as the temperature at which half of the strands are in a single-stranded state (ssDNA), i.e. non-hybridised. Since the probe-target hybridisation is reversible, heating samples beyond their melting temperature will cause the nanoparticle conjugates to once again be free in suspension. This leads to distinctive changes in the SPR of the nanoparticles, as shown in Figure 2.14 where mixtures of nanoparticle conjugates and either target or non-complementary DNA were subjected to four repeated heating and cooling cycles. For the target sample, the T_m value (55.2 °C) can be clearly seen as the temperature at which there is a sharp increase in the extinction value at 405 nm during heating of the sample, and both the extinction and T_m are little changed following repeated cycles. By contrast, no change in extinction at 405 nm is observed for the non-complementary sample. Results from both of these samples also highlight the stability of the conjugates at elevated temperatures. The data shown used the same conjugates and concentrations as in the previous reaction kinetics experiment, i.e. 10 pM each of KRU-P1 and KRU-P2 conjugates with 5 nM target/non-comp sequence in 0.3 M PBS. Samples were left to hybridise for two hours at room temperature prior to commencing the heat/cool cycles. Note that DNA has a λ_{max} of 260 nm, however it is present at such a low concentration relative to the nanoparticles that the peak is barely visible, therefore monitoring was carried out at the conjugate maximum instead.

As shown in Fig 2.14, the melting transition observed in nanoparticle assembly assays is very sharp, much more so than would be observed in a DNA-only system.[42] This is due to the co-operative melting effect as a result of the multiple DNA duplexes formed between each pair of nanoparticles. Melting temperature values depend on a range of factors, including nanoparticle size and orientation within the assemblies, surface density of probe DNA, target concentration, and the dielectric constant of the matrix.[42] Differences in melting temperature have been used to determine single-base mismatches within target DNA sequences using nanoparticle assembly assays.[42, 55]

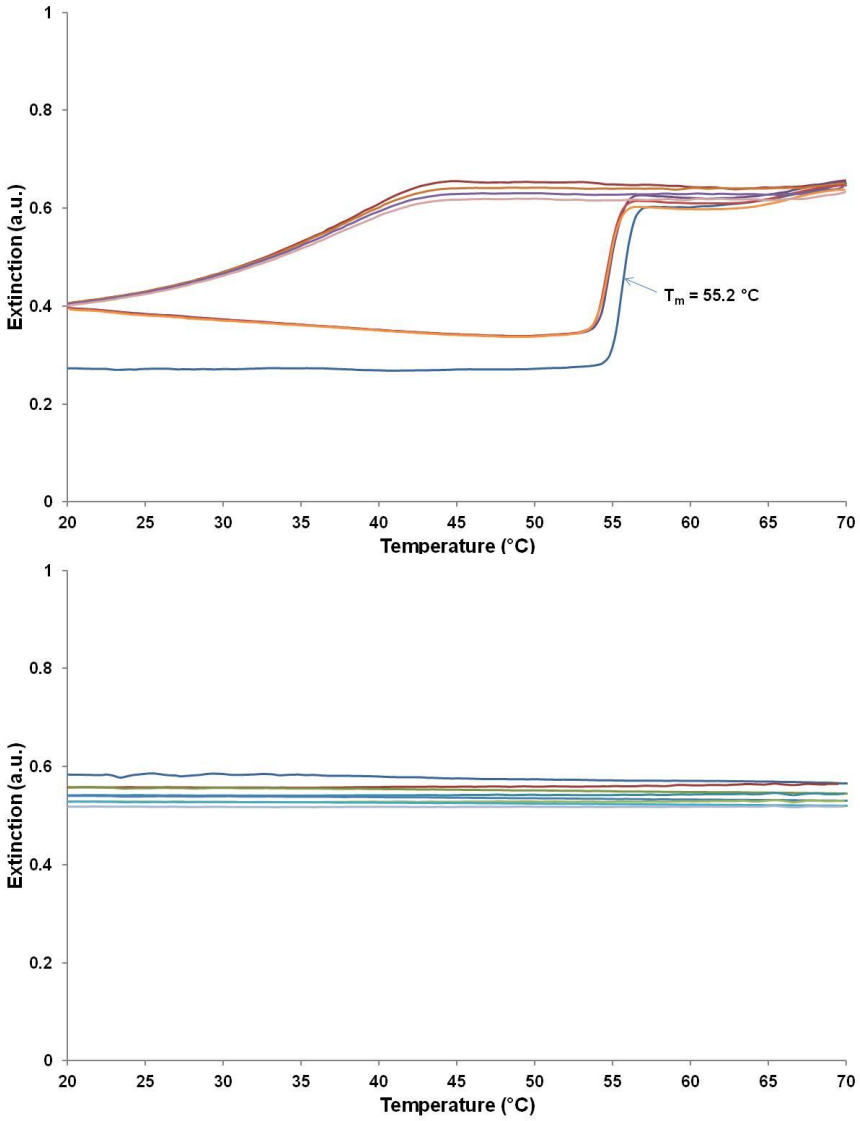

FIGURE 2.14: *Changes in extinction at 405 nm for samples of KRU-P1 and KRU-P2 probes with 5 nM target (top) or non-complementary sequence (bottom) in 0.3 M PBS, subjected to 4 heat/cool cycles (20 – 70 – 20 °C).*

2.3.2 DLS Measurements of Nanoparticle Assembly

Dynamic light scattering (DLS) can also be used as a means of confirming nanoparticle assembly by measuring changes in particle size upon addition of target DNA. Figure 2.15 shows changes in particle diameter for samples containing 5 pM of each of the KRU-P1-MP and KRU-P2 conjugates and 5 nM of either target or non-complementary DNA, in 0.3 M PBS buffer. Measurements were taken

immediately prior to target DNA addition, then at 20 min intervals for a total of 2 h following this, all at room temperature. The results show an increase in particle diameter from 69 nm before target addition to 426 nm 2 h after addition of target DNA, with no increase in size observed for the sample containing non-complementary DNA. Note that the particle sizes measured by DLS are larger than the true values since DLS measures the hydrodynamic diameter of particles.

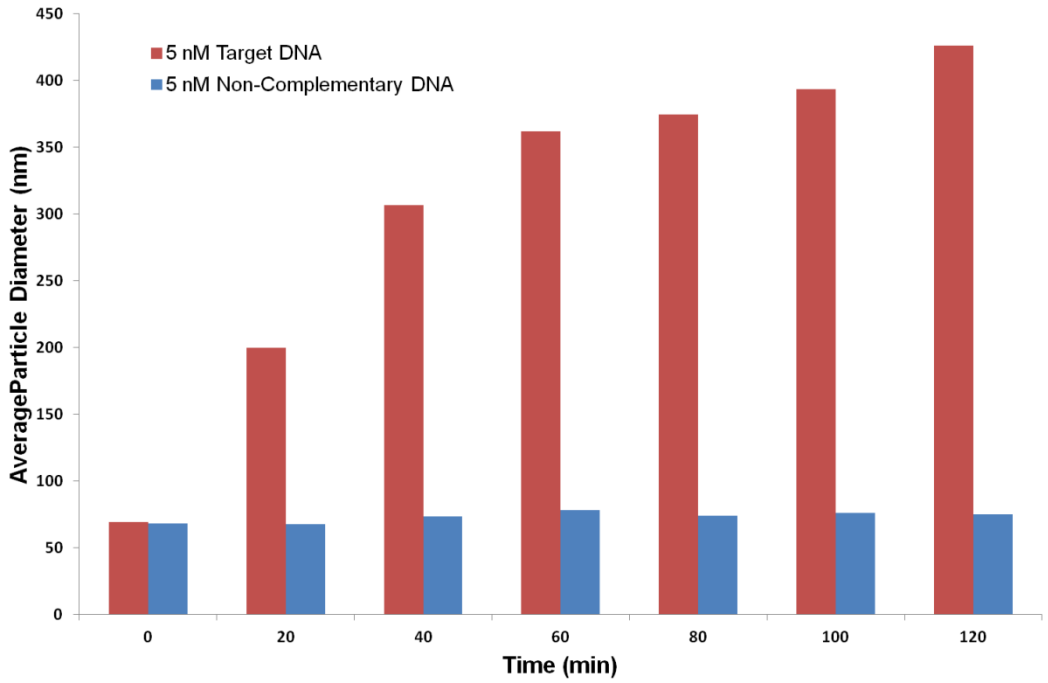

FIGURE 2.15: *Changes in hydrodynamic diameter over time for a sample of KRU-P1 and KRU-P2 conjugates in 0.3 M PBS following addition of either target or non-complementary DNA. Results are for single samples.*

2.3.3 SERS Measurements of Nanoparticle Assembly

i) Comparison of Magnetic Plug vs. Suspension Measurements

In the presence of target DNA, the Raman reporter attached to the AgNP experiences an enhancement in the electric field intensity of its immediate environment due to the induced nanoparticle aggregation.[36] This is illustrated in Figure 2.16a, which shows the change in intensity of the peak at 1179 cm^{-1} for MG over a 60 min period when a

mixture of ALB-P1-MG and ALB-P2 conjugates were mixed with either target or non-complementary DNA. These are suspension-based SERS measurements, carried out in cuvettes without the application of a magnet. A rapid increase in SERS intensity is observed for the 5 nM target sample, which plateaus after ~ 30 min. These samples were prepared in a total volume of 220 µL, therefore 5 nM equates to 1100 fmol of target DNA. For the non-complementary DNA sample, no increase in SERS intensity was observed throughout the sampling period. The increase in signal intensity for the target vs. non-complementary sample is ~ 4-fold after 60 min. When the target concentration was reduced to 1 nM (219 fmol), there was no discrimination between target and non-complementary DNA sequences.

Following these measurements, the same samples were pumped around a closed flow-cell loop with a magnet fixed underneath, allowing collection of a magnetic plug of the assemblies, which were then washed and SERS measurements taken. The results (Figure 2.16b) illustrate the strong signal enhancement that was achieved when SERS analysis was carried out on the concentrated magnetic plug compared to analysis of the sample in suspension, with a greater than 3-fold signal enhancement for both the 1 nM and 5 nM target concentrations. For the magnetic plug measurements, a greater than 10-fold signal enhancement was obtained for the 5 nM target vs. non-complementary sample. Further comparison of results obtained using the magnetic plug and the suspension assays is provided in Chapter 4.

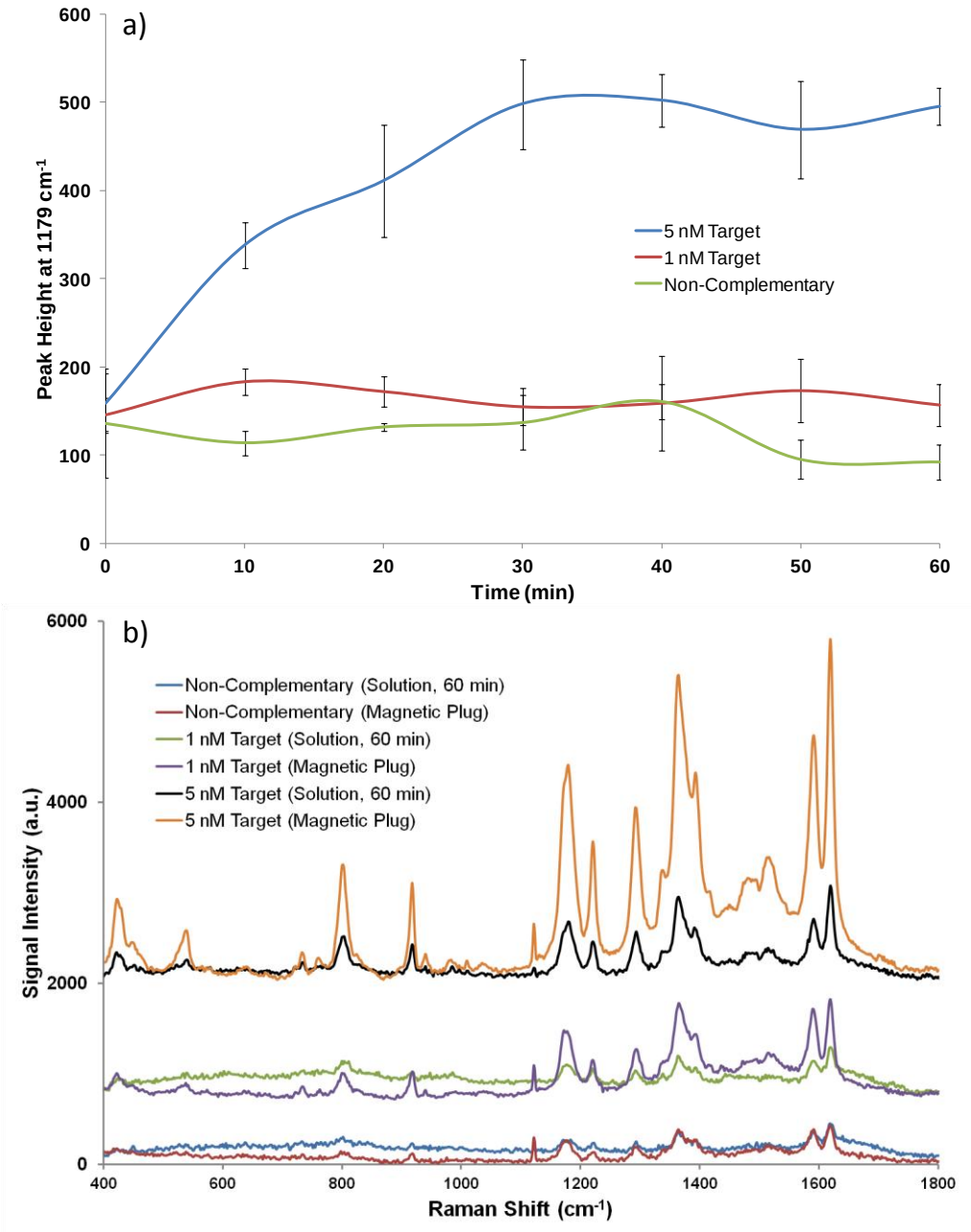

FIGURE 2.16: *Differences in MG signal intensity for samples containing ALB-P1-MG and ALB-P2 conjugates with either target or non-complementary DNA, showing a) change in peak height at 1179 cm^{-1} over 60 min for solution-based samples; and b) comparison of the SERS spectra for solution-based samples (after 60 min) vs. the magnetic plug of the same samples. Results shown for each sample type are mean average values from triplicate measurements from a single sample and error bars in a) represent ± one standard deviation.*

ii) Magnetic Plug Measurements

Figures 2.17 to 2.20 show the changes in SERS intensity of the Raman reporter for magnetic plug measurements of samples containing a range of concentrations of each of the four targets with their corresponding probes. The general conditions used for all of these samples involved combining the relevant P1 and P2 conjugates (e.g. 1 µL of each) in an Eppendorf tube with a pre-defined concentration of target DNA, typically made up to a total volume of 10 µL in 0.3 M PBS hybridisation buffer. Samples were left to hybridise for 60 min at room temp, then transferred to a glass capillary tube and collected on top of a magnet for 20 min. The magnetic plug of nanoparticle assemblies was then washed with 1 mL of 0.3 M PBS and directly interrogated with a 514 nm excitation laser to get the SERS measurements. Triplicate measurements were recorded for each sample, and 2 samples were separately prepared and analysed at each target concentration; the graphs show the average values of these six measurements and error bars represent ± one standard deviation. Note, the sharp peak at ~1125 cm^{-1} comes from the glass capillary tube.

In each case, there was a non-linear increase in signal intensity with increasing target concentration. While a low Raman reporter signal was observed in both blank samples (i.e. probes and buffer only) and samples containing non-complementary DNA, good discrimination in signal intensity was observed for low femtomole levels of target DNA for all target sequences. Compared with a corresponding sample containing the relevant probes and non-complementary DNA, the signal intensity was 4.9 times higher for a sample containing 20 fmol of KRU target; 3.6 times higher for a sample containing 20 fmol of ALB target; 12.6 times higher for a sample containing 10 fmol of model target (or 2.4 times higher for 3 fmol target); and 7.1 times higher for a sample containing 33 fmol of FUM target (or 1.7 times higher for 10 fmol target). For the ALB target, this represents more than a 10 times improvement in detection limit compared with suspension-based measurements.

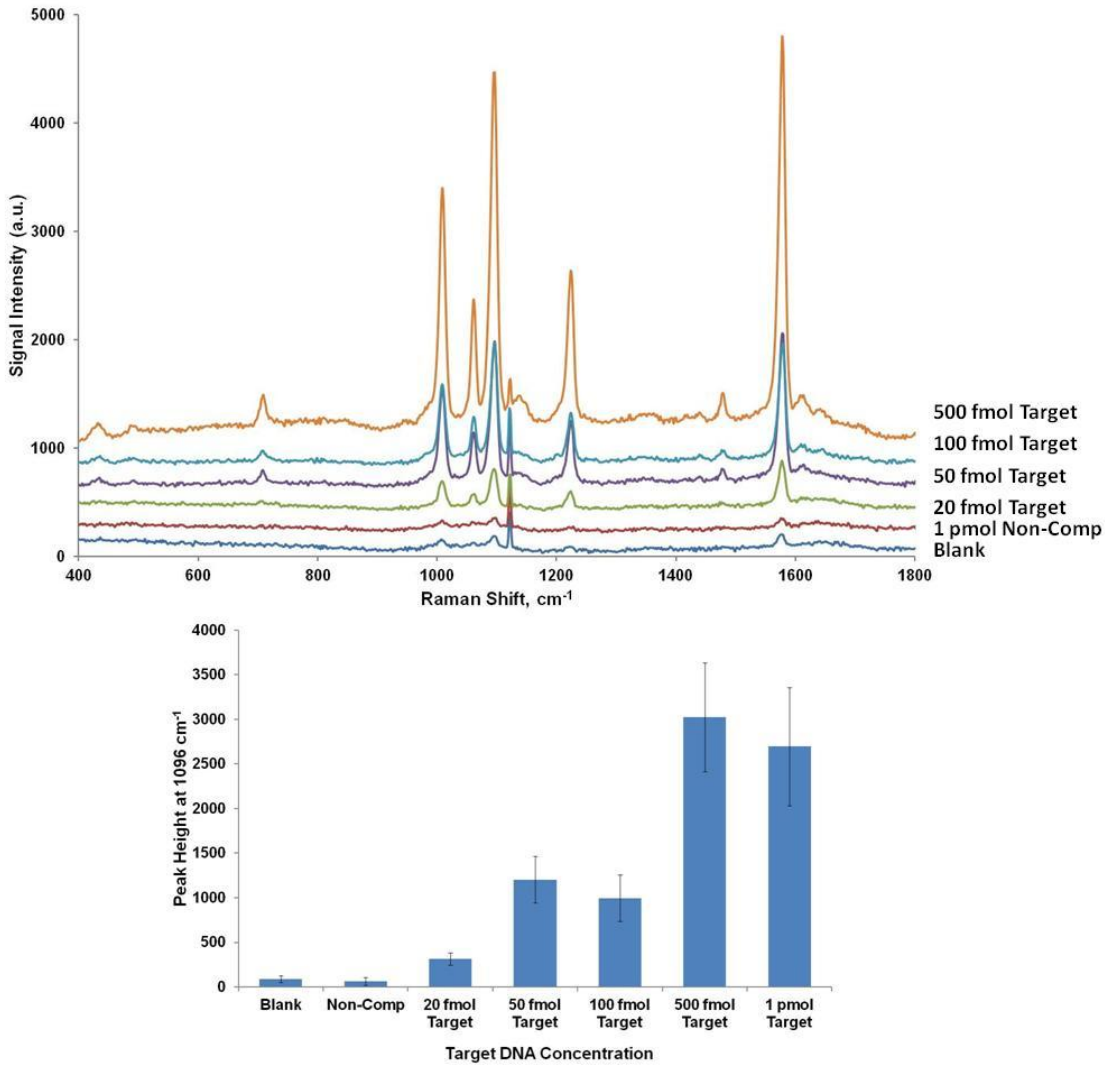

FIGURE 2.17: *Changes in 4-MP signal intensity for magnetic plug samples containing a range of synthetic KRU target concentrations, showing stacked averaged SERS spectra (top) and changes in the average peak height at 1096 cm^{-1} (bottom). Results shown are the mean average of triplicate measurements from each of two separate samples at each concentration, and error bars represent ± one standard deviation.*

Note that the SERS spectra for 4-MP shown in Figure 2.17 differs slightly from that shown in Figure 2.9. In particular, the peak at ~1004 cm^{-1} increases in intensity and the peaks at ~1250 cm^{-1} and 1604 cm^{-1} all but disappear when used within the nanoparticle assembly assay (Figure 2.17) compared with measurements of the dye directly on AgNPs (Figure 2.9). This is due to the different tautomeric forms that 4-MP adopts, which are very dependent on pH.[106]

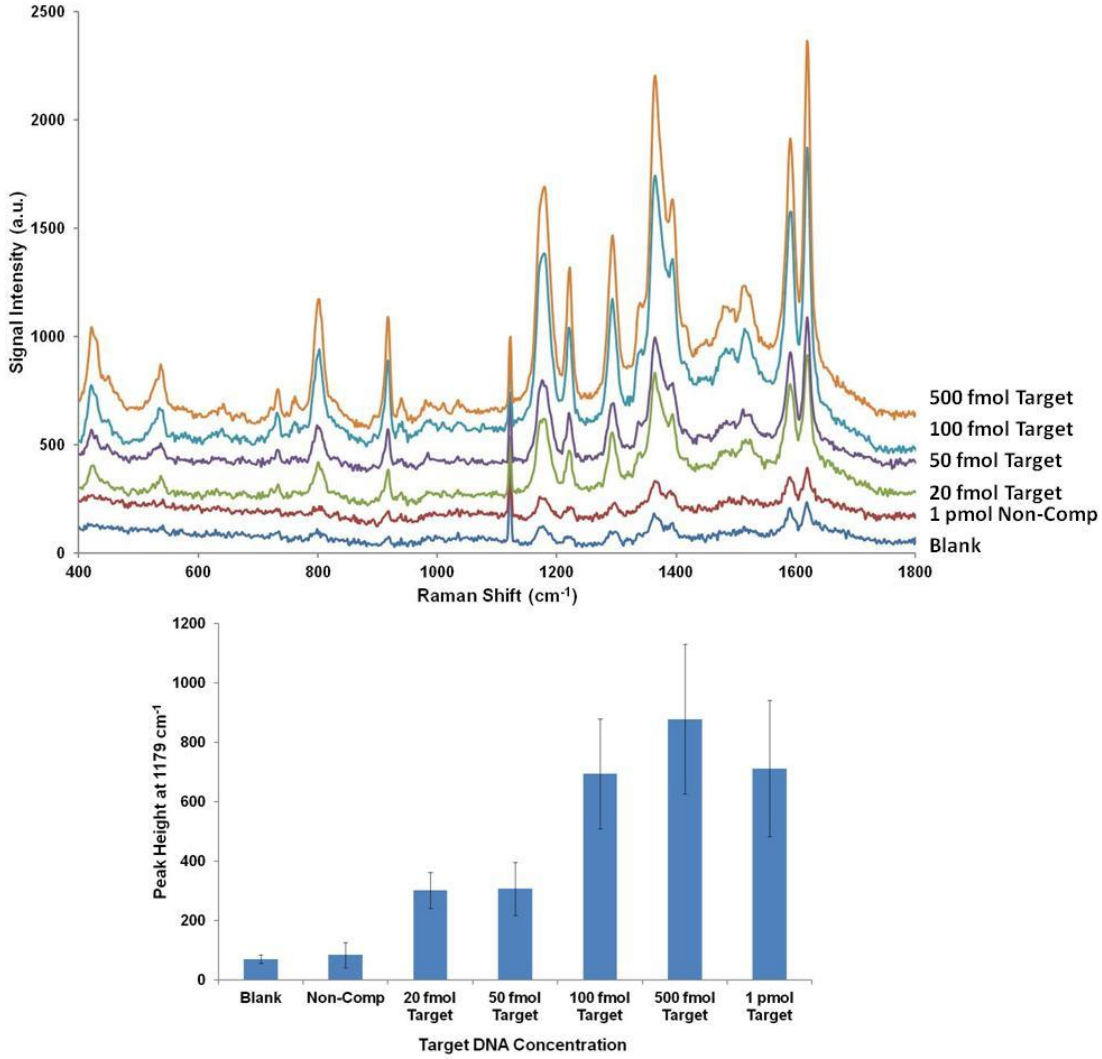

FIGURE 2.18: *Changes in MG.ITC signal intensity for magnetic plug samples containing a range of synthetic ALB target concentrations, showing stacked averaged SERS spectra (top) and changes in the average peak height at 1179 cm^{-1} (bottom). Results shown are the mean average of triplicate measurements from each of two separate samples at each concentration, and error bars represent ± one standard deviation.*

Each of the four Raman reporters has allowed a good level of discrimination between samples containing low concentrations of target DNA and samples containing no target, although in all cases the dye spectrum remains visibly present in blank samples. The intensity of these latter spectra could be reduced by using a lower ratio of Raman reporter to nanoparticles during conjugation, however this was at the expense of assay sensitivity.

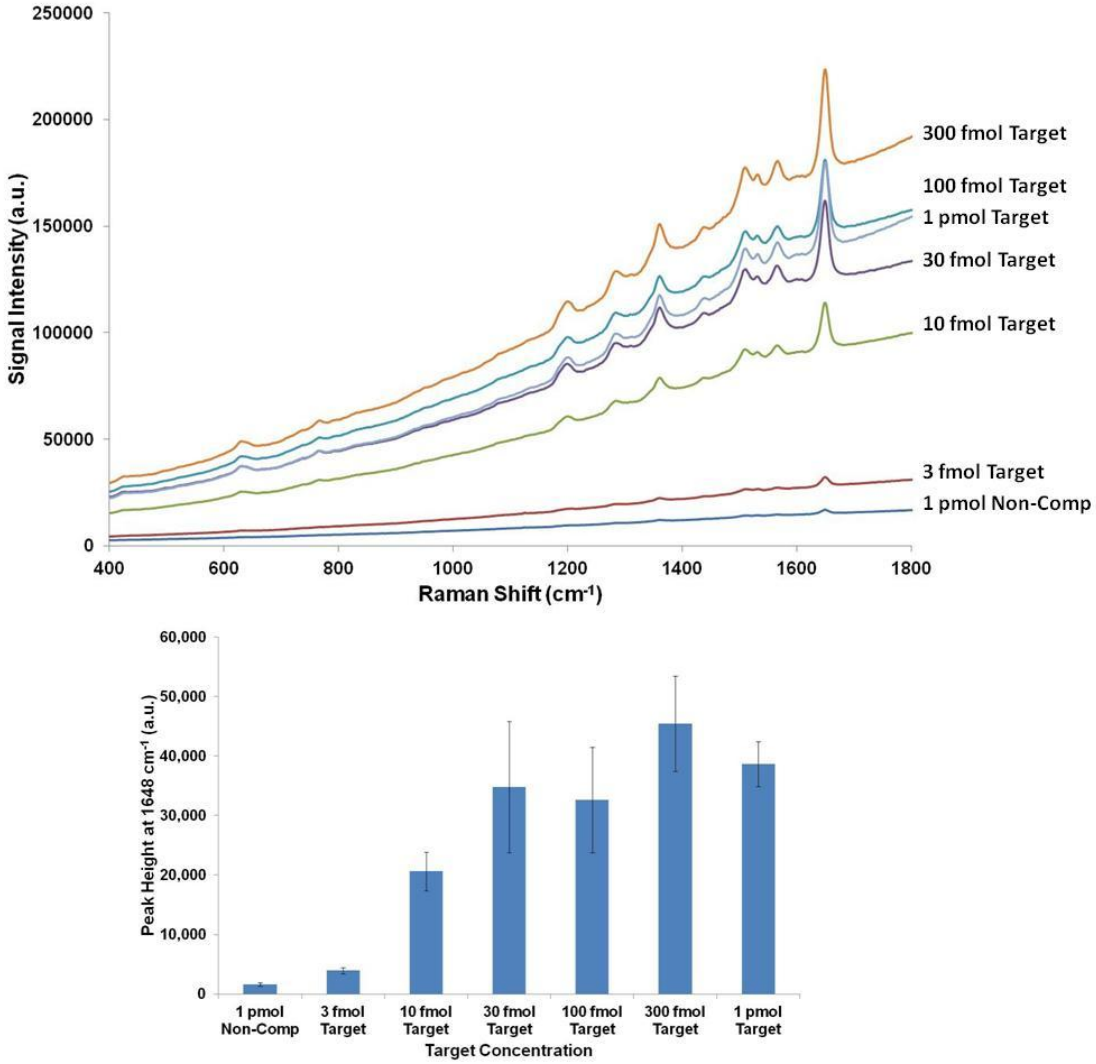

FIGURE 2.19: *Changes in RB.ITC signal intensity for magnetic plug samples containing a range of model target concentrations, showing averaged SERS spectra (top) and changes in the average peak height at 1648 cm^{-1} (bottom). Results shown are the mean average of triplicate measurements from each of two separate samples at each concentration, and error bars represent ± one standard deviation.*

The use of RB.ITC as a Raman reporter molecule resulted in much higher overall SERRS intensities than the other reporters, and this dye also allowed the highest level of discrimination between low concentrations of target and non-complementary DNA. However, the baseline of this dye was also much higher due to fluorescence, which led to difficulties when trying to multiplex with other Raman reporters with much lower baselines.

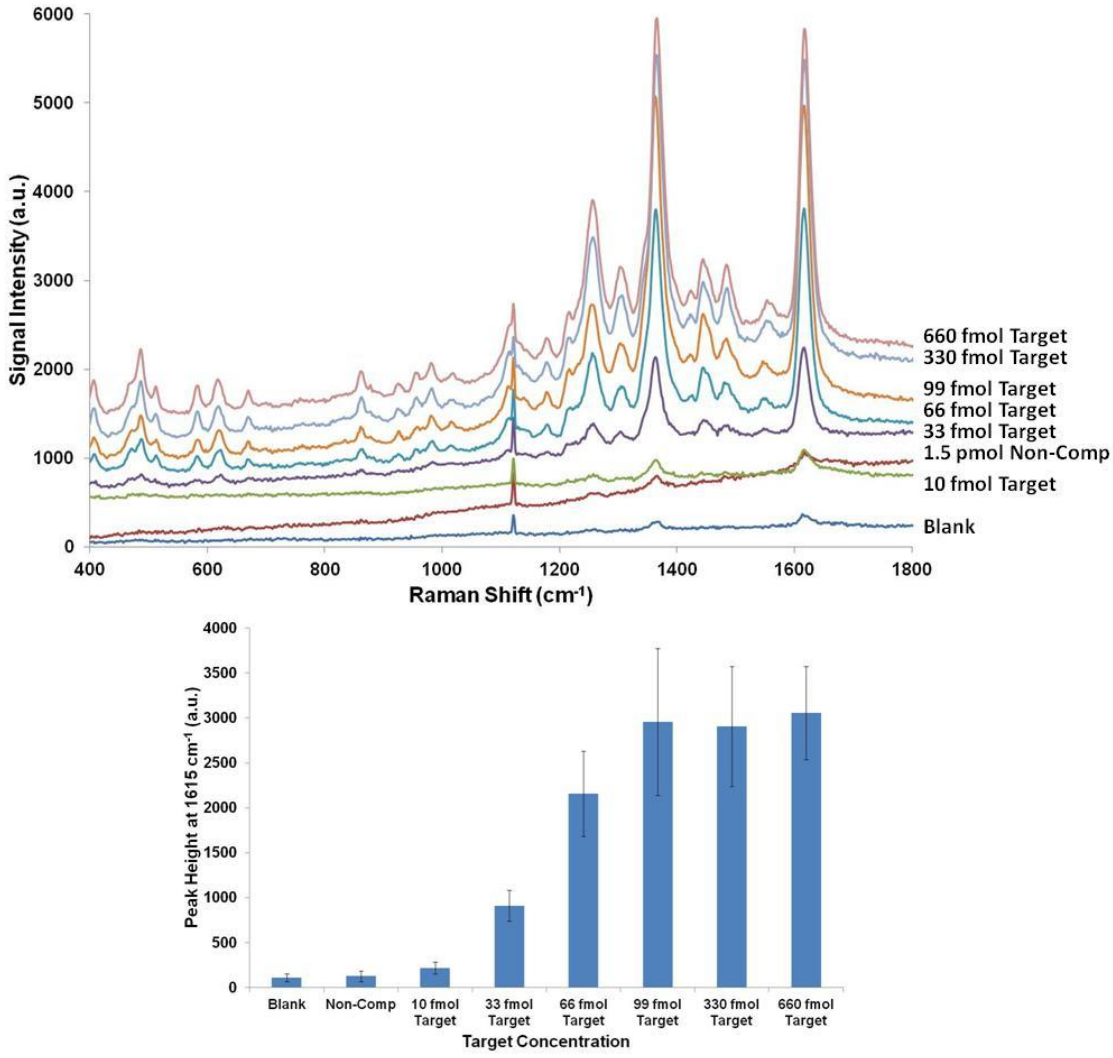

FIGURE 2.20: *Changes in RB1 signal intensity for magnetic plug samples containing a range of synthetic FUM target concentrations, showing stacked averaged SERS spectra (top) and changes in the average peak height at 1615 cm^{-1} (bottom). Results shown are the mean average of triplicate measurements from each of two separate samples at each concentration, and error bars represent ± one standard deviation.*

The multiplexing potential of SERS-based assays has been one of the driving factors in a number of studies dedicated to this technique in recent years.[111] In order to assess the functionality of the current assay in a duplex format, a new Ag@MNP-P2 conjugate was prepared containing an equal ratio of P2-ALB and P2-KRU oligonucleotide sequences, designated ALB/KRU-P2. Although not essential, having both probe sequences present on the same nanoparticle helps to minimise the

collection of excess MNPs that are not involved in any hybridisation event. Figure 2.21 shows the results for samples containing a combination of ALB-P1-MG, KRU-P1-MP and ALB/KRU-P2 conjugates in 0.3 M PBS, along with 100 fmol of either KRU or ALB synthetic target DNA. In the presence of ALB target, a strong SERS signal from MG was obtained, while in the presence of KRU target, a strong SERS signal from MP was obtained. While a low background level of reporter was observed in both samples, the presence of each of the target sequences can be clearly distinguished when present in this duplex format.

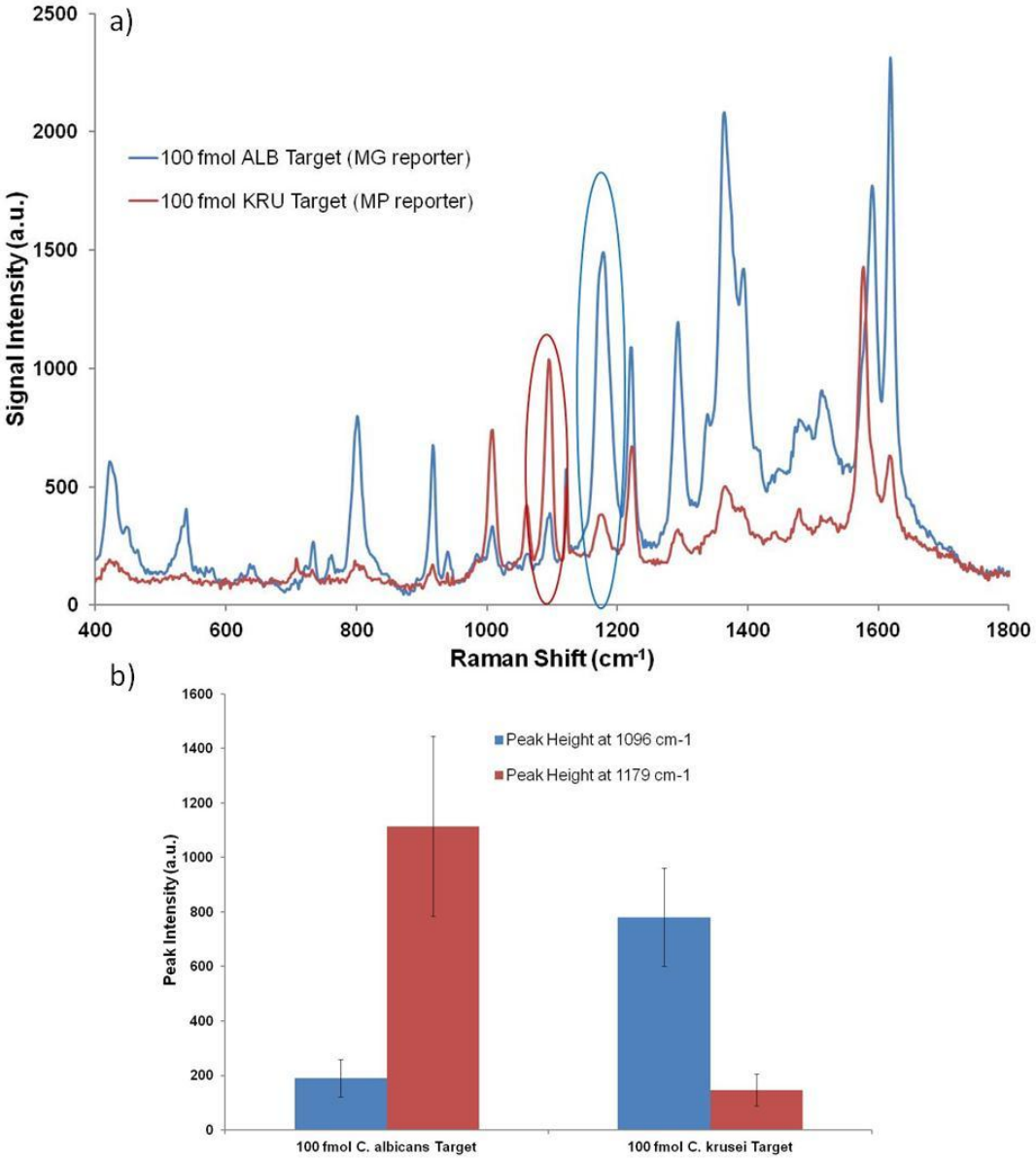

FIGURE 2.21: *Comparison of a) SERS spectra and b) signal intensity for peaks at 1096 cm^{-1} (relating to MP) and 1179 cm^{-1} (relating to MG), for samples containing 100 fmol of either KRU or ALB synthetic target DNA. NP probes relating to both targets are present in both samples. Results shown are the mean average of triplicate measurements from each of two separate samples for each target, and error bars represent ± one standard deviation.*

2.4 Assessment of Conjugate Stability

A study was carried out to assess how long the conjugates remained stable and functional when stored in buffer. The Probe 1 (P1) conjugates were prepared from hydroxylamine-reduced AgNPs using a 5000:1000:1 oligonucleotide:reporter:NP ratio. The Probe 2 (P2) conjugates were prepared using glucose-reduced Ag@MNPs and a 5000:1 oligonucleotide:NP ratio. 5'-thiol modified 12-base KRU probe sequences were used, such that a head-to-tail orientation resulted upon hybridisation with target. All conjugates were prepared following the standard fast, low pH method (see Experimental section) and stored in 10 mM phosphate buffer (pH 7.3) at approximately 4 °C.

Three different batches of conjugates were prepared in total. Batch 1 used MG.ITC as the Raman reporter, conjugated to AgNP-P1, and the conjugates were assessed over an 11-month period. Due to the results observed from these conjugates, a further two batches were subsequently prepared: batch 2 used RB1 as the Raman reporter, with assessment carried out over 6 months; batch 3 did not have any dye attached to P1, and was assessed over 5 months. Separate Ag@MNP-P2 conjugates were prepared alongside each batch of P1 conjugate.

All conjugates were first assessed within days of their preparation (0 months) then again at set periods of time following this. During assessment, conjugates were hybridised with either a 24-base synthetic KRU target sequence, or a 24-base non-complementary (non-comp) sequence.

2.4.1 Stability of Batch 1 Conjugates: MG.ITC Reporter

Figure 2.22 shows the SPR peaks for a 1:20 dilution of the individual AgNP-P1-MG.ITC and Ag@MNP-P2 conjugates in 0.3 M PBS, measured at 0 and 11 months from conjugate preparation. There is no difference in the λ_{max} and peak width of the conjugates, which indicates that there is no significant change in the size or composition of the nanoparticles throughout this period.

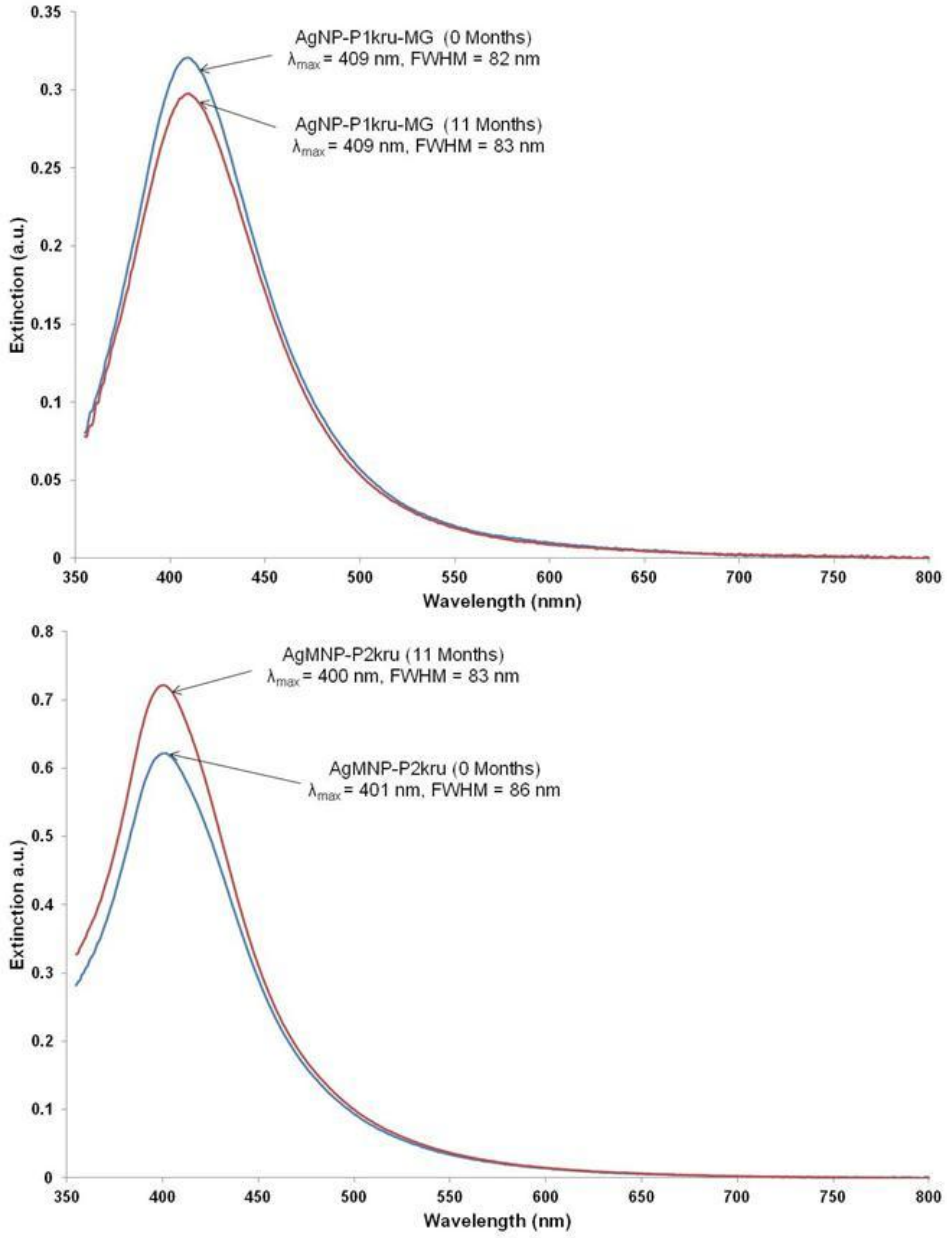

FIGURE 2.22: *Extinction spectra for a 1:20 dilution of the AgNP-P1-MG.ITC (top) and Ag@MNP-P2 (bottom) conjugates in 0.3 M PBS at 0 and 11 months since conjugate preparation.*

The functionality of the conjugates was assessed by measuring the SPR changes upon hybridisation of the P1 and P2 nanoparticle conjugates with a target sequence, as described earlier. Upon hybridisation with a 5 nM target sequence, the rate of nanoparticle assembly remained effectively unchanged for conjugates aged up to 6 months, however this rate was reduced for conjugates that were aged 9 months and

11 months (Figure 2.23). No nanoparticle assembly was observed for the sample containing a non-complementary sequence combined with 11 month-aged conjugates, highlighting the stability of these conjugates following an extended period of storage. Measurement of the melting transitions showed that the T_m remained unchanged throughout the 11 month period from conjugate preparation. For a sample containing 5 nM target, T_m = 48.7 ± 0.8 °C, and for a sample containing 1 nM target, T_m = 48.2 ± 1.2 °C.

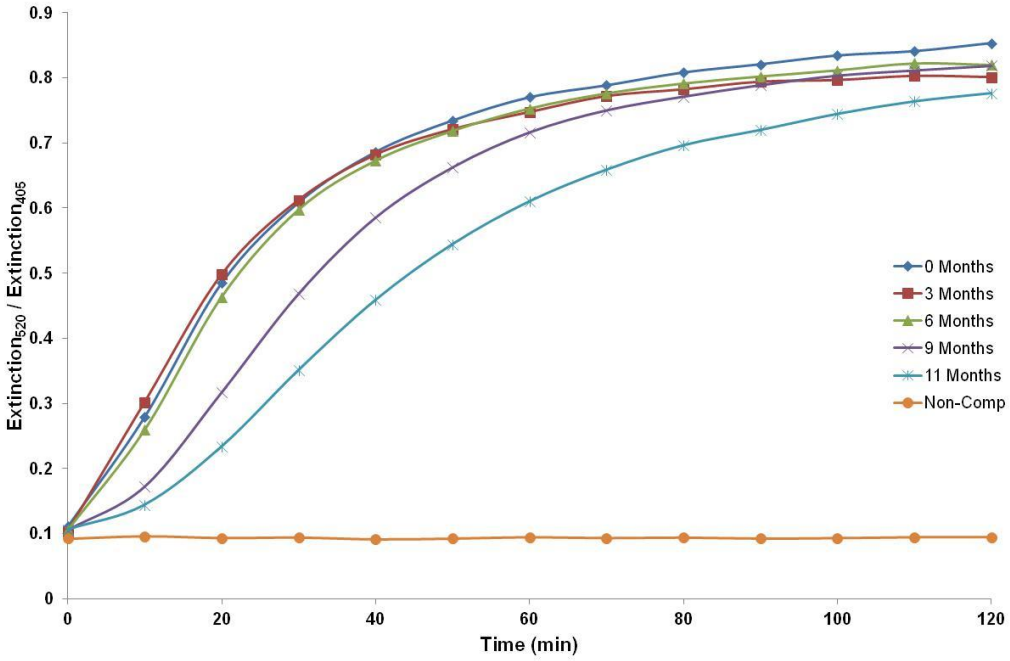

FIGURE 2.23: *Changes in nanoparticle assembly over a 2 h period for hybridisation of P1 and P2 conjugates (5 pM of each) with 5 nM Target in 0.3 M PBS buffer, using the same batch of P1/P2 conjugates at different periods of time following initial preparation (0 to 11 months). The Non-Comp sample uses conjugates that are aged 11 months. Results are for single samples.*

The SERS enhancement achieved with these conjugates was also compared over the 11 month period. This involved combining equal quantities of nanoparticle conjugate with either a target (100 fmol or 20 fmol) or non-complementary sequence (1 pmol) in 0.3 M PBS in an Eppendorf tube for one hour at room temperature, then transferring to a capillary tube and collecting on top of a magnet, rinsing with 1 mL

PBS and measuring the SERS signal of the magnetic plug of material (514 nm excitation). 3 measurements were taken of each sample and duplicate samples of each type were prepared. All data was normalised based on the signal intensity of a standard silicon wafer (peak at 520 cm^{-1}) measured at each time period.

The average spectra obtained for samples containing 100 fmol of target or no target (i.e. blank) at 0 and 11 months from conjugate preparation are shown in Figure 2.24. These results show a reduction in MG.ITC signal intensity for the target samples and an increase in intensity for the blank samples over this time period. A more detailed assessment of the results obtained throughout this period is provided in Figure 2.25, which compares changes in the height of the peak at 1588 cm^{-1} for samples with and without target DNA (error bars represent ± one standard deviation). The numerical value shown above each column is a measure of the level of discrimination between the target sample and the blank sample at that particular time period. These results highlight a decline in discrimination between target and blank samples for both the 100 fmol and 20 fmol target samples even for conjugates that are aged just 1 month. After 6 months there is no longer any discrimination between a 20 fmol target and a blank sample, while for a 100 fmol target sample, the level of discrimination has reduced more than 10-fold.

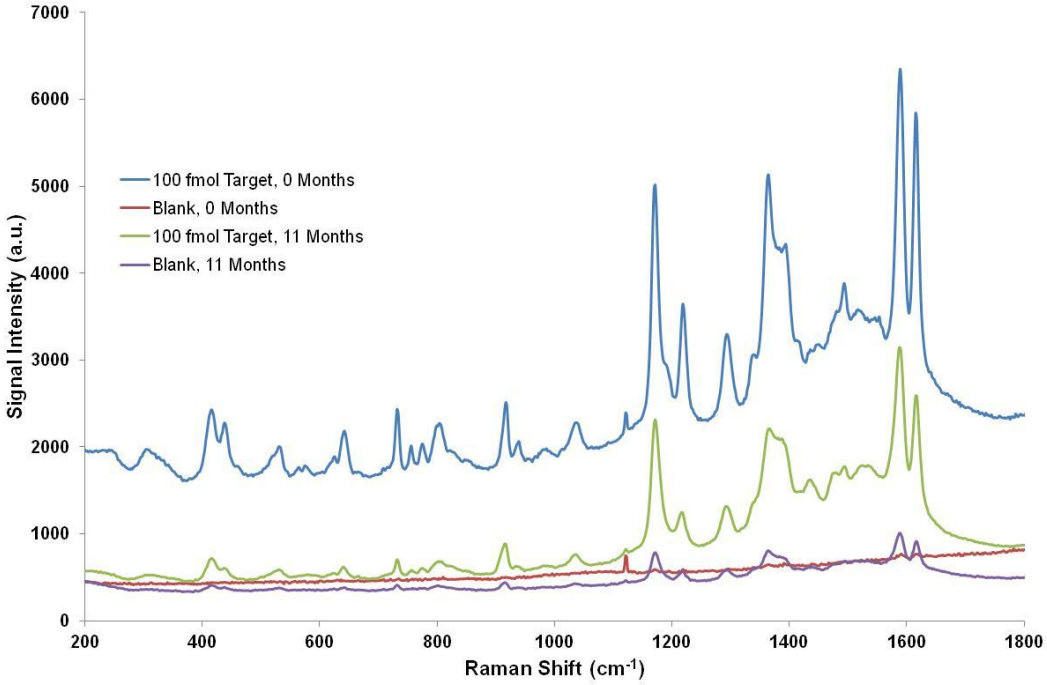

FIGURE 2.24: *Average uncorrected MG.ITC SERS spectra for samples containing 100 fmol target or no target (blank) collected 0 months and 11 months from the time of conjugate preparation. Results shown for each sample type are the mean average of triplicate measurements from each of two separate samples.*

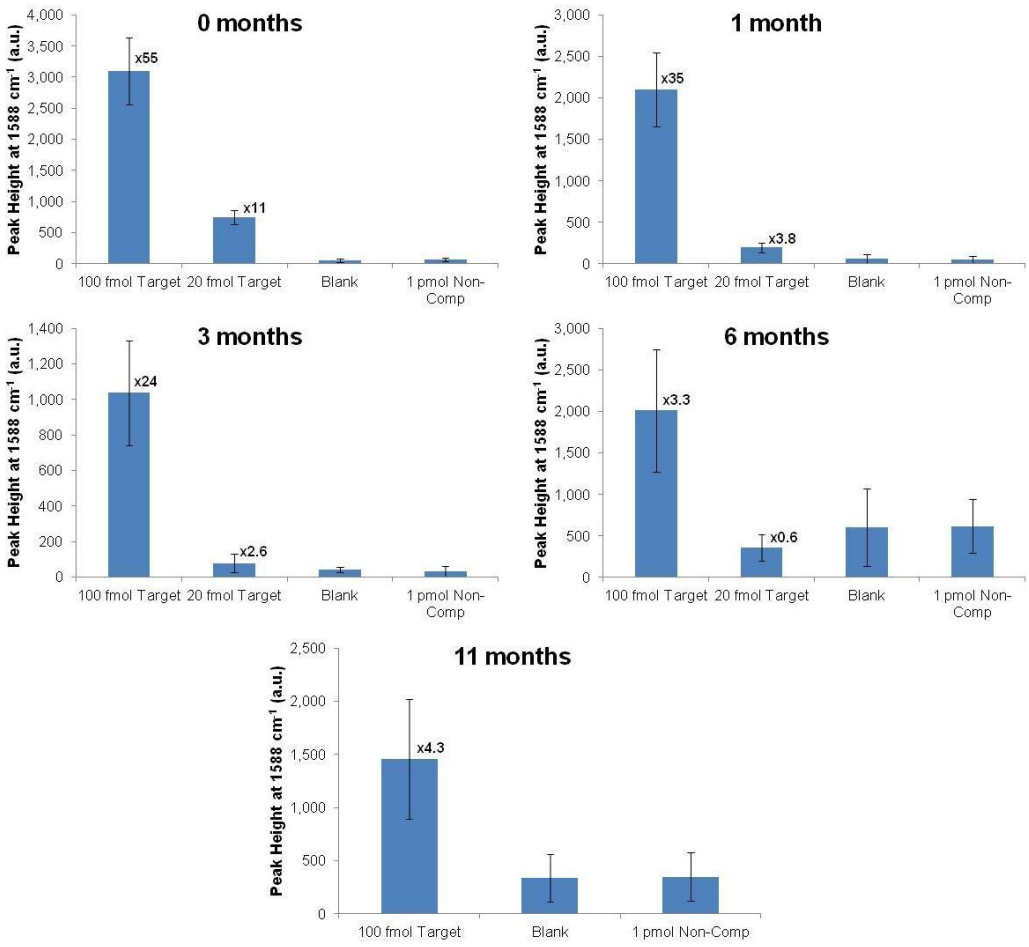

FIGURE 2.25: *Differences in MG.ITC signal intensity, measured as changes in average peak height at 1588 cm^{-1}, for samples containing target or non-comp DNA (or blank samples containing conjugates and buffer only), using conjugates aged from 0 to 11 months. Results shown for each sample type are the mean average of triplicate measurements from each of two separate samples, and error bars represent ± one standard deviation. Values above each target column refer to the level of discrimination vs. the blank sample from the same time period.*

2.4.2 Stability of Batch 2 Conjugates: RB1 Reporter

Given the changes in SERS intensities observed over time for the MG.ITC conjugates, a further set of conjugates was prepared using RB1 as the Raman reporter to determine if these same effects were observed. The average spectra obtained for a sample containing 100 fmol of target or no target (i.e. blank) at 0 and 6 months from conjugate preparation is shown in Figure 2.26. These results show a reduction in RB1 signal intensity for the target samples but no increase in intensity

for the blank samples over this time period. Figure 2.27 compares changes in the peak height at 1618 cm^{-1}, with values above each column again representing the level of discrimination between target and blank samples at that particular time period. These results show an initial reduction in target signal intensity and hence discrimination after 1 month, however no further reduction is noted up to a period of 6 months from conjugate preparation.

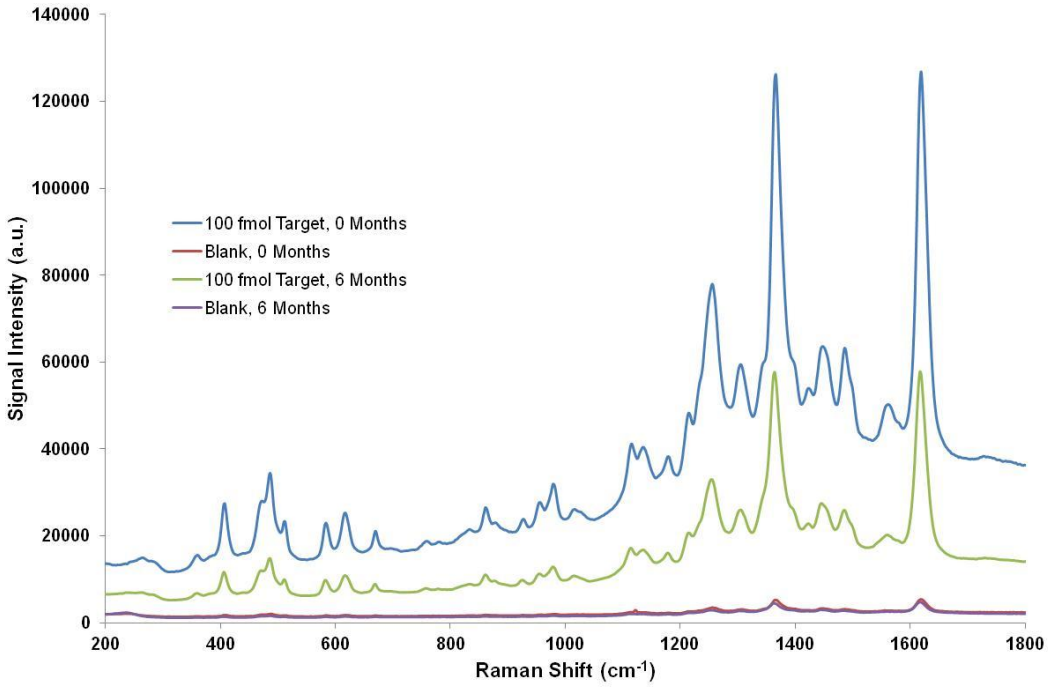

FIGURE 2.26: *Average uncorrected RB1 SERS spectra for samples containing 100 fmol target or no target (blank) collected 0 months and 6 months from the time of conjugate preparation. Results shown for each sample type are the mean average of triplicate measurements from each of two separate samples.*

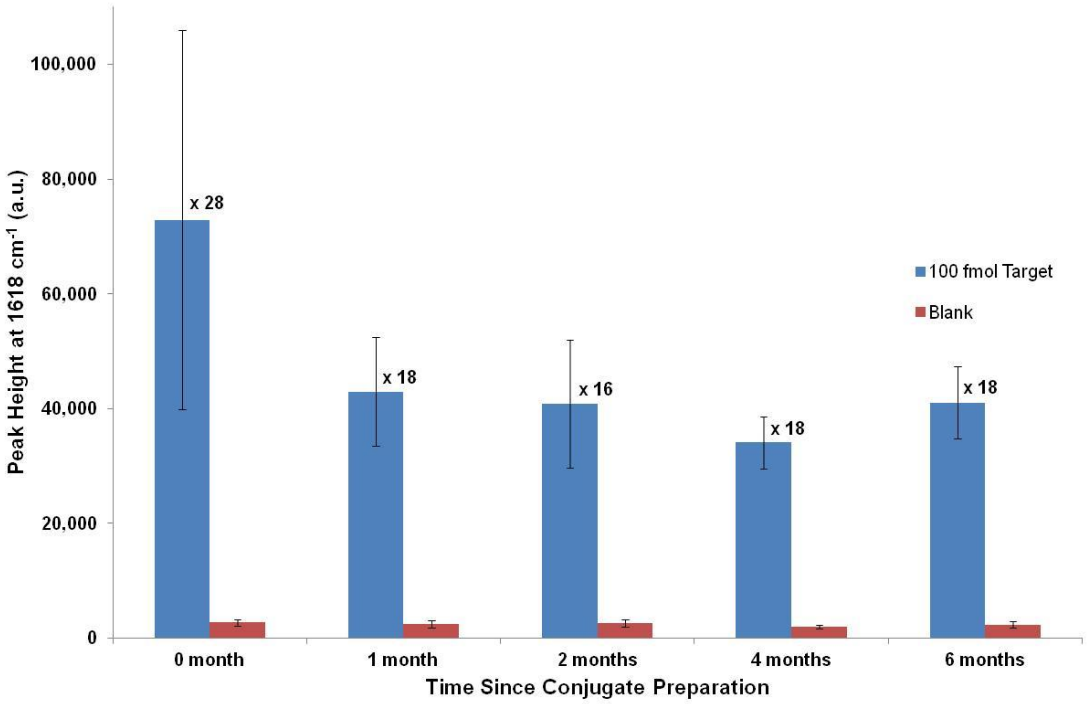

FIGURE 2.27: *Differences in RB1 signal intensity, measured as changes in average peak height at 1618 cm^{-1}, for samples containing 100 fmol target or blank samples (containing conjugates and buffer only), using conjugates aged from 0 to 6 months. Results shown for each sample type are the mean average of triplicate measurements from each of two separate samples, and error bars represent ± one standard deviation. Values above each target column refer to the level of discrimination vs. the blank sample from the same time period.*

For these conjugates, there was also a slight reduction in hybridisation rate after 6 months when mixed with 5 nM target and no observed instability in the sample containing a non-complementary sequence. The T_m value remained unchanged throughout the 6 month period since conjugate preparation, with a value of 56.6 ± 1.3 °C for a sample containing 5 nM target.

2.4.3 Stability of Batch 3 Conjugates: No Raman Reporter

These conjugates were prepared in order to assess hybridisation with lower concentrations of target. Figure 2.28 shows a summary of the nanoparticle assembly rates for these conjugates when newly prepared and after 5 months. For hybridisation with both 1 nM and 500 pM target, there is a reduction in nanoparticle assembly rate

for the older conjugates, although again there is no obvious instability in the blank sample using conjugates aged 5 months. The melting temperature remained unchanged throughout the 5 month period since conjugate preparation, with a value of 55.5 ± 0.4 °C for a sample containing 1 nM target, and 54.9 ± 0.8 °C for a sample containing 500 pM target.

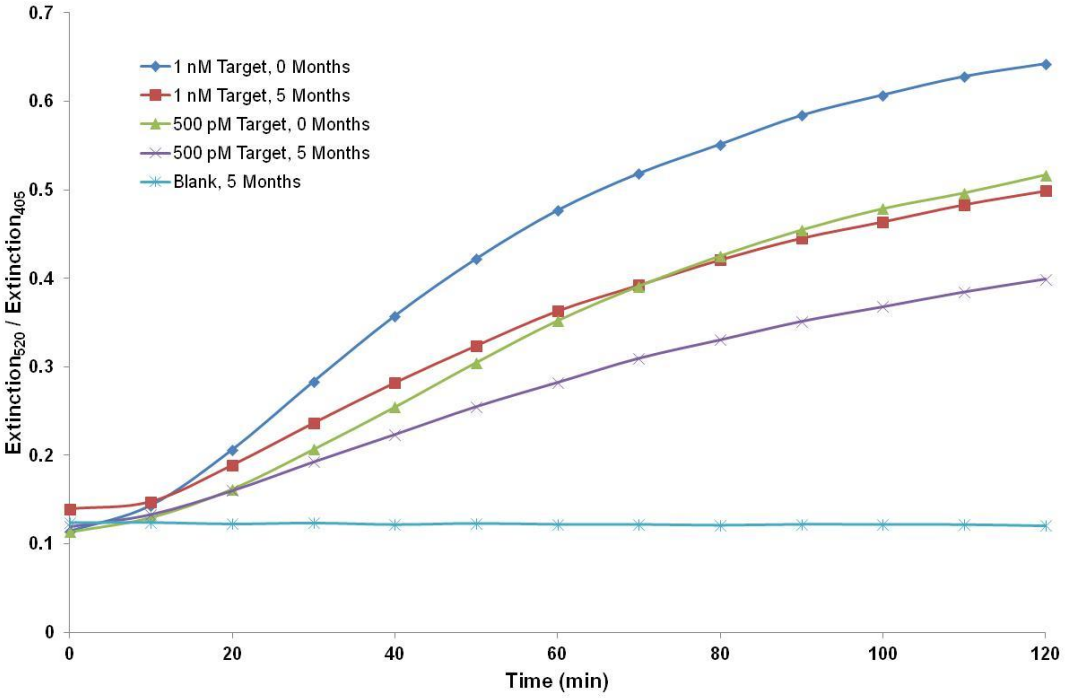

FIGURE 2.28: *Changes in nanoparticle assembly over a 2 h period for hybridisation of a combination of P1 and P2 conjugates (5 pM of each) with either 1 nM or 500 pM target DNA in 0.3 M PBS buffer, using the same batch of P1/P2 conjugates one day after preparation (0 months) then again after 5 months. The blank sample uses conjugates that are aged 5 months. Results shown are the average values from two different samples of each type.*

2.4.4 Summary of Stability Study

For all of the conjugates, a reduction in hybridisation rate was observed as the conjugates aged, although even after 11 months there was a good degree of hybridisation with 5 nM target. There was no measurable change in nanoparticle size throughout this period for either the P1 or P2 conjugates, and a mixture of conjugates in hybridisation buffer without any target showed no signs of aggregation, indicating

that a large proportion of the oligonucleotide probe strands remained on the nanoparticles throughout the 11 month period. Bhatt *et al.* studied the dissociation of thiolated DNA from gold nanoparticle surfaces, and found that high pH, high salt concentration, and high temperatures led to an increased level of DNA dissociation over time.[112] They found that the rate of dissociation was significantly reduced for conjugates stored at 4 °C, although not prevented completely. It seems likely therefore that the reduction in hybridisation rate over time for the conjugates is due to the gradual dissociation of the thiolated probe DNA from the AgNP/Ag@MNP surfaces during storage. These dissociated probe DNA strands are likely to hybridise with target DNA, effectively reducing the concentration of target available to hybridise with the nanoparticle conjugates, thus leading to a reduction in the rate and extent of nanoparticle assembly. As noted, the conjugates are stored at ~ 4 °C in a salt-free buffer, conditions that were intentionally chosen in order to minimise the dissociation of probe DNA from the nanoparticle surfaces.

An interesting point from this stability study is the variation in melting temperature between the batches of conjugates. The T_m values for batch 2 and 3 conjugates are similar to each other but ~ 7-8 °C higher than those for the batch 1 conjugates. Note that the batch 2 and batch 3 conjugates were prepared using the same AgNPs and Ag@MNPs, and these were different from the nanoparticles used to make the batch 1 conjugates. Figures 2.29 and 2.30 show the SPR peaks for each of the conjugates from the three batches. There is no significant difference in the SPR value or the width of the peak (as indicated by the full width at half height, FWHM, value) for the AgNP-P1 conjugates, indicating that they are of a similar average size and monodispersity. However, for the Ag@MNP-P2 conjugates, the SPR peak width is larger for the batch 1 conjugates, indicating a higher proportion of larger nanoparticles in this batch. Jin *et al.* demonstrated that larger nanoparticles result in reduced melting temperatures, while a higher density of probe DNA on the nanoparticle surface resulted in an increase in T_m.[42] All of the P2 conjugates were prepared at the same oligonucleotide:NP ratio, therefore the slightly larger size of the batch 1 nanoparticles could mean a slightly reduced density of oligonucleotide strands on their surface, and these combined effects could explain the observed

differences in T_m values between the conjugate batches. As mentioned, there was no measurable change in melting temperature within any of the conjugate batches over time when hybridised with target DNA, which further supports the conclusion that the majority of probe DNA strands remain attached to the nanoparticle surface during storage, since any significant reduction in probe density would be expected to result in a reduction in melting temperature.

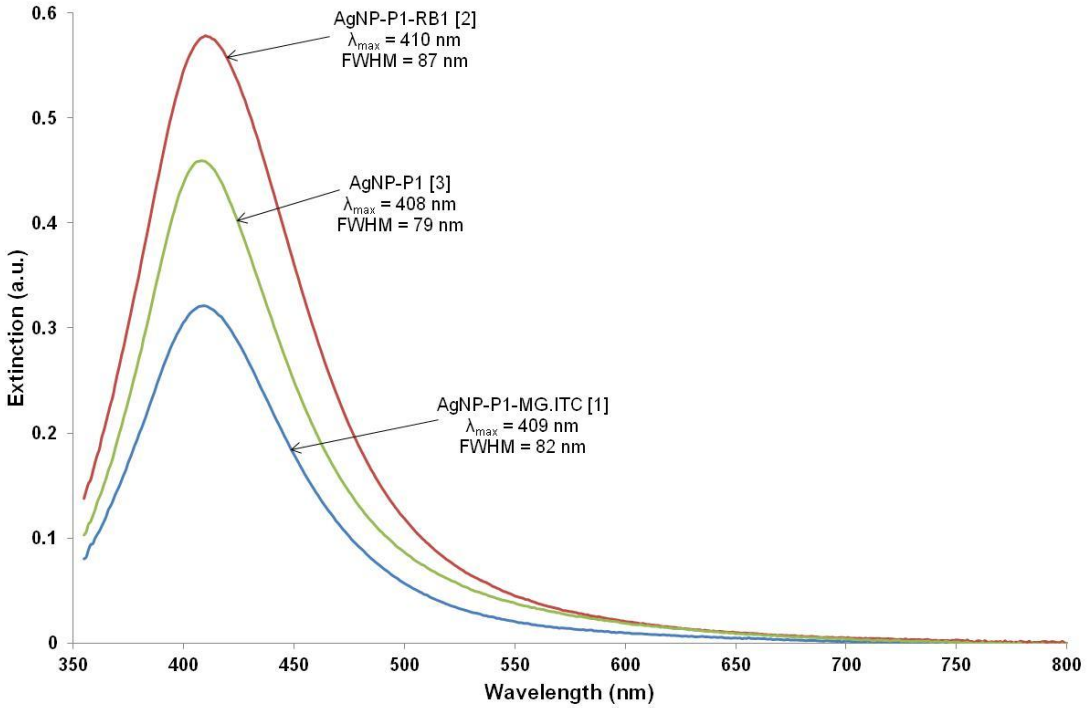

FIGURE 2.29: *Extinction spectra for three different batches of AgNP-P1 conjugates, all as 1:20 dilutions in 0.3 M PBS buffer*

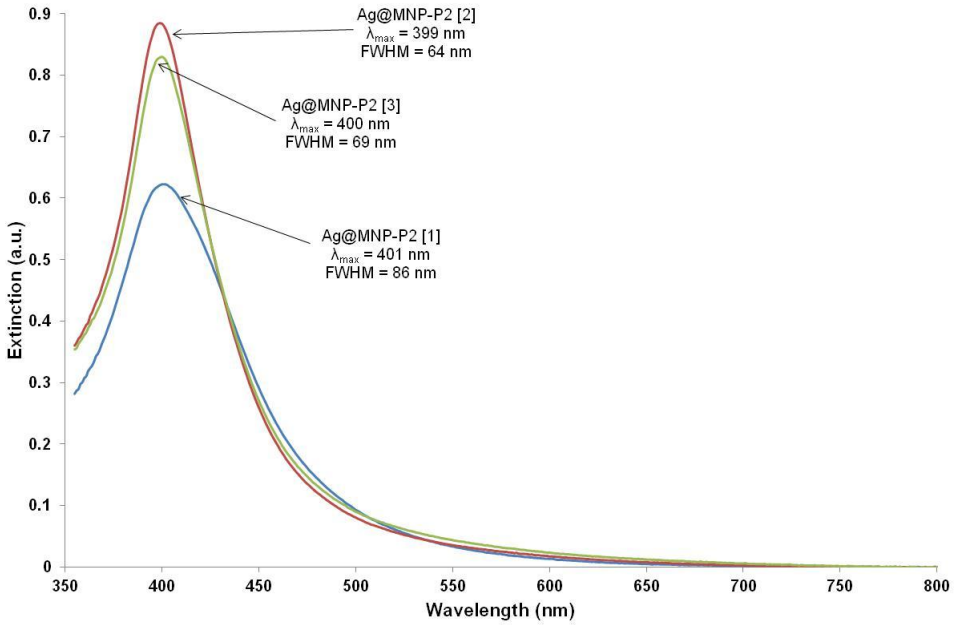

FIGURE 2.30: *Extinction spectra for three different batches of Ag@MNP-P2 conjugates, all as 1:20 dilutions in 0.3 M PBS buffer*

The use of MG.ITC as Raman reporter resulted in a significant reduction in discrimination between target and blank samples over 6 months, due to a combination of reduced signal intensity from the target samples and an increase in dye signal from the blank sample. As explained above, there is a reduction in hybridisation rate as the conjugates age due to detachment of some oligonucleotide strands during storage, which could partly explain the reduction in SERS signal for the target samples. In addition, any detachment of dye from the AgNP-P1 surface during storage could result in a reduction in signal intensity for target samples, as well as an increase in dye signal for blank samples due to attachment of free dye to the Ag@MNP-P2 surface during hybridisation.

For the conjugates using RB1 as reporter, there was no increase in signal intensity for the blank sample over the 6 month period, and hence the reduction in discrimination was much less severe. This could indicate that the benzotriazole-Ag bond is stronger than the isothiocyanate-Ag bond, resulting in less detachment of RB1 from the AgNP surface during storage compared with MG.ITC.

2.5 Summary of Assay Development

A stable assay with potential for molecular diagnostics has been developed, which combines the high sensitivity of SERS detection with the benefits of magnetic manipulation. Sensitive individual detection of four different synthetic DNA sequences was demonstrated, using four different Raman reporters, with typically ≤ 20 fmol of target being detected at > 3:1 level of discrimination compared with a blank sample. This highlights the flexibility of the assay, which has the ability to be adapted for use with a wide range of different target sequences. The assay was also shown to work in a duplexed format, i.e. using the same conjugates to detect the presence of either of two different target sequences. Some issues exist regarding background SERS levels of the Raman reporter which are observed in non-target samples, however clear discrimination is obtained at low target concentrations in both the individual and duplexed formats.

The stability of the nanoparticle-bound probes was investigated over an 11-month period. The probes remained stable and functional throughout this period when stored in 10 mM phosphate buffer in a refrigerator, although there was some displacement of both the thiolated oligonucleotide probe sequences and the Raman reporter over time. This was sufficient to affect the detection of low levels of target, although a good level of hybridisation and SERS enhancement was possible with higher target concentrations even after 11 months of conjugate storage.

This research represents the first combination of DNA-functionalised AgNPs and Ag@MNPs in a sandwich assay for DNA detection by SERS. All of the data in this chapter are based on the detection of 24-base synthetic target sequences, however the robust molecular recognition provided demonstrates the potential for further development of the assay to allow target DNA detection within a complex clinical sample matrix. This will rely on the ability of the assay to detect much longer DNA sequences, the presence of which can have a significant impact on nanoparticle assembly as discussed in detail in the following chapter.

CHAPTER 3: Investigation of Silver Nanoparticle Assembly Following Hybridisation with Different Lengths of DNA

Sections of the text and some figures used throughout this chapter have previously been published[113] and are reproduced by permission of John Wiley and Sons.

3.1 Introduction to Hybridisation Kinetics Study

A key factor when developing a successful nanoparticle assembly assay is achieving rapid and efficient hybridisation between the functionalised nanoparticles and target DNA. A number of factors are known to affect the rate of this controlled aggregation, such as concentration and length of the target sequence,[110] hybridisation temperature and hybridisation buffer,[42, 49] and the position of the probe hybridisation region within target DNA.[114] Methods have been developed to increase the hybridisation efficiency, such as the use of 'short internal complement' DNA[115] and the use of spacers between the nanoparticle and probe DNA sequence to reduce steric hindrance between neighbouring oligonucleotide strands.[45, 55, 57, 98]

The choice of hybridisation buffer is an important consideration in any molecular diagnostic assay, since the negative phosphate backbone on DNA requires charge screening between the probe and target oligonucleotides. Jin *et al.* found that the hybridisation rate was directly proportional to the salt concentration used in a gold nanoparticle sandwich assay, with no hybridisation taking place at sodium chloride concentrations less than 0.05 M.[42] The use of higher sodium chloride concentrations to achieve more rapid hybridisation between target and probe DNA was also demonstrated in the previous chapter (Figure 2.13). Buffers containing polymers have also been used to improve the efficiency of DNA hybridisation, with dextran sulfate shown to accelerate the hybridisation between probe DNA and a 281 base pair (bp) target PCR fragment in a gold nanoparticle assembly assay.[49] More recently, polyethylene glycol (PEG) was also shown to enhance DNA hybridisation to functionalised gold nanoparticles.[116]

During assay development, short lengths of synthetic target DNA are often used to assess the functioning and stability of the assay, with similar short lengths of probe DNA used to exactly match this, for instance two 12-mer probes with a 24-mer target[43, 55] or two 15-mer probes with a 30-mer target.[42] Indeed, the results detailed in Chapter 2 of this thesis all relate to the use of two 12-mer probes hybridised to a fully complementary 24-mer target. However, for the detection of clinically relevant DNA, the target sequence is likely to be much longer than the combined length of the probe DNA sequences, which may have a significant effect on the formation of the nanoparticle assemblies. Smith *et al.* investigated the effects of changing the length of the linker DNA on the kinetics of assembly and the melting transitions of a gold nanoparticle assembly assay.[110] Two 12-mer probe sequences were used throughout, while the target sequence was altered by adding non-hybridising bases either to the centre of the target DNA (i.e. as 'gaps') or to each end of the hybridising portion of the target DNA (i.e. as 'overhangs'). In both cases, the nanoparticle assembly process was found to be slower and the melting temperature decreased as more nucleotides were present, either as gaps or overhangs.[110] The effects of increasing the length of linker DNA as a means of increasing the distance between the nanoparticles following the assembly process has also been investigated, establishing that the rate of nanoparticle assembly was reduced as the length of linker DNA was increased both for gold[43] and silver[68] nanoparticles. In each of these examples, the length of probe DNA has remained constant while the linker DNA length has increased by adding bases that are not involved in hybridisation with probe DNA. The work detailed in this chapter seeks to assess the effects of both longer target and longer probe DNA sequences on the nanoparticle assembly process.

This chapter investigates the DNA-directed assembly of oligonucleotide-functionalised silver nanoparticles, with the aim of identifying the parameters that will maximise the efficiency of hybridisation with long target sequences, including probe length, orientation and hybridisation buffer effects. This is investigated by measuring the surface plasmon resonance changes that result from the near-field coupling of the nanoparticles during the assembly process. The aim of this work is to

contribute towards further development of the assay described in the previous chapter, to ultimately allow detection of clinically relevant samples of target DNA.

3.2 Probe and Target Sequences used to Investigate Hybridisation Effects

In order to determine the effects on the nanoparticle assembly process of varying the length and orientation of probe DNA, a range of oligonucleotide-functionalised silver nanoparticles were prepared using probe sequences of varying lengths. A thiol tether was attached to the 3' or 5' end of the oligonucleotide sequence such that the nanoparticles were arranged in either a 'head-to-tail' or a 'tail-to-tail' orientation upon hybridisation with target DNA. The number of bases on each probe was varied between 12 and 30, allowing ten different probe combinations to be compared; 3 in a head-to-tail and 7 in a tail-to-tail configuration (Figure 3.1). All probe sequences were attached to hydroxylamine-reduced silver nanoparticles; no magnetic nanoparticles were used throughout this section of work.

Four different lengths of target DNA sequence were assessed, consisting of 24, 48, 96 or 144 nucleotides in total ($Target_{24}$, $Target_{48}$, $Target_{96}$ and $Target_{144}$, respectively). Full details of the probe and target sequences used are shown in Table 3.1. In all cases, the combined probe sequence was exactly complementary to a central section of the target DNA, with no gaps. For all of the experiments in this chapter, each was carried out in duplicate under the same conditions; all graphs show the average of the two samples.

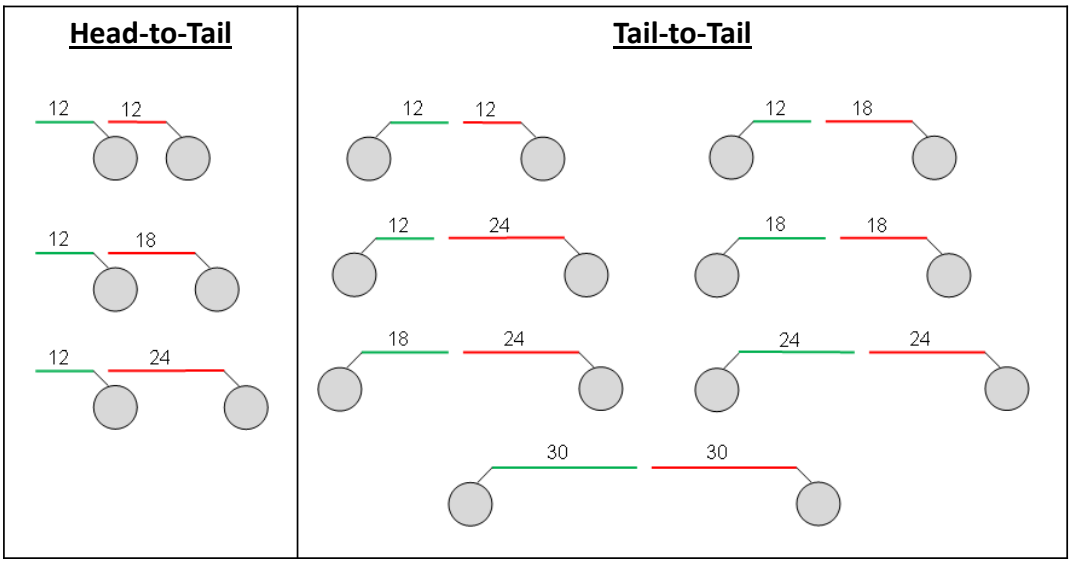

FIGURE 3.1: *Schematic representation of various combinations of different lengths of nanoparticle-bound probe DNA, showing the orientation that they would adopt (either head-to-tail or tail-to-tail) upon hybridisation with target DNA. P1 DNA is shown in red; P2 DNA is shown in green. All probe sequences are shown in a 3' to 5' direction.*

The target sequences are all specific for the fungal species *Candida krusei*. In assay development, synthetic target DNA sequences are chosen for use because they appear in a section of the PCR-amplified DNA fragment of interest. As the PCR DNA is double stranded (dsDNA), the target region may be selected to be on either one of these complementary strands. The 24-base KRU target sequence that was detailed in Chapter 2 relates to a section of DNA on one of the *C. krusei* PCR strands, while the targets that are used in this chapter relate to a section of DNA on the opposite PCR strand; the targets used here are designated as 'KRU_{mir}' to clarify this. Further detail on this is provided in the next chapter, when PCR detection is discussed.

TABLE 3.1: *Details of the different probe and target DNA sequences used to assess hybridisation kinetics, where $(HEG)_3$ denotes three hexaethylene glycol units (used as a spacer between the nanoparticle and the probe sequence)*

Probe/Target	Sequence (all 5' – 3')
$5'\text{-}P1_{12}$	HS-$(HEG)_3$- TCA AAG TAA TCG
$3'\text{-}P2_{12}$	TCC TGG TTC GCC -$(HEG)_3$-SH
$5'\text{-}P2_{12}$	HS-$(HEG)_3$- TCC TGG TTC GCC
$5'\text{-}P1_{18}$	HS-$(HEG)_3$- ATT TCC TCA AAG TAA TCG
$3'\text{-}P2_{18}$	TCC TGG TTC GCC CGA GGC -$(HEG)_3$-SH
$5'\text{-}P1_{24}$	HS-$(HEG)_3$- ACT CTA ATT TCC TCA AAG TAA TCG
$3'\text{-}P2_{24}$	TCC TGG TTC GCC CGA GGC TAG CCA -$(HEG)_3$-SH
$5'\text{-}P1_{30}$	HS-$(HEG)_3$- TTG AAC ACT CTA ATT TCC TCA AAG TAA TCG
$3'\text{-}P2_{30}$	TCC TGG TTC GCC CGA GGC TAG CCA GAA GGA -$(HEG)_3$-SH
$Target_{24}$	GGC GAA CCA GGA CGA TTA CTT TGA
$Target_{48}$	TGG CTA GCC TCG GGC GAA CCA GGA CGA TTA CTT TGA GGA AAT TAG AGT
$Target_{96}$	CTG TTG CGG CCG GGT CTT TCC TTC TGG CTA GCC TCG GGC GAA CCA GGA CGA TTA CTT TGA GGA AAT TAG AGT GTT CAA AGC AGG CCT TTG CTC GGA
$Target_{144}$	CGG ACG GTC TAC CTA TGG TAA GCA CTG TTG CGG CCG GGT CTT TCC TTC TGG CTA GCC TCG GGC GAA CCA GGA CGA TTA CTT TGA GGA AAT TAG AGT GTT CAA AGC AGG CCT TTG CTC GGA TAT ATT AGC ATG GAA TAA TAG AAT

3.3 Effects of Target Length on Hybridisation Kinetics

When two solid spherical metallic nanoparticles are brought into close proximity, coupling of the surface plasmons leads to a red-shift in the SPR peak. The extent of the shift is distance dependent, with an approximately exponential decrease in the extent of the red-shift with increasing nanoparticle separation, and no interaction when the distance between the nanoparticles is greater than 2.5 times their diameter.[52, 117] For the DNA-directed assembly of functionalised silver nanoparticles,

changes in the formation of the nanoparticle assemblies under different assay conditions were measured by plotting the ratio of the extinction peak height of the red-shifted assemblies over that of the individual nanoparticles, i.e. extinction$_{530}$ / extinction$_{410}$ as a function of time following addition of the target DNA (see Figure 3.2). The data shown relates to two 12-mer probes, hybridised with 24-base target DNA (Target$_{24}$) in a 'head-to-tail' orientation in 0.3 M PBS buffer. In this case, the red-shifted peak is very broad as it incorporates nanoparticle clusters of a range of different sizes due to the non-uniform nature of the assembly process.[68] When nanostructures become very large, multiple excitations are possible in addition to the dipole excitations of small nanoparticles, leading to the broadening of the LSPR peak and the appearance of a peak at higher wavelength.[30]

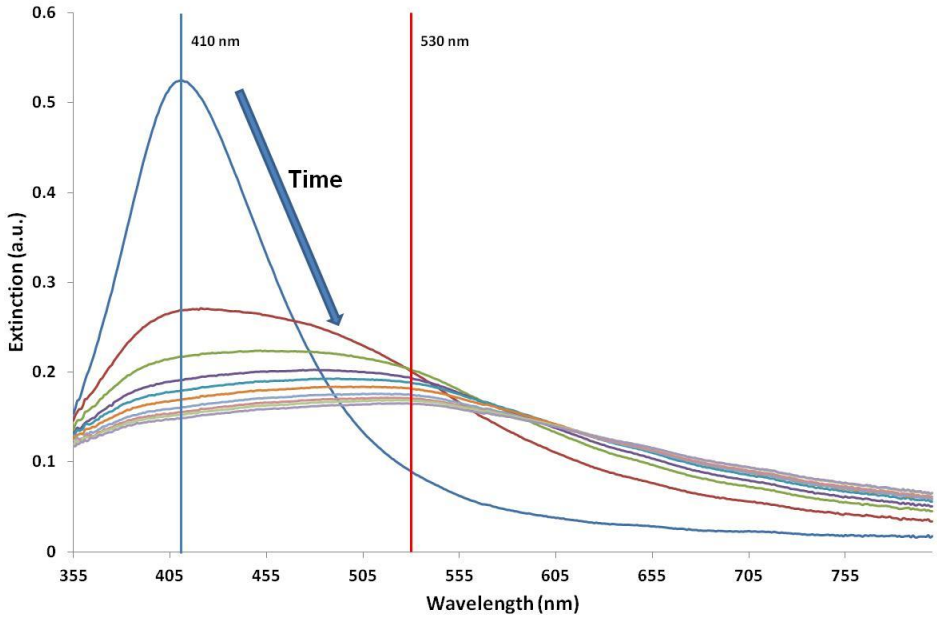

FIGURE 3.2: *Changes in extinction spectra over a 90 min period, showing spectra collected every 10 min following addition of 5 nM Target$_{24}$ to a solution of 10 pM P1 + 10 pM P2 conjugates in 0.3 M PBS buffer. The data relates to two 12-mer probes in a head-to-tail orientation. Results are for a single sample.*

The data in Figure 3.2 relates to a short length of synthetic DNA that exactly matches the combined length of the probe DNA, i.e. a 24-mer target with two 12-mer probes. In order to assess the functioning of the assay with longer DNA strands, target lengths of 48, 96 and 144-bases were added to the same conjugates using the same

experimental conditions (10 pM of each conjugate with 5 nM target in 0.3 M PBS buffer, hybridisations carried out at 25 °C over a 90 min period). In all cases the target length was extended by an equal number of nucleotides on each side such that the hybridising region remained in the centre (Figure 3.3a).

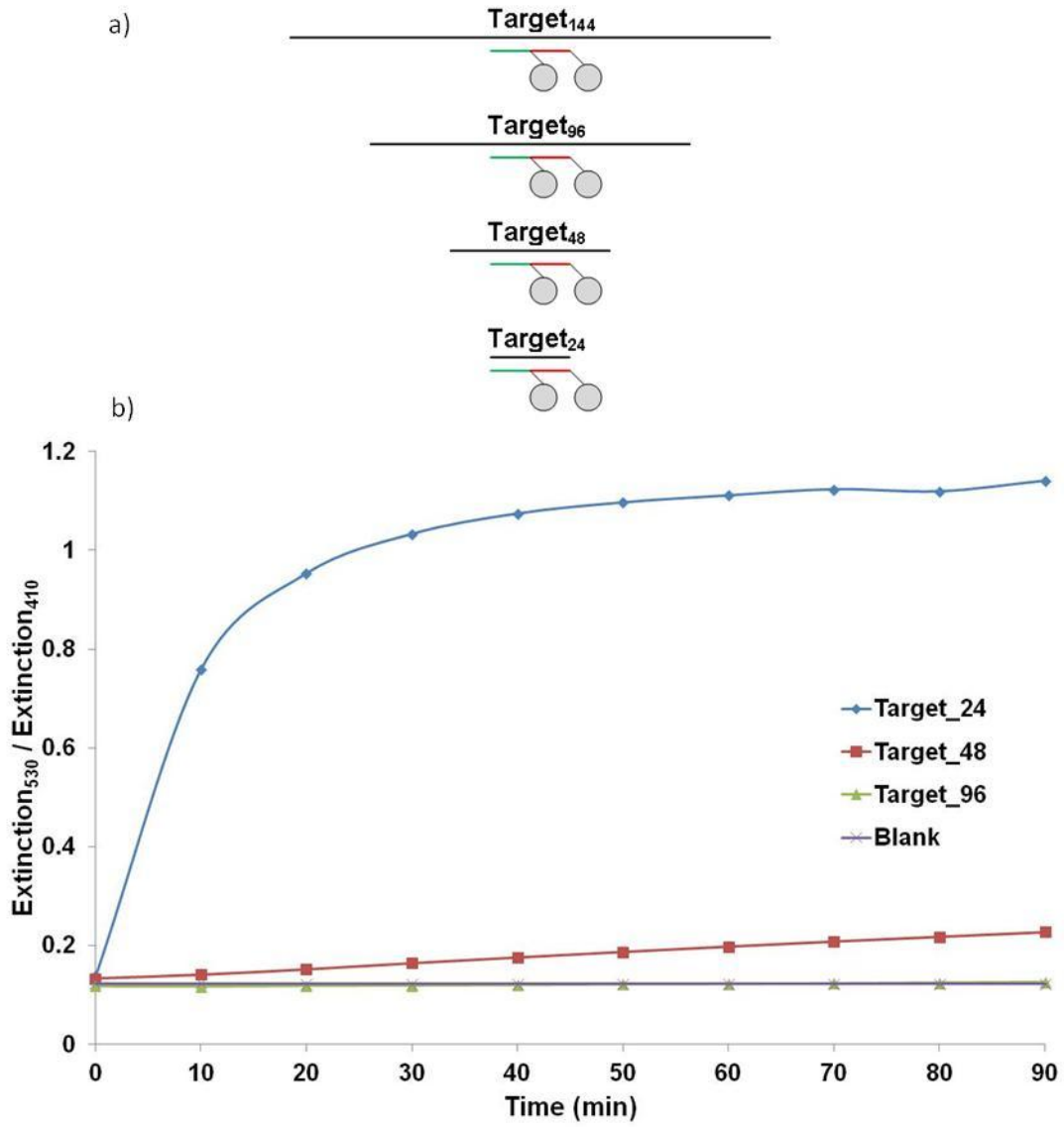

FIGURE 3.3: *a) Schematic showing the scale of different lengths of target DNA sequence against two 12-mer probes in a head-to-tail orientation; b) Changes in aggregation over a 90 min period following addition of 5 nM of three different lengths of target DNA to a solution of 10 pM P1 + 10 pM P2 conjugates in 0.3 M PBS buffer (blank samples contain no target); probes used are 12-12 head-to-tail. Results shown are the average values from two different samples of each type.*

Doubling the length of the target DNA from 24 to 48 bases was shown to significantly reduce the rate and extent of hybridisation with the 12-mer probes, as noted by a reduced change in the extinction profile over time (Figure 3.3b). Increasing the length further to 96 bases resulted in no obvious hybridisation within the 90 min analysis period (green line in Figure 3.3b, sitting directly underneath the purple 'blank' line). Results for $Target_{144}$ are not shown but are the same as for $Target_{96}$, i.e. there was no indication of hybridisation. These results are in agreement with those reported by Smith *et al.* in which 'overhangs' were found to reduce the rate of hybridisation in the assembly of DNA-functionalised gold nanoparticles,[110] and shows that the same effect is observed for silver nanoparticle assemblies.

The reduction in the rate of hybridisation with increasing target length is likely to be due to a combination of factors including the slower diffusion rate of the longer targets in the hybridisation buffer,[43] steric hindrance from the long strands that may limit the extent of hybridisation possible between neighbouring nanoparticles,[43] electrostatic repulsion between the non-hybridising bases on the longer targets and probe DNA on the nanoparticles,[110] and potential secondary structure formations for the long target sequences. The dramatic reduction in hybridisation efficiency with increasing target length could have significant implications for the use of nanoparticle assembly assays for detection of DNA in biological samples.[110]

3.4 Effects of Buffer on Hybridisation Kinetics

Changes were made to the hybridisation buffer to try to improve the efficiency of hybridisation of the functionalised silver nanoparticles with long strands of target DNA. Increasing the salt concentration is known to improve the rate of hybridisation between probe and target DNA by screening the charges from the DNA phosphate backbone to allow complementary strands to get close enough to hybridise.[42] For this current assay, when the buffer was changed from 0.3 M PBS to 1 M PBS (i.e. 10 mM phosphate buffer with either 0.3 M or 1 M NaCl), some hybridisation was observed

between $Target_{144}$ and two 12-mer probes, although the overall rate and extent of hybridisation was somewhat limited (see Figure 3.4). The salt concentration cannot be increased much higher than this or the nanoparticles become unstable and aggregate non-specifically (data not shown).

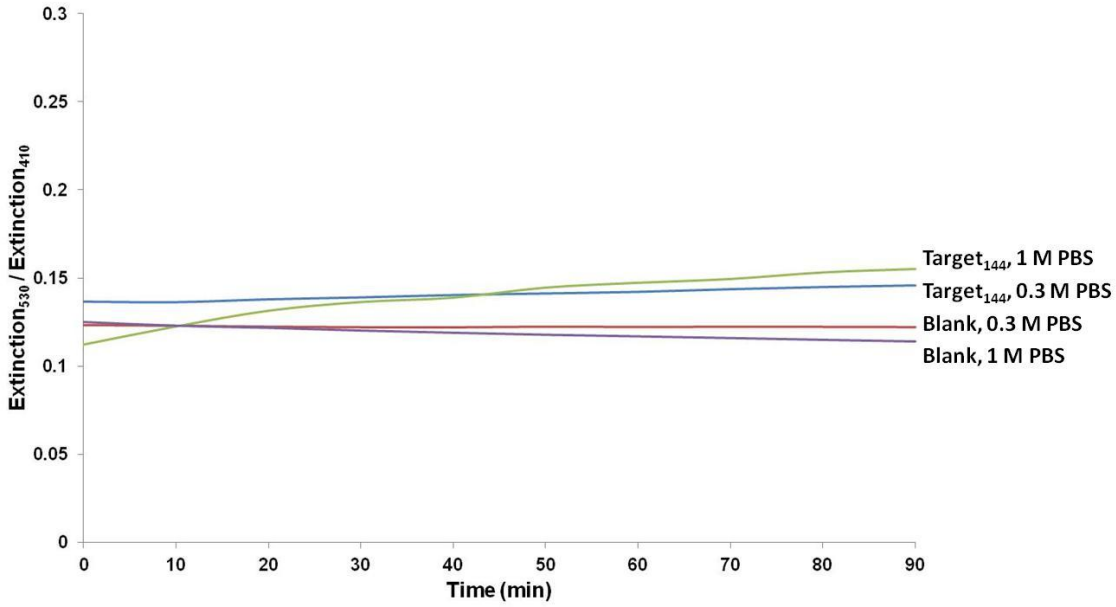

FIGURE 3.4: *Changes in aggregation over a 90 min period following addition of 5 nM $Target_{144}$ to a solution of 10 pM P1 + 10 pM P2 conjugates in either 0.3 M PBS or 1 M PBS buffer (blank samples contain no target); probes used are 12-12 head-to-tail. Results shown are the average values from two different samples of each type.*

To further improve the hybridisation kinetics with long targets, dextran sulfate was added to the buffer as this has been reported to increase the hybridisation rate of two DNA strands due to its volume excluding effect.[118] This polymer was also used to successfully increase the rate of hybridisation of long target DNA with oligonucleotide-functionalised gold nanoparticles,[49] although there appear to be no reports of its previous use in a silver nanoparticle assembly assay. In this current assay, the use of 5% w/v dextran sulfate in 0.3 M PBS buffer was found to significantly enhance the rate and extent of hybridisation of long targets (Figure 3.5) compared with hybridisation in 0.3 M PBS alone (Figure 3.3). In both cases, all other parameters were kept equal (conjugates, concentrations and temperature) with the

addition of the polymer to the buffer being the only point of difference. These results highlight the importance of using such an additive to allow a sufficient level of hybridisation with lengths of DNA that are more likely to be present in biological samples. The stability of the nanoparticle probes in this buffer, an important consideration in any nanoparticle assay, can be seen from the unchanging results for the blank sample (i.e. conjugates and buffer only).

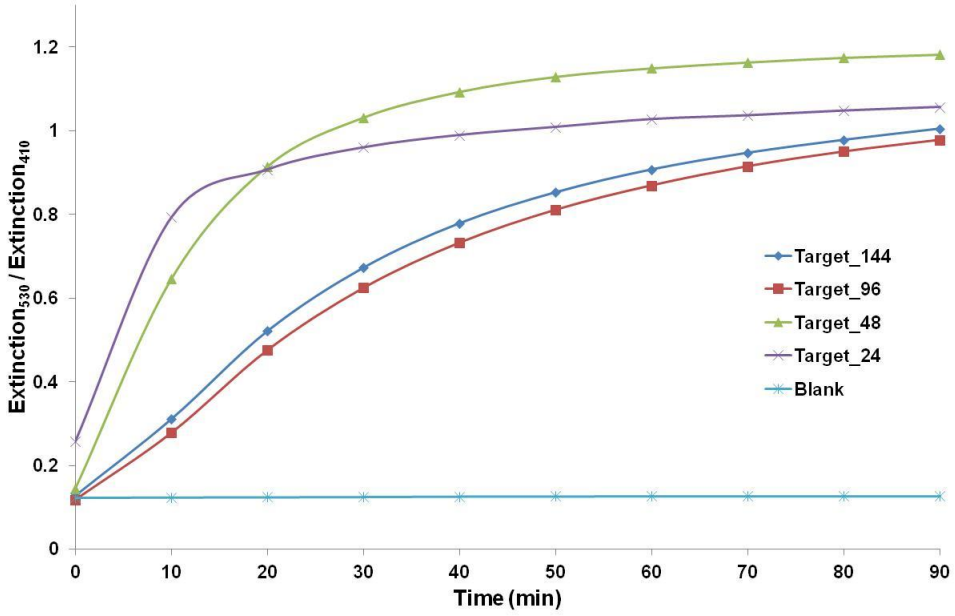

FIGURE 3.5: *Changes in aggregation over a 90 min period following addition of 5 nM of four different lengths of target DNA to a solution of 10 pM P1 + 10 pM P2 conjugates in 5% dextran sulfate/0.3 M PBS buffer (blank samples contain no target); probes used are 12-12 head-to-tail. Results shown are the average values from two different samples of each type.*

Hybridisation of $Target_{144}$ with the 12-mer probes was compared for 3 different concentrations of dextran sulfate (3%, 5% and 7% w/v, all in 0.3 M PBS), which showed that the rate increased with the concentration of polymer (see Figure 3.6). However, some instability was also observed for the blank sample in the 7% dextran buffer, indicating that there may be some non-specific hybridisation taking place between the probe DNA strands, or increased nanoparticle interaction as the nanoparticles are forced into closer proximity.

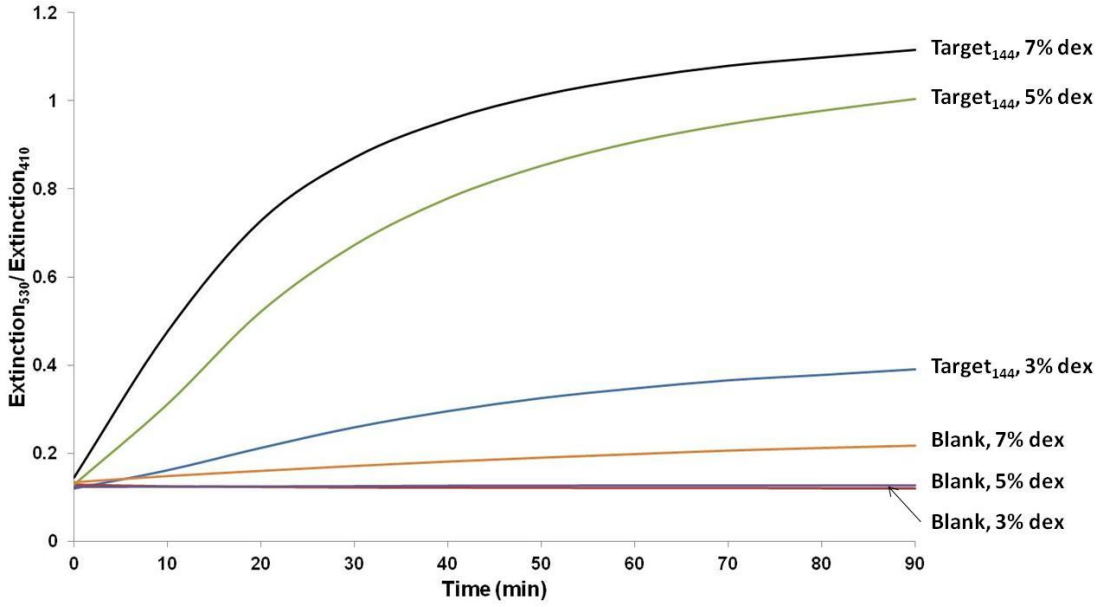

FIGURE 3.6: *Changes in aggregation over a 90 min period following addition of 5 nM Target$_{144}$ to a solution of 10 pM P1 + 10 pM P2 conjugates in either 3%, 5% or 7% dextran sulfate in 0.3 M PBS buffer ['dex'] (blank samples contain no target); probes used are 12-12 head-to-tail. Results shown are the average values from two different samples of each type.*

Similar comparisons were also carried out using polyethylene glycol (PEG) 10,000 in place of dextran sulfate as this has also previously been shown to increase the kinetics of hybridisation in a gold nanoparticle assembly assay,[116] although again there appear to be no reports of its use in a silver nanoparticle assay. PEG 10,000 was shown to produce very similar results to the dextran sulfate, with the rate of hybridisation and probe instability increasing with increasing PEG concentration (see Figure 3.7). PEG 2,000 in 0.3 M PBS buffer was also investigated but gave a significantly reduced level of hybridisation with Target$_{144}$ compared to the equivalent PEG 10,000 buffer (data not shown).

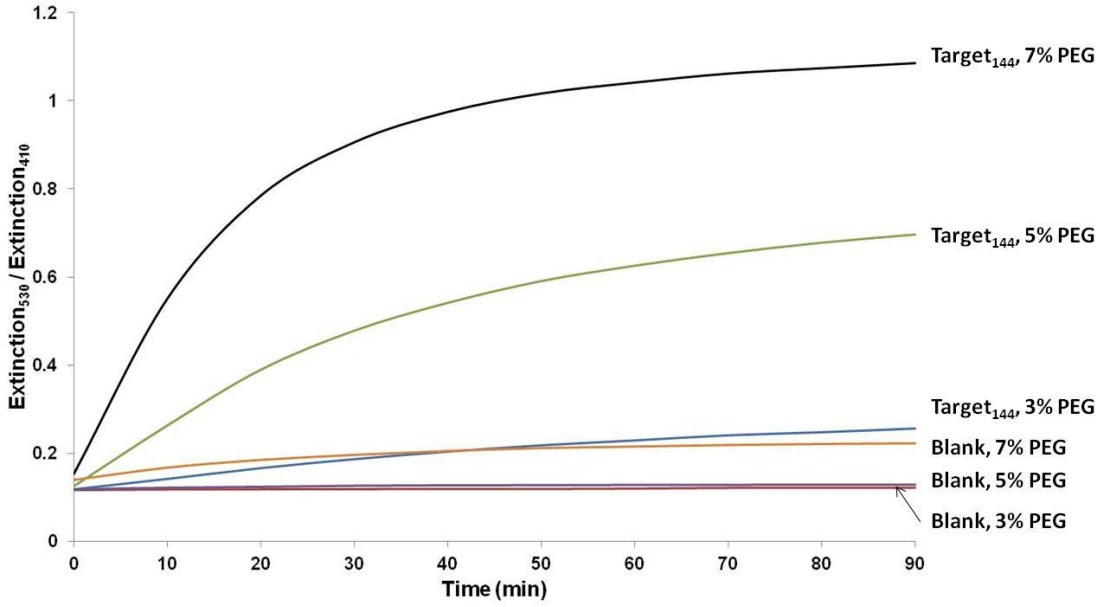

FIGURE 3.7: *Changes in aggregation over a 90 min period following addition of 5 nM Target$_{144}$ to a solution of 10 pM P1 + 10 pM P2 in either 3%, 5% or 7% PEG 10,000 in 0.3 M PBS buffer (blank samples contain no target); probes used are 12-12 head-to-tail. Results shown are the average values from two different samples of each type.*

3.5 Effects of Probe Length and Orientation on Hybridisation Kinetics

To assess the effects of the length and orientation of the probe sequences on the nanoparticle assembly process, each of the ten probe combinations outlined in Figure 3.1 was first hybridised with a 144-base length of target DNA. Note that this target is longer than the combined probe DNA length for all of the probe combinations investigated. All experiments were carried out using the same conditions throughout, i.e. 10 pM of each conjugate was mixed with 1 nM of target in 3% w/v dextran sulfate in 0.3 M PBS hybridisation buffer, and hybridised for 90 min at 25 °C. 3% dextran was used rather than 5% because, despite the 12-mer probes proving stable at the higher polymer concentration (Figure 3.6), some slight instability started to appear when the length of probe DNA was increased.

For the head-to-tail probe combinations, the extent and rate of nanoparticle assembly during hybridisation with $Target_{144}$ was enhanced as the length of P1 DNA increased from 12 to 24 bases (see Figure 3.8a). Similarly, hybridisation efficiency was increased for the tail-to-tail combinations as the combined probe DNA length increased from 24 to 48 bases, with a reduction in hybridisation for the two 30-mer probes (Figure 3.8b). Duplicate blank samples (i.e. probes and buffer only) were also analysed for each probe combination; in all cases there was no significant change in the height or width of the silver nanoparticle plasmon throughout the analysis period, indicating that all probes were stable in the buffer used (data not shown).

When the length of probe DNA is increased, a number of complex and interacting factors are involved that could potentially affect hybridisation with a long target sequence, including: i) increased base-pair interactions between probe DNA and the long target DNA, which would lead to stronger, more thermodynamically favourable duplexes compared to probes with fewer bases available for hybridisation; ii) increased nanoparticle separation, which could result in reduced electrostatic and steric hindrance between the nanoparticles, but also reduced inter-particle salt concentrations due to smaller overlaps of the electric double layers surrounding the DNA-nanoparticle conjugates;[68] iii) reduced electrostatic and steric repulsion between the target overhangs and the nanoparticles as the effective length of the overhangs is reduced due to a longer hybridising section; iv) slower diffusion within the hybridising buffer of nanoparticles bound to longer probe sequences; v) possible secondary structure formation and greater strand-to-strand interactions for the longer probe DNAs; vi) possible differences in probe density on the nanoparticle surface with different lengths of probe DNA. A combination of some or all of these factors could potentially affect the nanoparticle assembly process with long target sequences, and the extent of each contributing factor may vary depending on the length and sequence of both the probe and the target DNA.

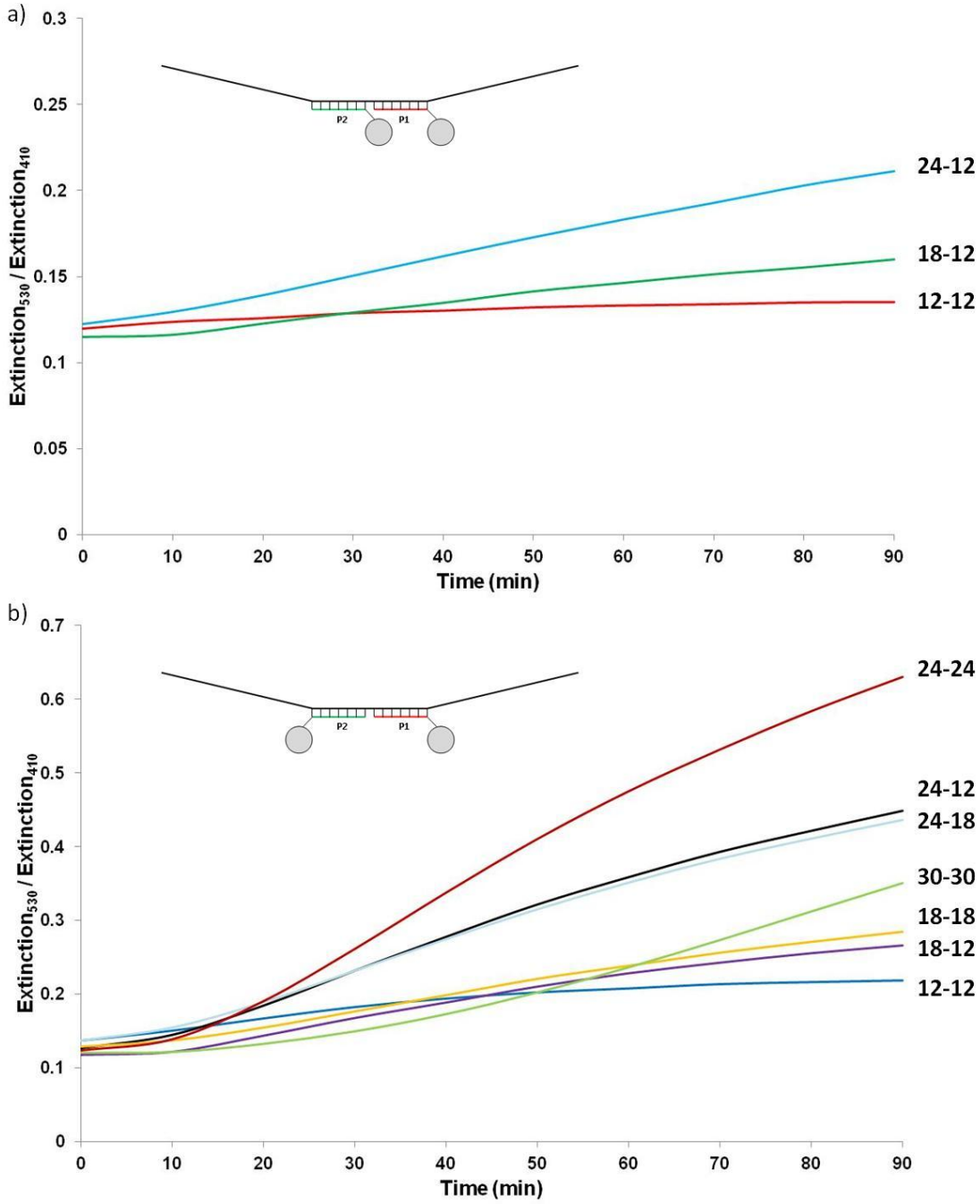

FIGURE 3.8: *Changes in nanoparticle assembly over a 90 min period following addition of 1 nM of 144-base length target DNA to a solution of 10 pM P1 + 10 pM P2 conjugates in 3% dextran sulfate/0.3 M PBS buffer for different a) head-to-tail and; b) tail-to-tail probe combinations. Captions to right of graphs indicate the number of bases in P1 and P2, respectively. Results shown are the average values from two different samples of each type.*

Comparisons can also be made for assemblies with the same length of duplex but a different probe orientation, e.g. the $P1_{12}$-$P2_{12}$, $P1_{18}$-$P2_{12}$ and $P1_{24}$-$P2_{12}$ probe combinations in either a head-to-tail or tail-to-tail orientation when hybridised to $Target_{144}$. As shown in Figure 3.9, the hybridisation rate was higher in each case when the nanoparticles were spaced further apart in the tail-to-tail configuration, which is likely due to the reduced electrostatic and steric hindrance between the silver nanoparticles.

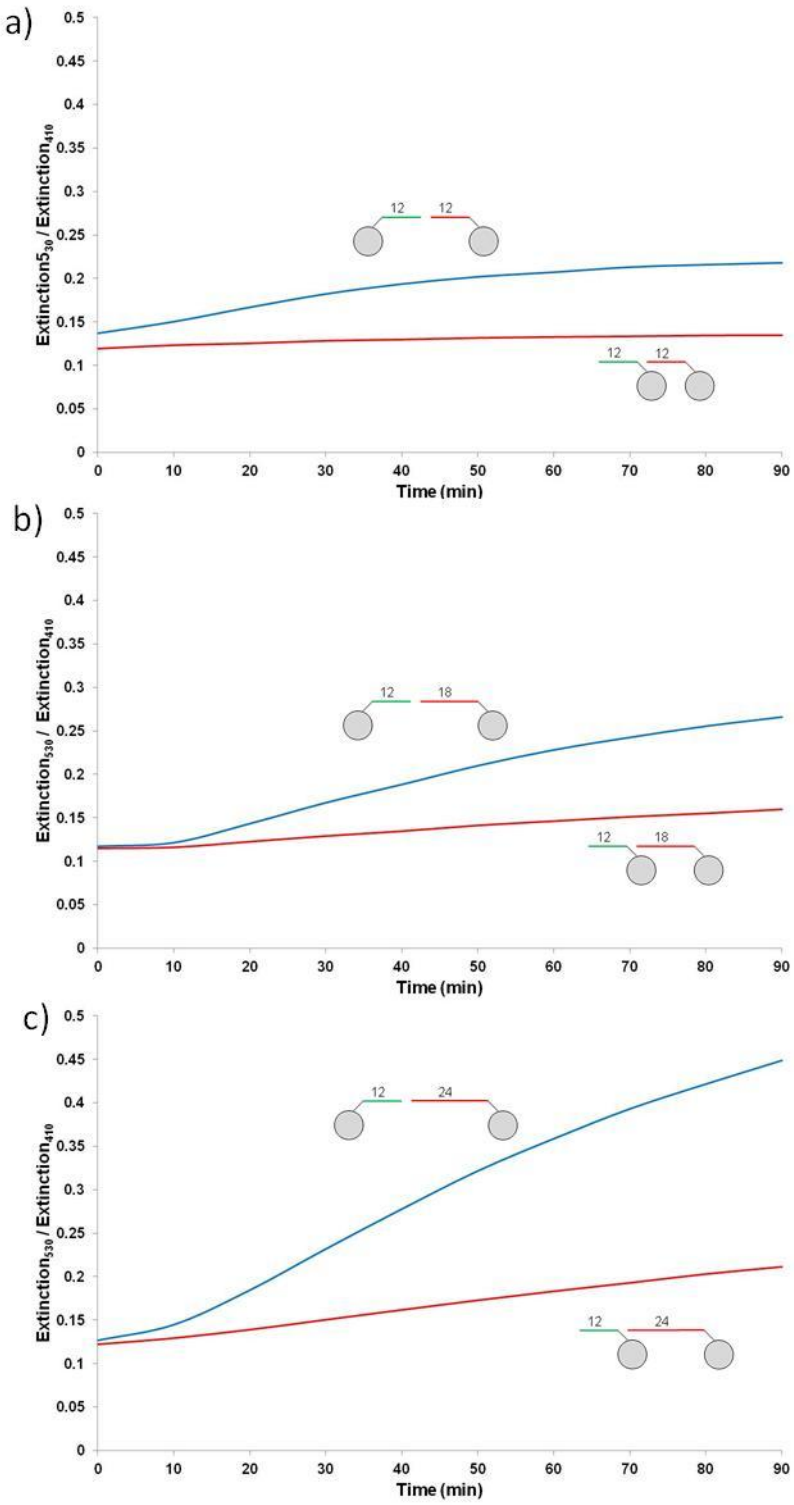

FIGURE 3.9: *Changes in aggregation over a 90 min period following addition of 1 nM of 144-base length target DNA to a solution of 10 pM P1 + 10 pM P2 conjugates in 3% dextran sulfate/0.3 M PBS buffer, comparing head-to-tail (in red, bottom line) and tail-to-tail (in blue, top line) probe combinations for a) $P1_{12}$ + $P2_{12}$ conjugates; b) $P1_{18}$ + $P2_{12}$ conjugates; and c) $P1_{24}$ + $P2_{12}$ conjugates. Results shown are the average values from two different samples of each type.*

When Storhoff *et al.* investigated the aggregation rate of DNA-gold nanoparticle conjugates in the presence of varying lengths of dsDNA linker, they found that longer linkers resulted in a slower rate of aggregation.[43] Guerrini *et al.* also found that increasing the length of dsDNA linker between DNA-silver nanoparticle conjugates led to a reduction in the rate of hybridisation.[68] However, in both cases the length of the probe DNA remained constant throughout, and therefore the number of possible base-pair interactions in the hybridising duplexes was unchanged. In order to separate out the effects of changing probe DNA length with changing number of base pair interactions, as well as any electro-steric effects with target overhangs, the nanoparticle assembly process was assessed using a selection of probe combinations hybridised with a 24-base length of target DNA. In this case, the length of duplex formed remained constant (24 bp), while the probe length and configuration was varied. Experiments were carried out following the same conditions as before but using half the target concentration, i.e. 10 pM of each conjugate mixed with 500 pM of target, hybridised for 90 min at 25 °C in 3% w/v dextran sulfate in 0.3 M PBS hybridisation buffer.

Under these conditions, the rate of hybridisation was found to decrease as the length of probe DNA was increased, and was also slower for the two 12-mer probes when in a tail-to-tail configuration compared with head-to-tail (see Figure 3.10). This is essentially the reverse situation to that which occurs for hybridisation with a long sequence of target DNA. For short target sequences, therefore, probe orientations that result in increased nanoparticle separation lead to a reduction in hybridisation, in agreement with the work of Storhoff *et al.*[43] and Guerrini *et al.*.[68] This may be due to a combination of slower diffusion of the longer nanoparticle-probe conjugates, increased strand-strand interactions in longer probes, and electrostatic repulsion between the hybridising and non-hybridising bases on the probe DNA, which has been found to hinder formation of the duplex.[119] Different levels of oligonucleotide loading on the nanoparticles may also contribute to the effect noted.

Comparison of Figure 3.10 with Figure 3.8 shows that the nanoparticle assembly process is enhanced for all conjugate combinations upon hybridisation with $Target_{24}$ compared with $Target_{144}$, noting also that the shorter target is present at a lower concentration (500 pM of $Target_{24}$ vs. 1 nM of $Target_{144}$). This is in agreement with the data presented in Figure 3.3, whereby increasing the length of target DNA dramatically reduced the rate of hybridisation in 0.3 M PBS buffer.

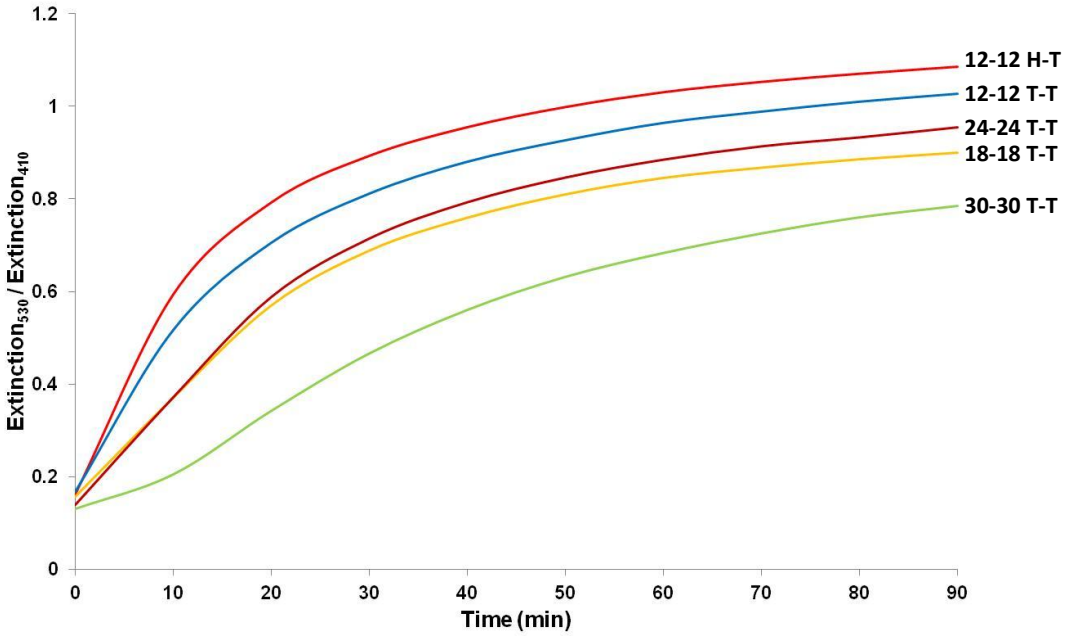

FIGURE 3.10: *Changes in aggregation over a 90 min period following addition of 500 pM of 24-base target DNA to a solution of 10 pM P1 + 10 pM P2 conjugates in 3% dextran sulfate/0.3 M PBS buffer, comparing head-to-tail (H-T) and tail-to-tail (T-T) probe combinations for different lengths of probe DNA. Results shown are the average values from two different samples of each type.*

Overall, these results have shown the importance of using longer sequences of probe DNA in nanoparticle conjugates, oriented in a tail-to-tail configuration, in order to get the maximum rate and extent of hybridisation with long target sequences. In this case, the increased base-pairing interactions, reduced steric hindrance between the nanoparticles, and reduced electro-steric interactions between the target overhangs and the nanoparticles appear to be the dominant factors in maximising target-probe DNA hybridisations. However, if the length of probe DNA is increased too much,

hybridisation rate is reduced due to slower diffusion of the conjugates and potential strand-strand interactions and secondary structure effects in the probe DNA.

3.6 Effects of Hybridisation Parameters on Melting Transitions

The melting temperature (T_m) of DNA-nanoparticle assemblies, i.e. the temperature at which the probe and target DNA strands dissociate, indicates the thermodynamic stability of the system. The sharp, reproducible melting transitions can be important to allow detection of single base mismatches in both gold[42] and silver nanoparticle assemblies.[55] A number of factors are known to affect the T_m of a nanoparticle assembly assay, such as probe and target concentration,[98] probe density, particle size, salt concentration, length of spacer, and probe orientation.[42]

The T_m was determined in this current assay by measuring the change in intensity of the SPR peak at 410 nm with temperature; this change occurs due to the nanoparticle assemblies separating and reverting back to free nanoparticles in suspension as the probe and target DNA strands dissociate once the melting temperature is reached. Samples were prepared by combining 10 pM of each conjugate with 5 nM of target DNA in 3% dextran sulfate/0.3 M hybridisation buffer and allowing to hybridise for 3 h at 25 °C prior to analysis. The target concentration and hybridisation period were both greater than for the kinetics experiments, which was required to reduce the effect of varying quantity of duplex formed between probe combinations. Samples were then heated from 25-70 °C (or 25-90 °C for samples with higher melting temperatures) at 1 °C/min while monitoring the extinction at 410 nm.

Measurements for a range of probes hybridised with $Target_{144}$ showed that an increase in probe length led to an increase in T_m for both the head-to-tail and tail-to-tail combinations (see Table 3.2 and Figure 3.11). This change is significant, with a $\geq$ 30 °C increase in T_m for the two 30-mer probes compared to two 12-mer probes in a tail-to-tail orientation. This is likely due to the increased base stacking interactions[110] and co-operative melting effects due to the longer duplexes formed, as

well as a possible increase in the amount of duplex formed[98] due to increased hybridisation, as explained in the previous section.

TABLE 3.2: *Comparison of melting temperature (T_m) values for a range of different probe combinations for samples containing 10 pM P1 + 10 pM P2 conjugates with 5 nM $Target_{144}$ in 3% dextran sulfate/0.3 M PBS hybridisation buffer. Note: temperature could not be increased above 90 °C, hence unable to get exact T_m for final probe combination. Results shown are the average values from two different samples of each type.*

Probes	Orientation	Duplex Length (bp)	T_m (°C)
$P1_{12}$ + $P2_{12}$	Head-Tail	24	50.2
$P1_{18}$ + $P2_{12}$	Head-Tail	30	59.5
$P1_{24}$ + $P2_{12}$	Head-Tail	36	63.9
$P1_{12}$ + $P2_{12}$	Tail-Tail	24	58.2
$P1_{18}$ + $P2_{12}$	Tail-Tail	30	65.9
$P1_{24}$ + $P2_{12}$	Tail-Tail	36	71.1
$P1_{18}$ + $P2_{18}$	Tail-Tail	36	72.7
$P1_{24}$ + $P2_{18}$	Tail-Tail	42	83.7
$P1_{24}$ + $P2_{24}$	Tail-Tail	48	88.1
$P1_{30}$ + $P2_{30}$	Tail-Tail	60	>88

To determine the extent of the effect of the increased duplex length on T_m, the two 30-mer probes (tail-to-tail orientation) were also hybridised with $Target_{24}$ under the same conditions. In this case the T_m dropped to 62.5 °C, compared with > 88 °C when hybridised with $Target_{144}$ (Table 3.2). This result is interesting since Smith *et al.* found that there was a large decrease in T_m as a result of increased 'overhangs' in the target DNA due to electrostatic repulsion,[110] and therefore highlights that the formation of stronger duplexes as a result of more probe-target DNA interactions is more significant than the increased electrostatic repulsion when moving to a longer target length. Comparison of the T_m values for the same lengths of duplex with a change in probe orientation reveals that a tail-to-tail orientation consistently gives rise to a higher melting temperature than head-to-tail (Table 3.2), similar to the result observed by previous authors investigating a gold[42] and a silver[55] nanoparticle assembly assay. This effect is likely due to the reduced steric hindrance and electrostatic repulsion as the nanoparticles are spaced further apart, combined with the increased hybridisation efficiency, as found in the hybridisation experiments.[42]

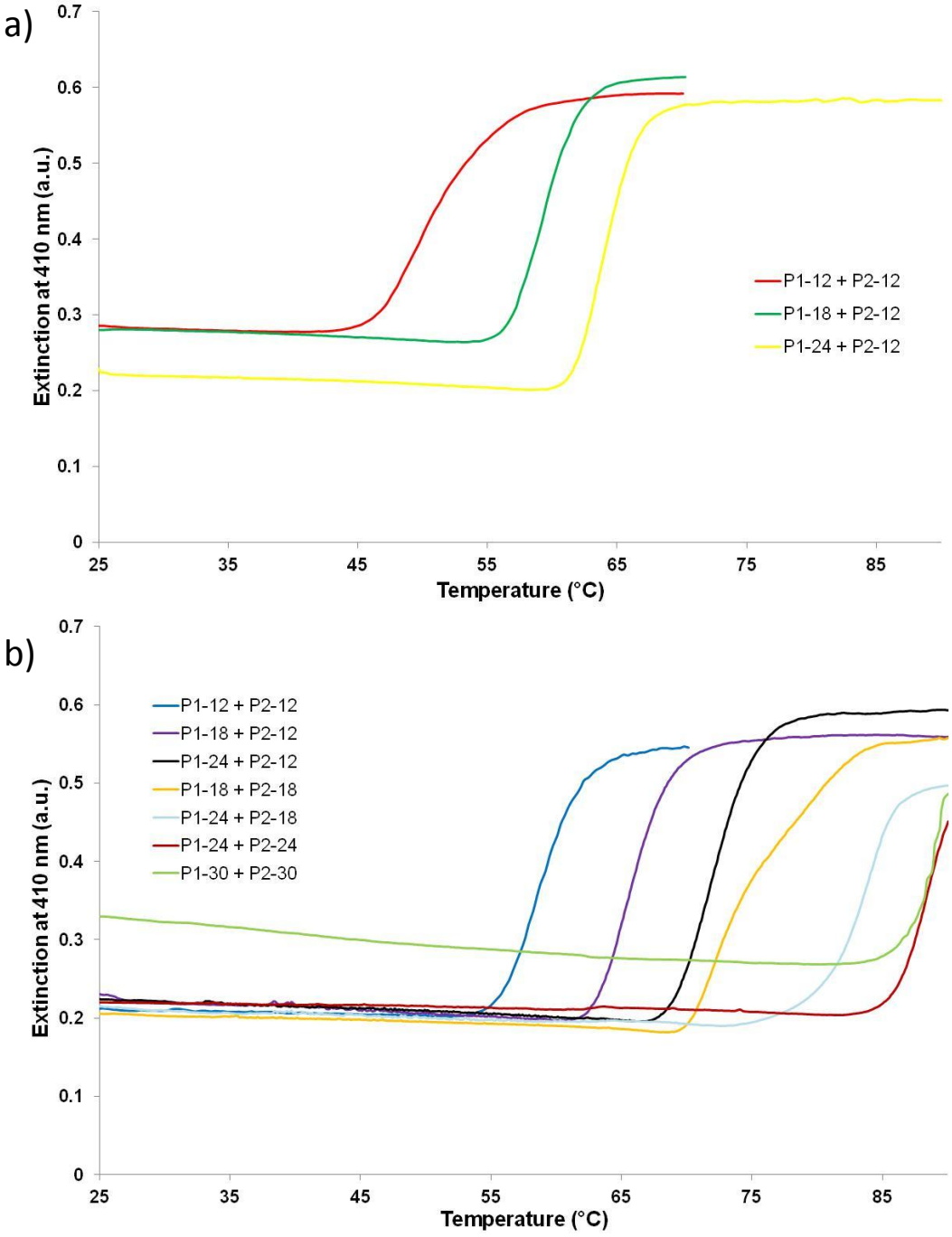

FIGURE 3.11: *Changes in extinction at 410 nm with temperature for different probe combinations (10 pM P1 + 10 pM P2 conjugates) following a 3 h hybridisation with 5 nM Target$_{144}$ in 3% dextran sulfate/0.3 M PBS buffer, showing probes in a) head-to-tail and b) tail-to-tail configuration. Results are for single samples.*

3.7 Use of Short Internal Complement (sic) DNA

As stated earlier in this chapter, the use of 3% rather than 5% dextran sulfate in 0.3 M PBS buffer has been used for many of the hybridisations since the higher dextran content resulted in instability in some of the nanoparticle conjugates, particularly those with longer probe sequences. Greater instability was also observed for the P1 conjugates than for the P2 conjugates in these higher concentration buffers (data not shown). As can be seen from the probe sequences shown in Table 3.1, all of the P1 conjugates have 33.3% GC content, while for each of the P2 conjugates the GC content is ≥ 63.3%. It therefore seems likely that the observed probe instability at higher dextran concentrations is due to an increased level of non-specific hybridisation between the probe DNA strands, which is particularly evident for the stronger GC pairings, causing the nanoparticles to be pulled close together.

In an attempt to prevent or minimise these interactions, the use of short internal complement DNA (sicDNA) was investigated, which consists of a short section of DNA that is complementary to a section of the probe DNA. Its use was first reported by Prigodich *et al.*,[115] who used the technique to allow better hybridisation of nanoparticle-bound probe DNA with target sequences by creating duplexes within the probe DNA to extend the sequence further away from the nanoparticle surface, thus making it more available for hybridisation with target DNA. In this current work, the intention was rather to use the sicDNA to act as short 'blocking' sequences on the probe DNA to prevent inter-strand hybridisation and hence reduce instability of the conjugates. It was hoped that by improving stability of the nanoparticle conjugates, a higher concentration of polymer could be used in the hybridisation buffer, which should allow a much higher degree of hybridisation with long target sequences (as shown in Figures 3.6 and 3.7).

For this, the 24-24 tail-to-tail probe sequences were used (5'-$P1_{24}$ and 3'-$P2_{24}$), with a 12-base sequence of sicDNA complementary to a section of each one, as shown in Scheme 3.1. In order to anneal the sicDNA sequences onto nanoparticle-bound probe DNA, each of the sicDNA sequences was added to an aliquot of the corresponding nanoparticle conjugate at a 1000:1 sicDNA:AgNP ratio, and the buffer concentration

adjusted to 0.5 M PBS. These samples were heated rapidly from 25-70 °C then slowly cooled to 25 °C at 0.5 °C/min. Hybridisation kinetics experiments were then carried out using both the original conjugates, and also the conjugates containing sicDNA.

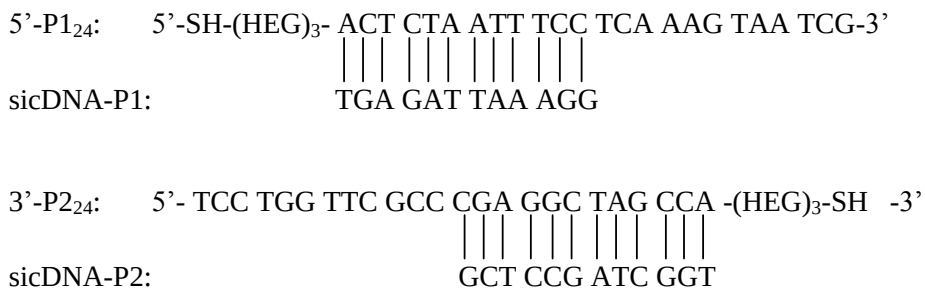

SCHEME 3.1: *Representation of two 12-base sicDNA sequences and the corresponding 24-base probe DNA sequences to which they were annealed.*

10 pM of each of the 5'-P1$_{24}$ and 3'-P2$_{24}$ conjugates, either with or without sicDNA, was combined with 100 pM of a 144-base length of target DNA in 6% dextran sulfate/0.3 M PBS hybridisation buffer. Equivalent blank samples were also prepared containing conjugates and buffer only; a single sample of each type was prepared and analysed. Extinction spectra were then collected for each of these samples every 10 min over a period of 80 min, with samples maintained at room temperature throughout. By comparing the rate of formation of the nanoparticle assemblies (Figure 3.12) it is clear that the conjugates without sicDNA added are not stable in this hybridisation buffer (blank sample, green line), whereas the conjugates with sicDNA are much more stable throughout the analysis period (blank sample, purple line). Furthermore, the presence of sicDNA in the conjugates does not seem to have limited the rate of hybridisation with long target DNA, as seen from comparison of the red and blue lines in Figure 3.12.

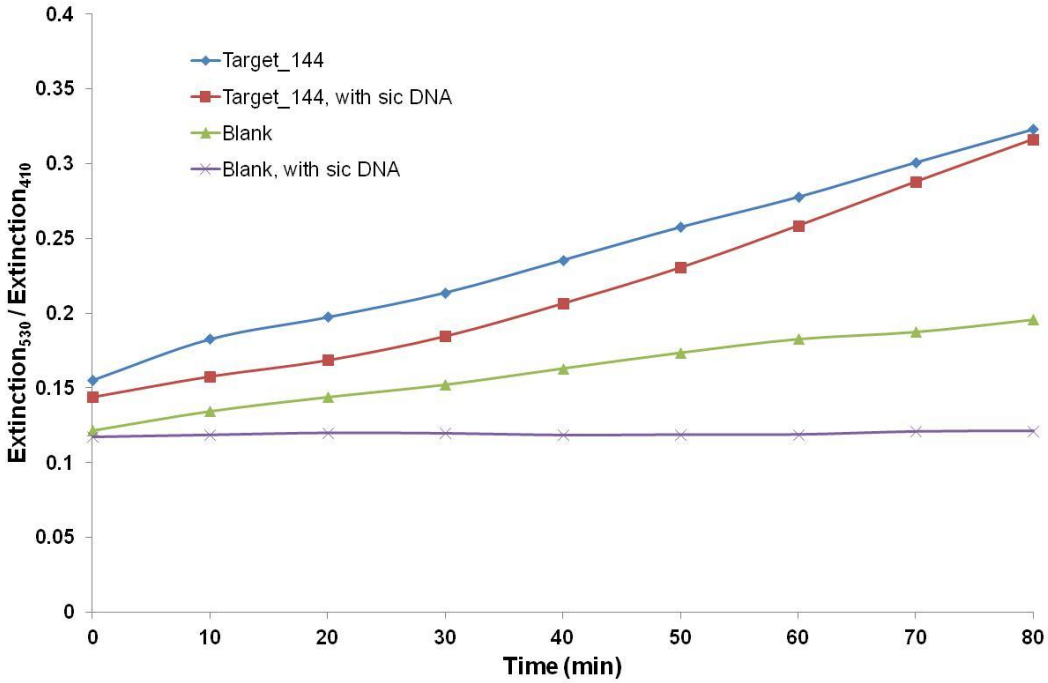

FIGURE 3.12: *Changes in aggregation over an 80 min period following addition of 100 pM of 144-base target DNA to a solution of 10 pM 5'-P1$_{24}$ + 10 pM 3'-P2$_{24}$ conjugates (either with or without sic DNA added) in 6% dextran sulfate/0.3 M PBS buffer. Blank samples contain conjugates and buffer only. Results shown are the average values from two different samples of each type.*

The use of sicDNA does therefore seem to offer the opportunity to use a buffer containing a higher concentration of polymer to accelerate the rate of hybridisation, by binding to sections of probe DNA and thus preventing non-specific hybridisation between strands of probe DNA on different nanoparticles. Moreover, it seems that these short sicDNA strands are readily displaced from the probe DNA in the presence of longer target DNA as they do not appear to affect the rate of hybridisation between probe and target DNA. Unfortunately, this experiment was carried out at the very end of my PhD and no time was available to investigate this further.

3.8 Conclusions

Increasing the length of target DNA was shown to limit the nanoparticle assembly process for silver nanoparticles functionalised with short oligonucleotide sequences. The effect became more pronounced with further increases in target length, and is thought to be primarily due to the electrostatic and steric hindrance between the non-hybridising nucleotides on the target sequence and the nanoparticle-probe conjugates, along with slower diffusion of the longer target sequences. The use of a volume excluding polymer, such as dextran sulfate or polyethylene glycol, was shown to dramatically improve the hybridisation of short probe sequences with long target sequences, due to the probes and target being forced into closer proximity by the polymer. To ensure stability of a range of different nanoparticle conjugates, a buffer consisting of 3% w/v dextran sulfate in 0.3 M PBS was used for most of this work. For target DNA that is longer than the combined probe DNA, increasing the length of probe DNA and using a tail-to-tail configuration was shown to significantly enhance hybridisation by creating more base-pair interactions and reducing electrostatic and steric interactions within the system. This leads to the formation of very strong duplexes with high melting temperatures. However, if the length of probe DNA is increased too much, hybridisation rate is reduced due to slower diffusion of the conjugates and potential strand-strand interactions and secondary structure effects in the probe DNA. For short target sequences, maximum hybridisation was achieved when the combined probe DNA length matched the length of the target DNA, highlighting the range of complex interactions that take place in a nanoparticle assembly assay.

It is worth noting that this work does not aim to accurately define the relationship between nanoparticle separation and hybridisation. This would not be possible from the data shown since there is known to be some flexibility in the DNA hybrids formed as a result of the breaks in the probe DNA,[37, 120] as well as flexibility from the hexaethylene glycol spacer units that are present between the nanoparticle and probe DNA sequence. Rather, it is a practical assessment of the factors that affect DNA-directed nanoparticle assembly that provides useful information for the design of

DNA probes, particularly when used for the detection of long sequences of target DNA.

In Chapter 2, the number of oligonucleotide strands that are conjugated to a 48 nm silver nanoparticle was calculated as 1,300 ± 200. This was based on a 12-mer thiol-modified probe sequence with a HEG_3 spacer. In the case of longer probe sequences, it is likely that the extent of loading on the nanoparticle will change. It has been shown that moving to a polyethylene glycol spacer rather than a T_{10} or A_{10} spacer resulted in a greater than 3-fold increase in the loading of a 15-base oligonucleotide sequence onto a gold nanoparticle.[46] This was explained as being due to the inter-strand repulsion due to the negatively charged phosphate backbone on the A_{10} and T_{10} spacers, which limits the extent of loading on the nanoparticle. For this current work, it therefore seems likely that the increased electrostatic repulsion that would result from an increased number of nucleobases could lead to a reduced extent of loading onto a silver nanoparticle for longer probe sequences. An increased surface density of probe DNA strands has been said to enhance DNA hybridisation,[44] and therefore the reduction in hybridisation of a 24-base target DNA sequence with increasing lengths of probe DNA could partly be explained by a corresponding reduction in probe density on these nanoparticle conjugates. In the case of longer target sequences, this effect is superseded by the longer duplexes formed and the reduced steric hindrance when hybridised with longer probe sequences.

CHAPTER 4: Use of Magnetic Assay with SERS for Detection of Long Target Sequences and PCR DNA

Chapter 2 described the development of a magnetic nanoparticle assembly assay with SERS analysis for the detection of short, specific sequences of target DNA. Chapter 3 then discussed the importance of using longer probe sequences and buffer additives in order to achieve successful hybridisation with long sequences of target DNA. This was investigated using two AgNP probes and by measurement of the plasmonic changes upon nanoparticle interaction. This current chapter now investigates the use of these different probe combinations and hybridisation accelerants for the detection of long target sequences using the AgNP-Ag@MNP assay, with measurement of the SERS enhancements achieved. This chapter focuses on the detection of targets specific for the fungal species *A. fumigatus* and *C. krusei*. Hybridisation is investigated with different lengths of synthetic target DNA, as well as with samples of PCR-amplified plasmid DNA.

An important issue that needs to be considered is whether sufficient SERS enhancement can be achieved with the larger nanoparticle separations that occur as a result of using longer probe DNA sequences, and by using a tail-to-tail probe orientation. Scheme 4.1 shows a to-scale representation of the separation between two 48 nm silver nanoparticles, each conjugated with a 24-mer probe sequence with a HEG_3 spacer, hybridised to a 48-nucleotide sequence of target DNA in a tail-to-tail orientation. The dimensions are based on the length of 10 base pairs being 3.4 nm[1] and the length of a HEG_3 spacer being approximately 6-7 nm.[121] If the HEG spacers and probe DNA sequences were extended fully towards each other, as shown in the diagram, this would result in a nanoparticle separation of approximately 30 nm. It is known, however, that the nanoparticle assembles are not structurally rigid, and that there is some flexibility as a result of the break in the centre of the probe DNA strands,[120] and the HEG spacer units will also provide some degree of flexibility. Furthermore, Scheme 4.1 represents just two nanoparticles, whereas the nanoparticle assemblies formed involve large numbers of nanoparticles linked in a 3-dimensional

network, with undefined spacing and orientations of the nanoparticles relative to each other. Nonetheless, given that it has been shown that two nanoparticles should be in sub-nanometre proximity in order to achieve maximum SERS enhancement,[36] it is important to determine whether the described changes in probe length and orientation affect the enhancements obtained in the magnetic nanoparticle assembly assay.

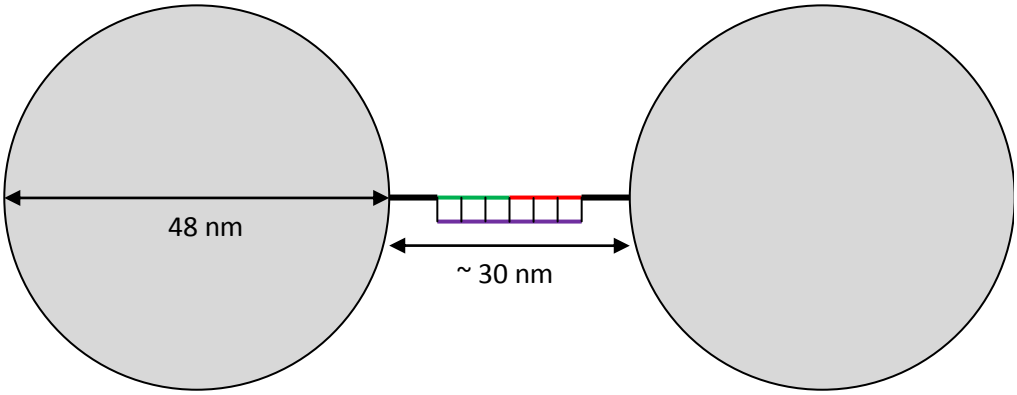

SCHEME 4.1: *To-scale representation of the separation between two 48 nm silver nanoparticles, each conjugated with a 24-mer probe sequence (red and green lines) with a HEG_3 spacer (black lines), hybridised to a 48-base length of target DNA (purple line) in a tail-to-tail orientation.*

4.1 Detection of *Aspergillus fumigatus* Targets using Magnetic Assay and SERS

Detection of long target sequences specific for *A. fumigatus* (FUM) were investigated using 2 different probe combinations: 12-12 head-to-tail (H-T) and 18-18 tail-to-tail (T-T), see Scheme 4.2. Differences in these 2 probe combinations were compared for hybridisation with 4 different lengths of synthetic target sequence: 24nt, 50nt, 100nt and 150nt. Full details of the probe and target sequences used are shown in Table 4.1. In all cases, the combined probe sequence was exactly complementary to a section of the target DNA, with no gaps. Scheme 4.3 shows the relative position of the 18-18 tail-to-tail probes when hybridised to each of these

lengths of target. The probe 1 oligonucleotide sequences were attached to hydroxylamine-reduced AgNPs (FUM-P1) and the probe 2 sequences were attached to glucose-reduced Ag@MNPs (FUM-P2).

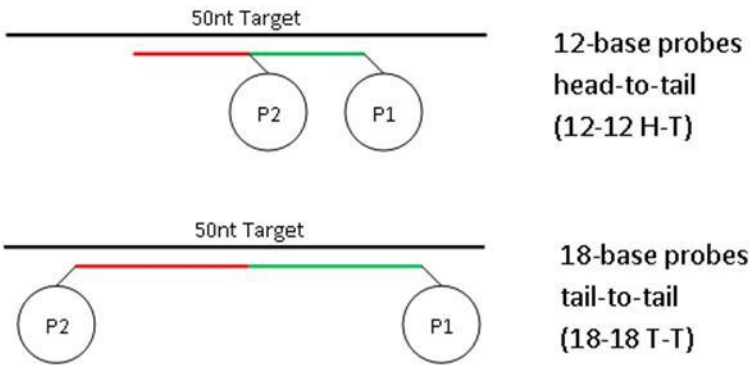

SCHEME 4.2: *Illustration of the two probe combinations used to investigate detection of long target FUM sequences, showing the position of the probe sequences relative to a 50nt target sequence*

TABLE 4.1: *Details of the different probe and target FUM DNA sequences used, where $(HEG)_3$ denotes three hexaethylene glycol units (used as a spacer between the nanoparticle and the probe sequence)*

Probe/Target	Sequence (all 5' – 3')
5'-$P1_{12}$	HS-$(HEG)_3$- CCC TCG GAA TGT
5'-$P2_{12}$	HS-$(HEG)_3$- ATC ACC TCT CGG
5'-$P1_{18}$	HS-$(HEG)_3$- CAA AGG CCC TCG GAA TGT
3'-$P2_{18}$	ATC ACC TCT CGG GGT GTC -$(HEG)_3$-SH
24nt Target	CCG AGA GGT GAT ACA TTC CGA GGG
50nt Target	GCT ATA AGA CAC CCC GAG AGG TGA TAC ATT CCG AGG GCC TTT GAC CGG CC
100nt Target	GCT ATA AGA CAC CCC GAG AGG TGA TAC ATT CCG AGG GCC TTT GAC CGG CCG CCC AAA CCG ACG CTG GCC CGC CCA CGG GGA AGT ACA CCG GCA CGA ATG C
150nt Target	CAG GCC GCA TTG CAC CCT CGG CTA TAA GAC ACC CCG AGA GGT GAT ACA TTC CGA GGG CCT TTG ACC GGC CGC CCA AAC CGA CGC TGG CCC GCC CAC GGG GAA GTA CAC CGG CAC GAA TGC CGG CTG AAC CCC GCG GGC GAG TCT GGT CGC

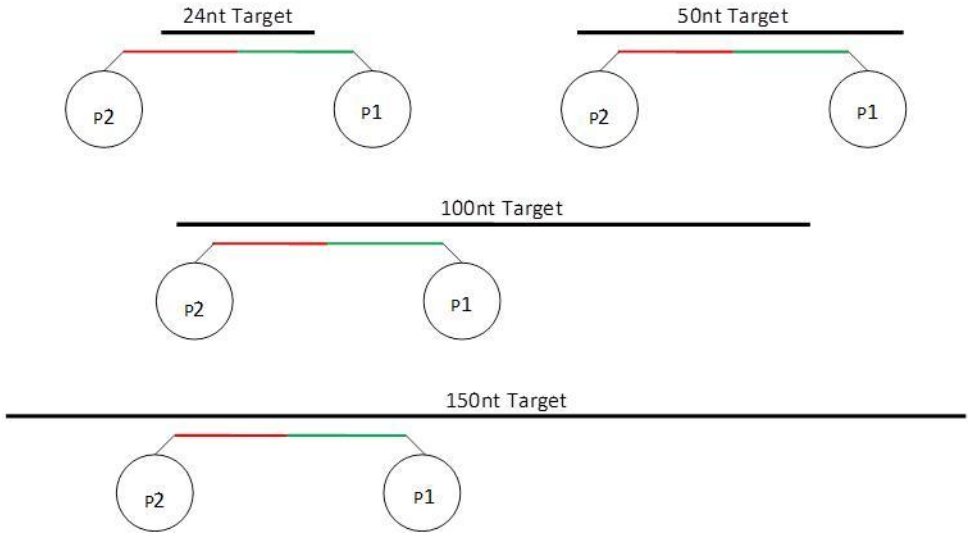

SCHEME 4.3: *Illustration of the relative position of the 18-18 tail-to-tail FUM probe combination when hybridised to four different lengths of target sequence*

4.1.1 Detection of Different Lengths of Synthetic Target DNA

i) Extinction Spectroscopy Measurements

Reaction kinetics experiments were carried out to determine the rate and extent of nanoparticle assembly for the two probe combinations with different lengths of synthetic target DNA. This was done by combining FUM-P1 and FUM-P2 conjugates (5 pM of each) with 5 nM target sequence in hybridisation buffer at room temperature and collecting the extinction spectra of the samples at 10 min intervals from the point at which target was added. Differences in the nanoparticle assembly process were compared for different samples by plotting the ratio of the extinction of the nanoparticle assemblies to that of the individual nanoparticles (i.e. extinction_{520} / extinction_{405} for these conjugates) against time, as described in previous chapters.

In 0.3 M PBS hybridisation buffer, no hybridisation was observed with the 50nt or 100nt target sequences using the 12-12 H-T probe combination (Figure 4.1a). When the buffer was changed to 5% dextran sulfate in 0.3 M PBS, hybridisation was observed with all four target lengths using this same probe combination (Figure 4.1b), while the rate and extent of hybridisation with the longer target sequences (50nt to 150nt) was increased when the 18-18 T-T probe combination was used (Figure 4.1c). These results mirror those reported in the previous chapter and

highlight that the explanations provided for this behaviour also apply to the conditions used here, i.e. with different target and probe sequences and using a AgNP-Ag@MNP assay.

For the samples in 5% dextran sulfate/0.3 M PBS hybridisation buffer (Figure 4.1b-c), the same samples were then heated to determine their melting temperature, following a 2 hour hybridisation at room temperature. The extinction value of the individual nanoparticles (i.e. $extinction_{405}$) was monitored while heating the hybridised samples from 20 to 70 °C (or 90 °C for higher melting samples) at 1 °C/min. The melting temperatures were calculated from the sharp melting transitions and are shown in Figure 4.2 and Table 4.2 for both probe combinations with each of the four lengths of target DNA.

For the 12-12 H-T probe combination, increasing the length of the target sequence leads to a reduction in the melting temperature, which is likely due to a reduction in the amount of duplex formed due to the reduced level of hybridisation as shown in Figure 4.1. For the 18-18 T-T probe combination, T_m values for all lengths of target are higher than for the 12-12 H-T probes; this is due to a combination of increased length of duplex formed (for the 50nt, 100nt and 150nt targets) along with reduced steric hindrance as a result of the increased nanoparticle separation.[42] With these 18-18 T-T probes the T_m value is greater for a 50nt vs. 24nt target sample due to the increased length of duplex formed, however this then reduces as the target length is increased further to 100nt and 150nt. This is likely due to increased electrostatic repulsion from the larger overhangs on the target sequence.[110]

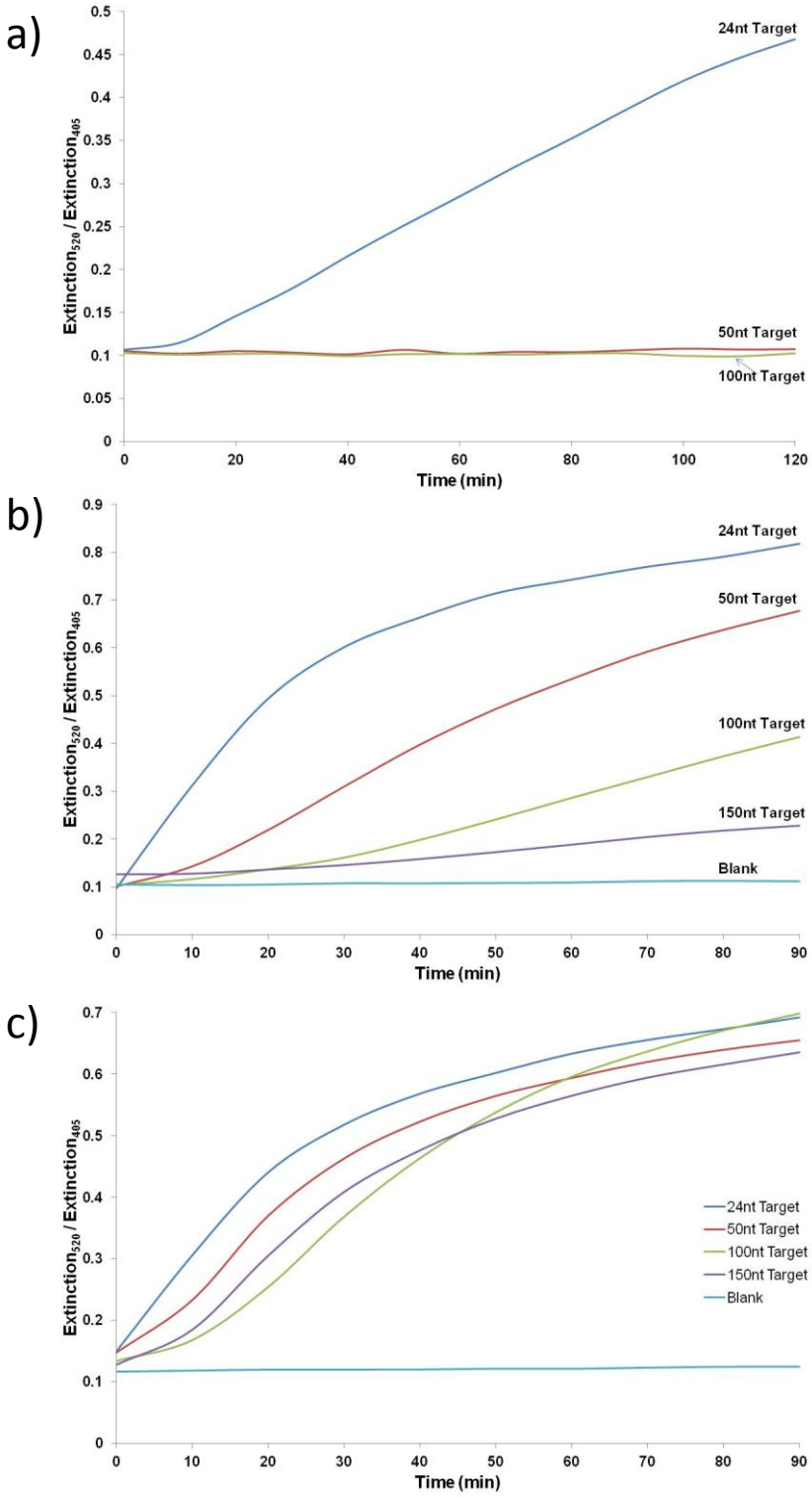

FIGURE 4.1: *Changes in nanoparticle assembly rate for samples of FUM-P1 and FUM-P2 (5 pM of each) hybridised with different lengths of 5 nM target, showing: a) 12-12 H-T probes in 0.3 M PBS buffer; b) 12-12 H-T probes in 5% dextran sulfate/0.3 M PBS buffer and; c) 18-18 T-T probes in 5% dextran sulfate/0.3 M PBS buffer. Results are based on one sample for each target length/probe combination.*

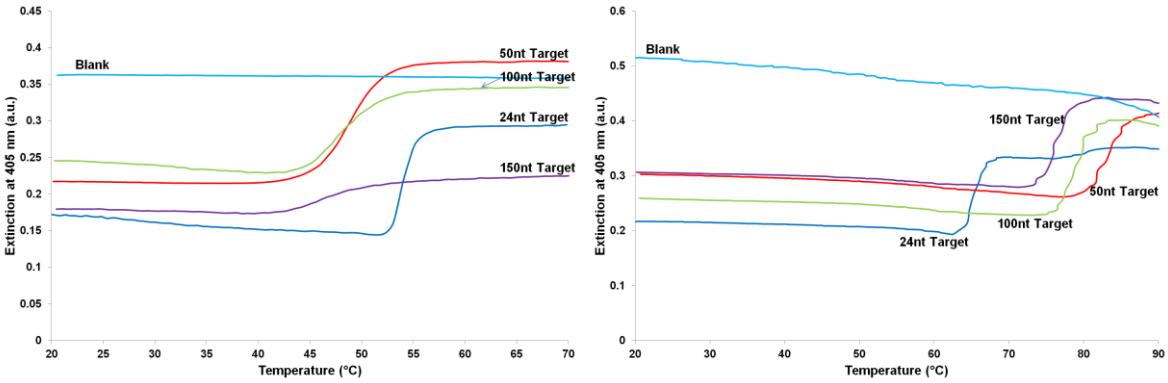

FIGURE 4.2: *Melting transitions for samples of 5 pM FUM-P1 and FUM-P2 conjugates hybridised with different lengths of 5 nM target in 5% dextran sulfate/0.3 M PBS buffer, showing results for 12-12 H-T probes (left) and 18-18 T-T probes (right). Results are based on one sample for each target length/probe combination.*

TABLE 4.2: *T_m values calculated from the melting transitions shown in Figure 4.2*

Conjugates	Melting Temperature (°C)			
	24nt Target	50nt Target	100nt Target	150nt Target
12-12 Head-Tail	53.5	49.0	47.1	45.6
18-18 Tail-Tail	64.4	81.6	80.0	75.9

ii) SERS Measurements

SERS measurements were carried out to determine the effect that the different probe combinations may have on the SERS enhancement for hybridisation with each of the four lengths of target DNA. While the extinction spectroscopy data has clearly demonstrated that the 18-18 tail-to-tail probes allow better hybridisation with longer target sequences, it was unknown whether the increased nanoparticle separation that results from this probe combination would allow sufficiently strong SERS enhancement of the reporter molecule. Malachite green isothiocyanate was used as the Raman reporter, attached to the AgNP-P1 conjugate (FUM-P1-MG).

Samples were prepared by combining 1 µL of each of FUM-P1-MG and FUM-P2 conjugates with a certain quantity of target (e.g. 1 µL of 40 nM target for 40 fmol target) to a total of 12 µL in hybridisation buffer (5% dextran sulfate in 0.3 M PBS) in an Eppendorf tube. Samples were allowed to hybridise for 1 hour at room temperature then transferred to a glass capillary tube, collected on top of a magnet for 20 min and washed with 1 mL of 0.3 M PBS. The magnetic plug was then directly interrogated with a 514 nm excitation laser and the data collected (5 x 1 s accumulations). Figures 4.3 and 4.4 show the results obtained for the 12-12 H-T and 18-18 T-T probe combinations, respectively, with 3 different concentrations of each of the 4 target lengths. Results represent triplicate measurements of a single sample at each concentration (duplicate blank samples were analysed).

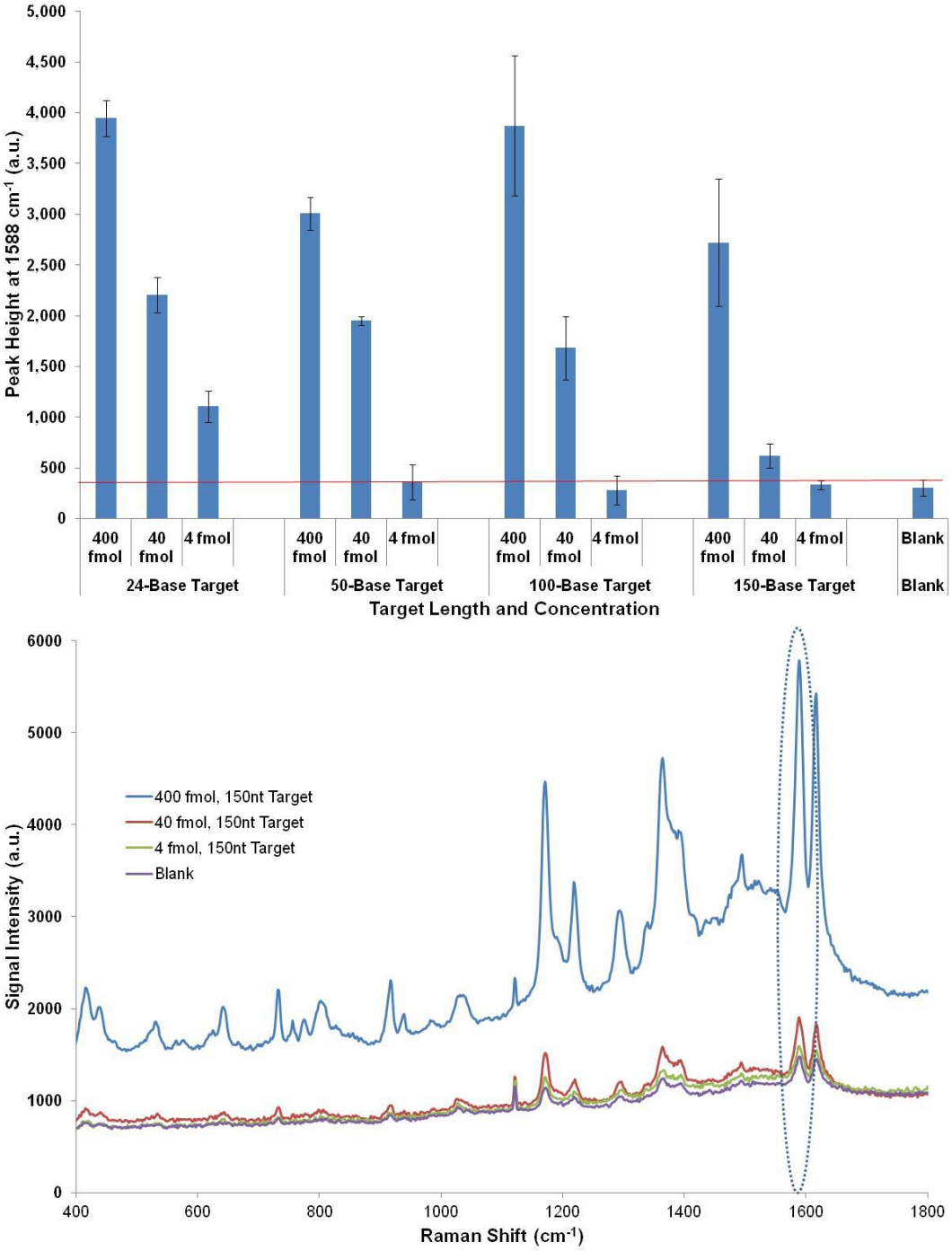

FIGURE 4.3: *SERS results from interrogation of magnetic plug from samples of 12-12 H-T FUM probes hybridised with different lengths and concentrations of synthetic FUM target in 5% dextran sulfate/0.3 M PBS buffer, showing change in peak height at 1588 cm^{-1} for the MG.ITC reporter (top), and comparison of uncorrected MG.ITC SERS spectra with 3 concentrations of 150nt target (bottom). Results are the mean average from triplicate measurements from a single sample at each concentration (triplicate measurements from two different blank samples), and error bars represent ± one standard deviation.*

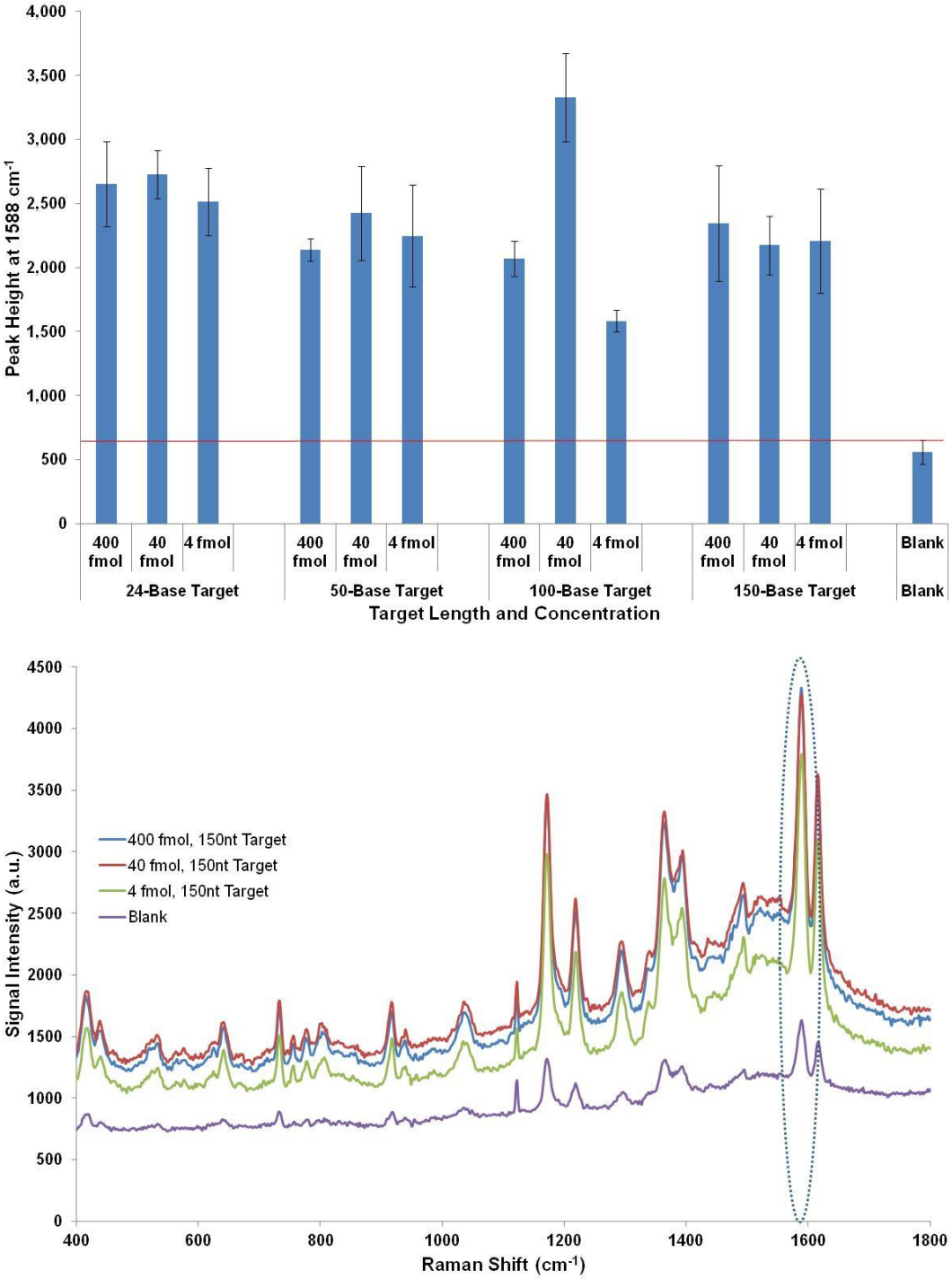

FIGURE 4.4: *SERS results from interrogation of magnetic plug from samples of 18-18 T-T FUM probes hybridised with different lengths and concentrations of synthetic FUM target in 5% dextran sulfate/0.3 M PBS buffer, showing change in peak height at 1588 cm^{-1} for the MG.ITC reporter (top), and comparison of uncorrected, average MG.ITC SERS spectra with 3 concentrations of 150nt target (bottom). Results are the mean average from triplicate measurements from a single sample at each concentration (triplicate measurements from two different blank samples), and error bars represent ± one standard deviation.*

These results show that the 18-18 T-T probes allow better SERS enhancement with low concentrations of the long target sequences compared with the 12-12 H-T probes, which is likely due to the improved level of hybridisation as shown in the kinetics graphs (Figure 4.1). These data demonstrate that the larger nanoparticle separation inherent with the 18-18 T-T probe combination does not prevent the measurement of a strong SERS signal from the Raman reporter following nanoparticle assembly. For the 18-18 T-T probes, the results also show a reduction in intensity of the SERS signal in the presence of higher concentrations of target, along with an increase in the background dye signal in blank samples, resulting in reduced discrimination between some target and blank samples. Nonetheless, use of the 18-18 T-T probes does allow an enhancement in signal intensity of > 3:1 for a sample containing just 4 fmol of a 150-base length of synthetic target DNA compared with a blank sample. A further important point worth noting from these results is that the use of dextran sulfate in the hybridisation buffer has not caused any interference in the SERS spectra, as can be seen by comparison of the spectra in Figures 4.3/4.4 with that in Figure 2.6 (chapter 2).

4.1.2 Detection of PCR DNA

The supplied PCR-amplified sequence of *A. fumigatus* dsDNA consists of a 252 bp sequence, including the primer regions on each side. The full PCR sequence is shown in the Experimental section. Scheme 4.4 illustrates the relative location within the PCR sequence at which the 18-18 T-T probes hybridise. The strand of DNA containing the target region is the same strand that contains the biotinylated primer sequences.

SCHEME 4.4: *Illustration of relative position of 18-18 T-T probes hybridising to section of A. fumigatus PCR-amplified plasmid DNA*

The PCR-amplified DNA has been through 45 amplification cycles, from an initial 10^3 input copy number. This could produce a maximum of 3 x 10^{16} target copies/5 x 10^{-8} moles of DNA, i.e. 1 mM DNA for each 50 µL aliquot made from each PCR batch. This is based on 2^n copies of a molecule being produced for *n* cycles,[9] although it is known that the amplification is not always exponential and therefore the actual yield of target DNA is likely to be much lower. Typically, 5 µL of a 1:10 dilution of PCR product was used; this is equivalent to a maximum of approximately 500 pmol of target DNA.

Initially, attempts were made to hybridise the 18-18 T-T probes with a sample of dsPCR DNA by first heating the sample to separate the two DNA strands then cooling slowly back to room temperature to try to anneal the nanoparticle-probe sequences onto the target strand. These efforts were unsuccessful, based on extinction spectroscopy and SERS measurements. This is likely due to the preference of the two strands of PCR DNA to rehybridise with each other, rather than with the probe DNA, which is attached to a bulky nanoparticle. The slow kinetics of the target-probe DNA interaction are to be expected, given the large degree of steric hindrance from the nanoparticle and electrostatic repulsion from the multiple oligonucleotide strands on its surface.

As a result of these problems, attempts were instead made to separate the dsDNA into ssDNA prior to addition of the probe sequences. This process made use of the biotinylated primers that are used during the PCR amplification process, which then become part of one of the strands of amplified DNA. The PCR DNA was combined with streptavidin-coated magnetic beads, allowing the dsDNA to attach onto the beads through the biotinylated primers. The dsDNA was then denatured using either heat or NaOH, leaving the strand containing biotinylated primers attached to the magnetic bead, and the non-biotinylated strand in the supernatant (see Scheme 4.5). These strands could then be easily separated using a magnet and collected individually.

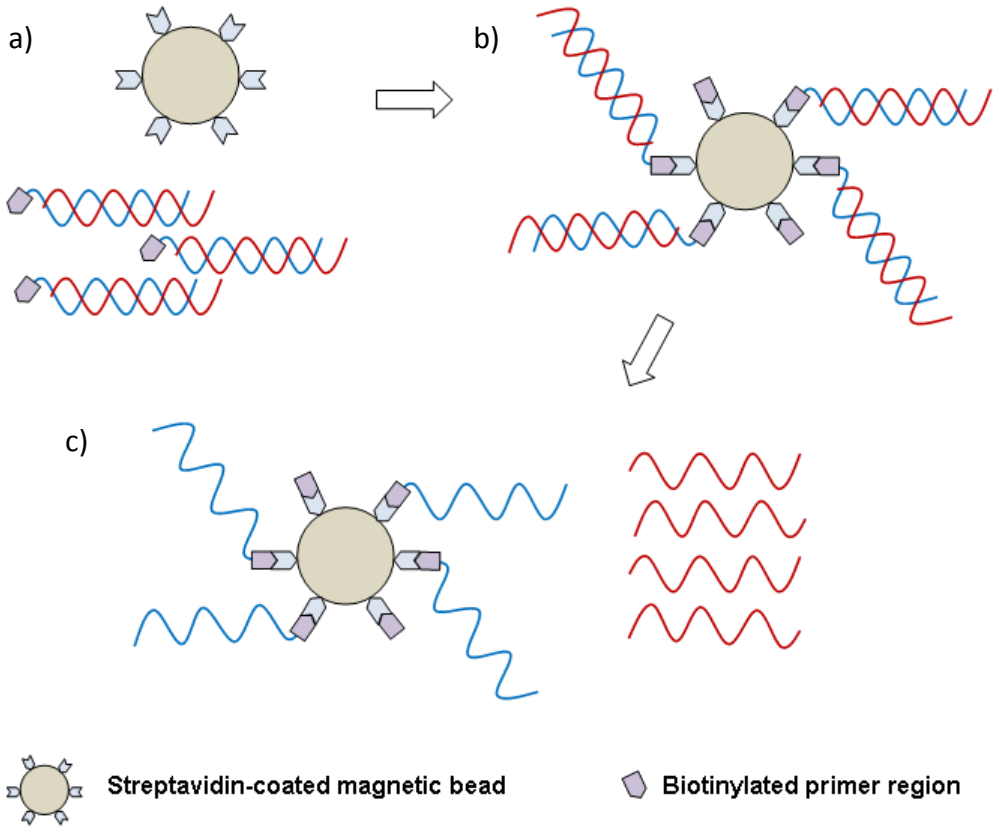

SCHEME 4.5: *Schematic illustration of the separation of dsDNA to ssDNA showing a) streptavidin-coated magnetic beads mixed with biotinylated dsDNA; b) creation of steptavidin-biotin links to attach dsDNA to magnetic beads; c) denaturation of DNA strands leaving biotinylated strand attached to magnetic bead and non-biotinylated strand free in solution.*

Denaturation of dsDNA by alkaline treatment was found to give better results than heat separation, therefore this method was used in most of the experiments. The use of streptavidin beads and NaOH to produce ssDNA from PCR DNA is one of the most convenient and commonly used methods available, and has been shown to produce high yields of single stranded template, more so than with the heat-separation method.[122] For *A. fumigatus* PCR DNA, the target sequence is contained within the biotinylated strand, which remains fixed to a magnetic bead following denaturation. A negative control was prepared at the same time as the FUM PCR sample, which consisted of a portion of streptavidin-coated magnetic beads treated in exactly the same way but without any PCR product added.

In order to measure the extent of any hybridisation between conjugates and PCR DNA, an aliquot of NaOH-separated PCR DNA (or negative control) was mixed with FUM-P1-MG and FUM-P2 conjugates (5 pM of each) in 5% dextran sulfate/0.3 M PBS hybridisation buffer and the extinction spectra measured over a period of 90 min at room temperature. Following this, these same samples were then heated from 25 to 90 °C while monitoring the extinction at 405 nm, in order to determine the presence of any melting transition. Results from these experiments are shown in Figures 4.5 and 4.6.

For the sample containing FUM PCR DNA (shown in Figure 4.5), the SPR peak dropped significantly and broadened over the 90 min period, indicating that nanoparticle assembly has taken place. A small melting transition at 68.6 °C is also observed, which verifies that the nanoparticle assembly is due to a DNA hybridisation event. For the negative control sample (see Figure 4.6), the SPR peak also dropped over the 90 min period, although to a lesser extent than the PCR sample and without any corresponding broadening of the peak. This is believed to be due to the presence of the large magnetic beads within the solution, which are likely to settle out to some extent during the analysis period, potentially pulling some of the Ag@MNP-P2 conjugates with them. Furthermore, no melting transition is observed for this sample.

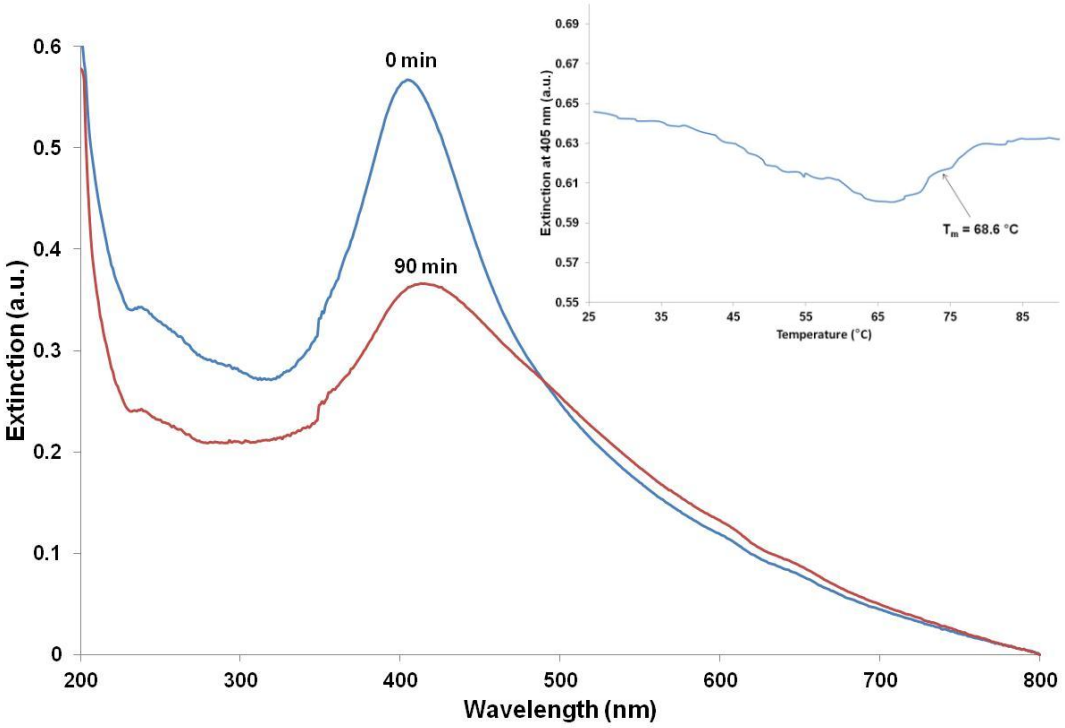

FIGURE 4.5: *Changes in extinction spectra 0 min and 90 min after addition of NaOH-separated FUM PCR sample (5 µL) to a mixture of FUM-P1-MG and FUM-P2 conjugates (5 pM of each) in 5% dextran sulfate/0.3 M PBS hybridisation buffer at room temp, and (inset) change in extinction at 405 nm of this same sample upon heating from 25 to 90 °C at 1 °C/min, showing a melting transition with T_m = 68.6 °C.*

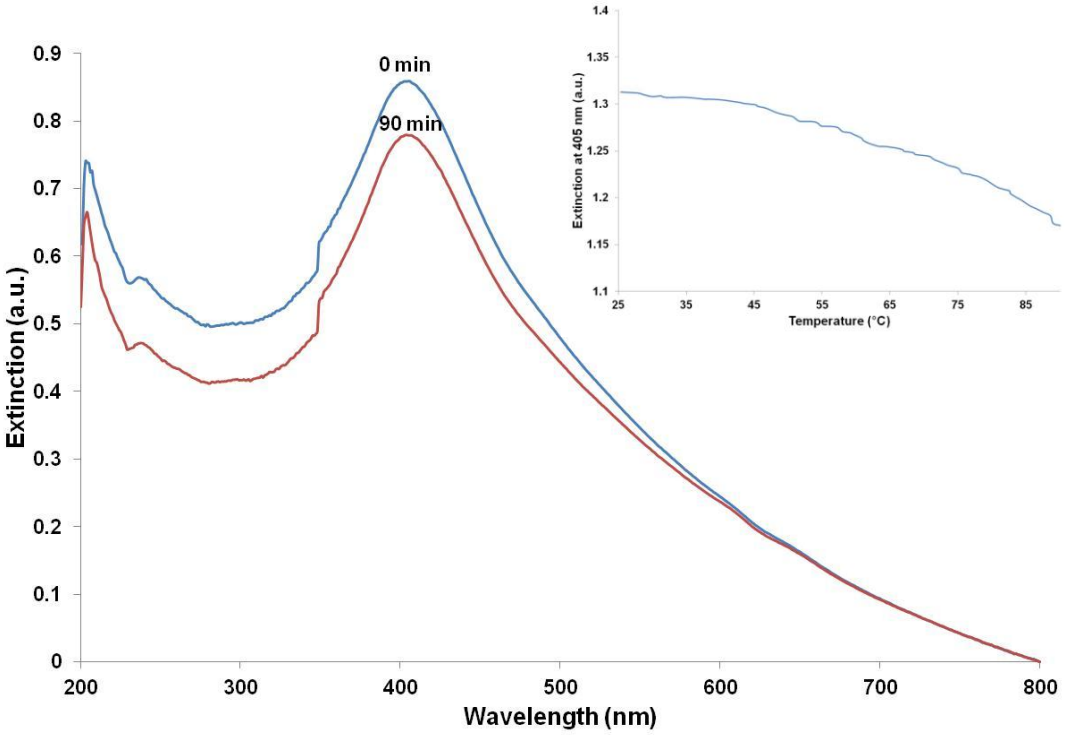

FIGURE 4.6: *Changes in extinction spectra 0 min and 90 min after addition of NaOH-treated negative control sample (5 µL) to a mixture of FUM-P1-MG and FUM-P2 conjugates (5 pM of each) in 5% dextran sulfate/0.3 M PBS hybridisation buffer at room temp, and (inset) change in extinction at 405 nm of this same sample upon heating from 25 to 90 °C at 1 °C/min, showing no melting transition.*

SERS measurements were also carried out on mixtures of the FUM PCR and negative control samples with FUM probes. For these experiments, 1 µL of the NaOH-separated samples were mixed with FUM-P1-MG and FUM-P2 conjugates (1 µL of each) to a total of 12 µL in 5% dextran sulfate/0.3 M PBS buffer. Samples were allowed to hybridise for 60 min at room temperature in Eppendorf tubes then transferred to glass capillary tubes, collected on top of a magnet, washed with 0.3 M PBS then directly interrogated with a 514 nm excitation laser (5 x 1 s accumulations). 3 separate samples were prepared for each of the PCR DNA and negative control, and triplicate SERS measurements were taken from each of these. Figure 4.7 shows the average SERS spectra for both types of sample, demonstrating that SERS enhancement is obtained with the PCR sample compared with a negative control.

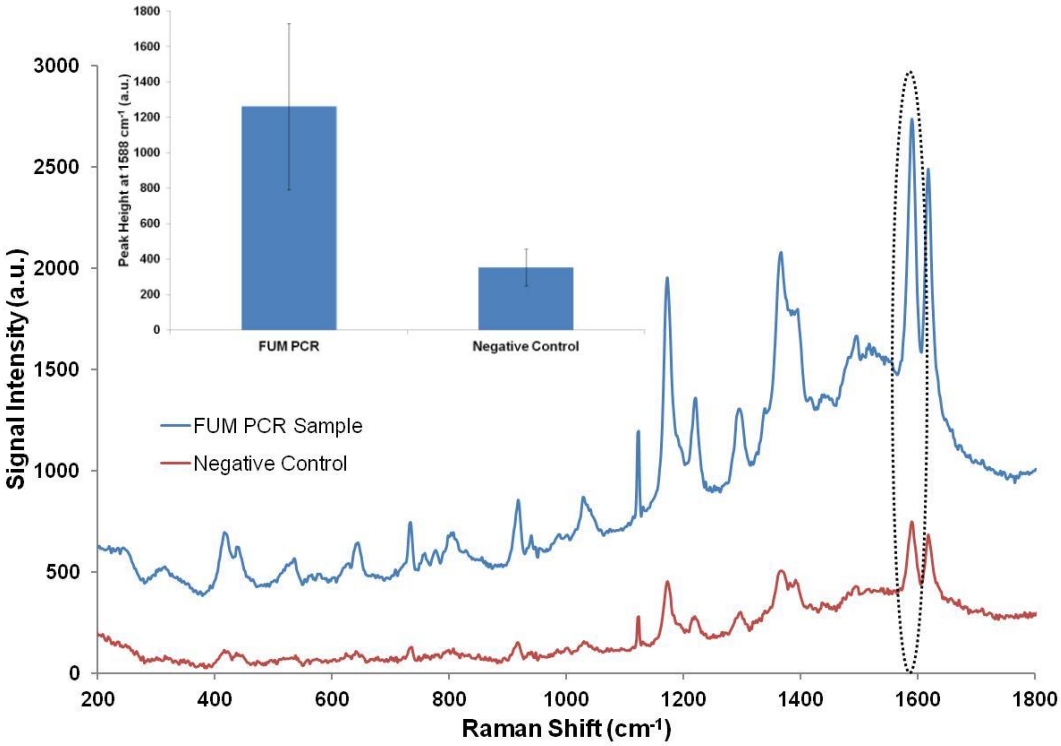

FIGURE 4.7: *Changes in MG.ITC signal intensity for samples of NaOH-separated FUM PCR DNA and a negative control sample hybridised with FUM-P1-MG and FUM-P2 conjugates in 5% dextran sulfate/0.3 M PBS buffer, showing stacked SERS spectra and (inset) change in peak height at 1588 cm^{-1}. Results are the mean average of triplicate measurements from each of 3 samples of each type, and error bars represent ± one standard deviation.*

These results have shown that the 18-18 tail-to-tail probe configuration gives better hybridisation with long sequences of FUM targets than the 12-12 head-to-tail configuration, and that the addition of dextran sulfate to the buffer also increases the rate of hybridisation with these long target sequences. These results are in agreement with those reported in the previous chapter. It has also been shown that good SERS enhancement can be achieved using this 18-18 T-T probe configuration, despite the increased spacing between the nanoparticles in the assembly, and that no spectral interference occurs due to the presence of the polymer. Under these conditions, successful hybridisation of nanoparticle-probes with a sample of FUM PCR DNA has been demonstrated, along with SERS enhancement of the assemblies formed using MG.ITC as a Raman reporter.

4.2 Detection of *Candida krusei* Targets using Magnetic Assay and SERS

Five different probe combinations were used to investigate the SERS detection of long target sequences specific for *C. krusei* (KRU_{mir})[c] using the AgNP-Ag@MNP assay: 12-12 head-to-tail (12-12 H-T), 12-12 tail-to-tail (12-12 T-T), 18-18 tail-to-tail (18-18 T-T), 24-24 tail-to-tail (24-24 T-T) and 30-30 tail-to-tail (30-30 T-T) (see Scheme 4.6). This is a subset of the probes used in Chapter 3 and the sequence details are the same as those provided there (Table 3.1). The probe 1 oligonucleotide sequences were attached to hydroxylamine-reduced AgNPs, along with RB1 as the Raman reporter (KRU_{mir}-P1-RB1). The probe 2 sequences were attached to glucose-reduced Ag@MNPs (KRU_{mir}-P2). These probes were hybridised with a 144nt length of target DNA, with the probes hybridising to a central section of the target sequence in all cases.

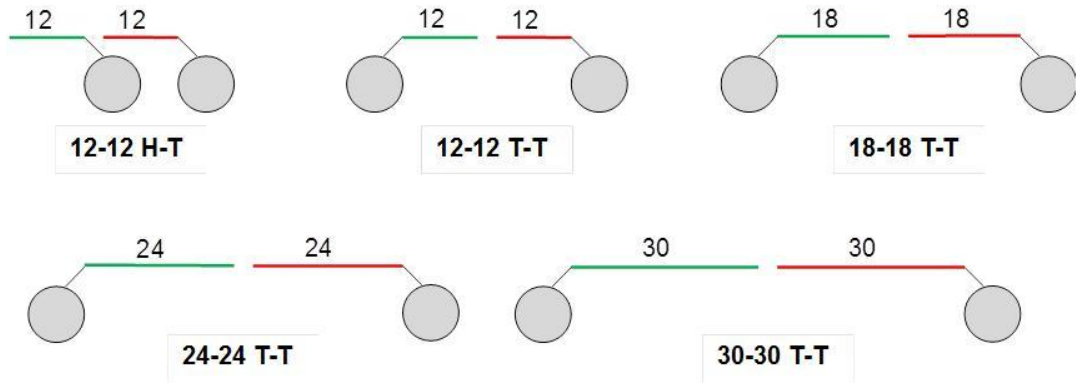

SCHEME 4.6: *Illustration of the five KRU_{mir} probe sequence combinations used to investigate the SERS detection of a long target DNA sequence.*

4.2.1 Detection of Long Synthetic Target DNA

For each of the five probe combinations hybridised with the 144nt target sequence, the SERS signal was measured both from the hybridised sample in suspension, as well as from the magnetic plug following magnetic collection and washing. This was

[c] As explained in Chapter 3, these *C. krusei* target sequences (designated as 'KRU_{mir}') are complementary to those used in Chapter 2 (designated as 'KRU' sequences) to reflect the fact that the desired target sequence on a section of KRU PCR DNA is on the non-biotinylated strand. The corresponding probe sequences were therefore also altered to suit the modified target sequence.

done to allow a comparison of the SERS enhancement obtained from the two sampling methods. Such a comparison was also shown in Chapter 2 (Figure 2.16), although in that case it was only for a 12-12 H-T probe combination hybridised to a 24nt target sequence.

Samples were prepared by combining the KRU_{mir}-P1-RB1 and KRU_{mir}-P2 conjugates (40 pM of each, typically 1.0-1.3 µL) with a certain quantity of target DNA (e.g. 4 µL of 25 nM 144nt target for 5 nM final concentration) to a total volume of 20 µL in 3% PEG 10,000/0.3 M PBS hybridisation buffer. Note that PEG 10,000 was used rather than dextran sulfate for this set of experiments due to problems with dextran sulfate contamination at the time. Blank samples consisted of conjugates and hybridisation buffer only. Samples were prepared in Eppendorf tubes and allowed to hybridise for 60 min at room temperature, then 10 µL transferred to a glass capillary tube. Triplicate SERS measurements were taken of the hybridised solution within the capillary tube using a 514 nm excitation laser (5 x 1 s accumulations). Following this, a magnet was placed under the solution in the capillary tube and the magnetic assemblies allowed to collect on top of this for 10 min then washed with 1 mL of 0.3 M PBS. Triplicate SERS measurements were then taken of the magnetic plug of assembled nanoparticles within the capillary tube using the same conditions as with the sample in suspension.

For each of the five probe combinations, results for samples containing 50 fmol of 144nt target DNA per 10 µL sampled volume were compared with those for blank samples. Three separate samples of each type were prepared and analysed, with the average of these shown in Figures 4.8 to 4.12, i.e. results are the average of triplicate measurements from three individually hybridised samples of each type. The bar charts show the change in intensity of the peak at 1617 cm^{-1}, with error bars representing ± one standard deviation. The numerical values above each blue target column represent the level of discrimination between the target and its corresponding blank sample, e.g. for the 12-12 H-T combination shown in Figure 4.8, the peak height at 1617 cm^{-1} for the magnetic plug 50 fmol 144nt target sample is 3.5 times greater than for the magnetic plug blank sample.

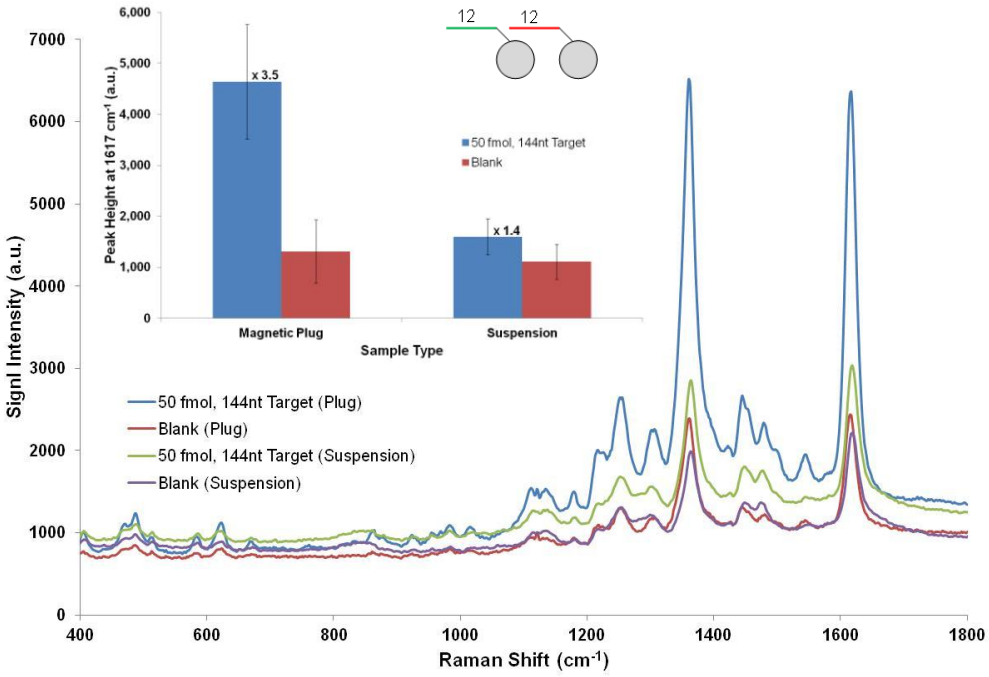

FIGURE 4.8: *Differences in RB1 signal intensity for samples of KRU_{mir} conjugates in a 12-12 H-T combination with either target or no target DNA in 3% PEG/0.3 M PBS hybridisation buffer, showing results for samples in suspension vs. the magnetic plug of the same samples. Results for each sample type are the mean average from triplicate measurements from each of three different samples, and error bars represent ± one standard deviation. Numerical values above each target column refer to the level of discrimination vs. the corresponding blank sample.*

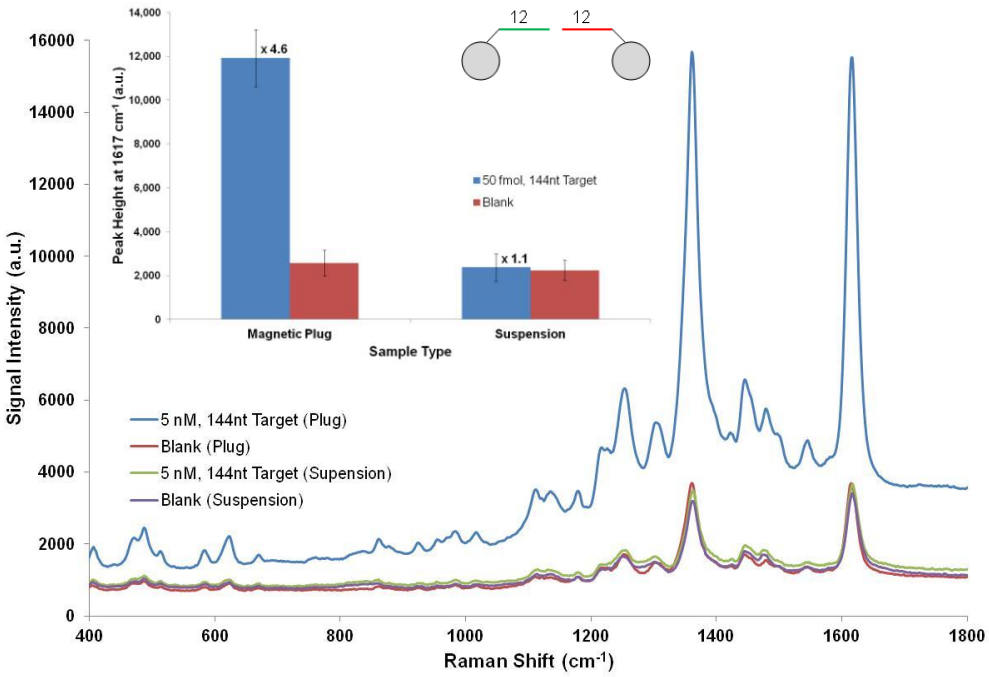

FIGURE 4.9: *Differences in RB1 signal intensity for samples of KRU_{mir} conjugates in a 12-12 T-T combination with either target or no target DNA in 3% PEG/0.3 M PBS hybridisation buffer, showing results for samples in suspension vs. the magnetic plug of the same samples. Results for each sample type are the mean average from triplicate measurements from each of three different samples, and error bars represent ± one standard deviation. Numerical values above each target column refer to the level of discrimination vs. the corresponding blank sample.*

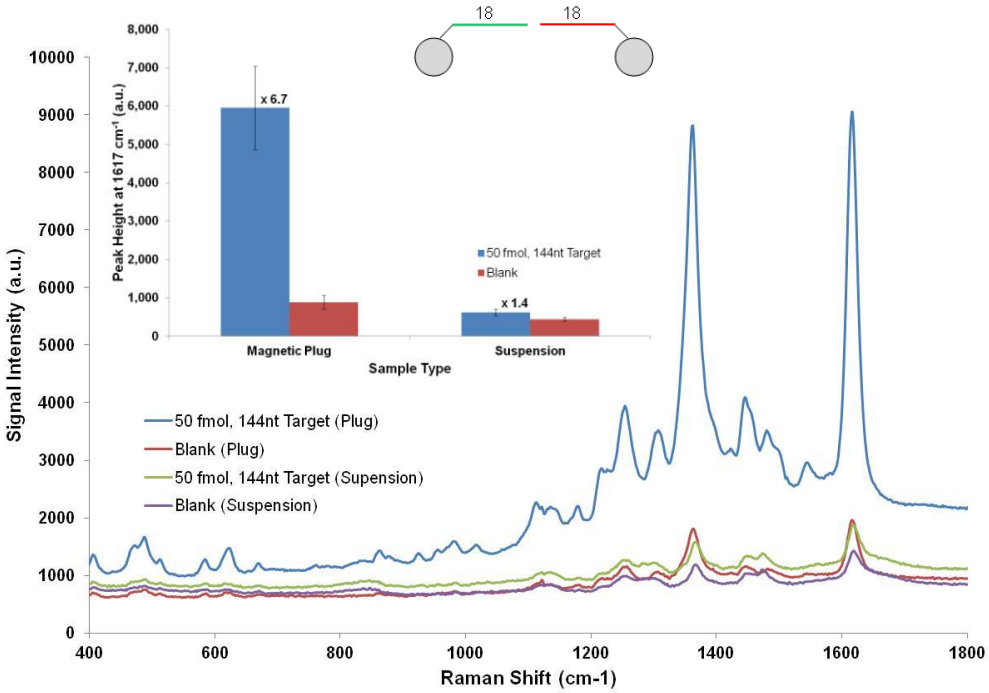

FIGURE 4.10: *Differences in RB1 signal intensity for samples of KRU$_{mir}$ conjugates in an 18-18 T-T combination with either target or no target DNA in 3% PEG/0.3 M PBS hybridisation buffer, showing results for samples in suspension vs. the magnetic plug of the same samples. Results for each sample type are the mean average from triplicate measurements from each of three different samples, and error bars represent ± one standard deviation. Numerical values above each target column refer to the level of discrimination vs. the corresponding blank sample.*

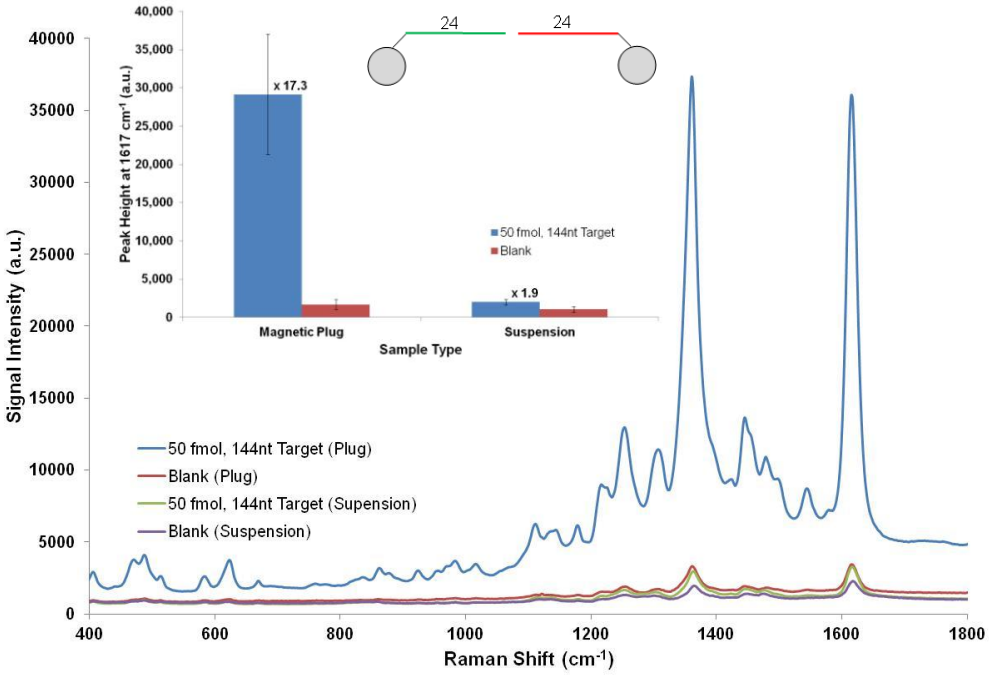

FIGURE 4.11: *Differences in RB1 signal intensity for samples of KRU_{mir} conjugates in a 24-24 T-T combination with either target or no target DNA in 3% PEG/0.3 M PBS hybridisation buffer, showing results for samples in suspension vs. the magnetic plug of the same samples. Results for each sample type are the mean average from triplicate measurements from each of three different samples, and error bars represent ± one standard deviation. Numerical values above each target column refer to the level of discrimination vs. the corresponding blank sample.*

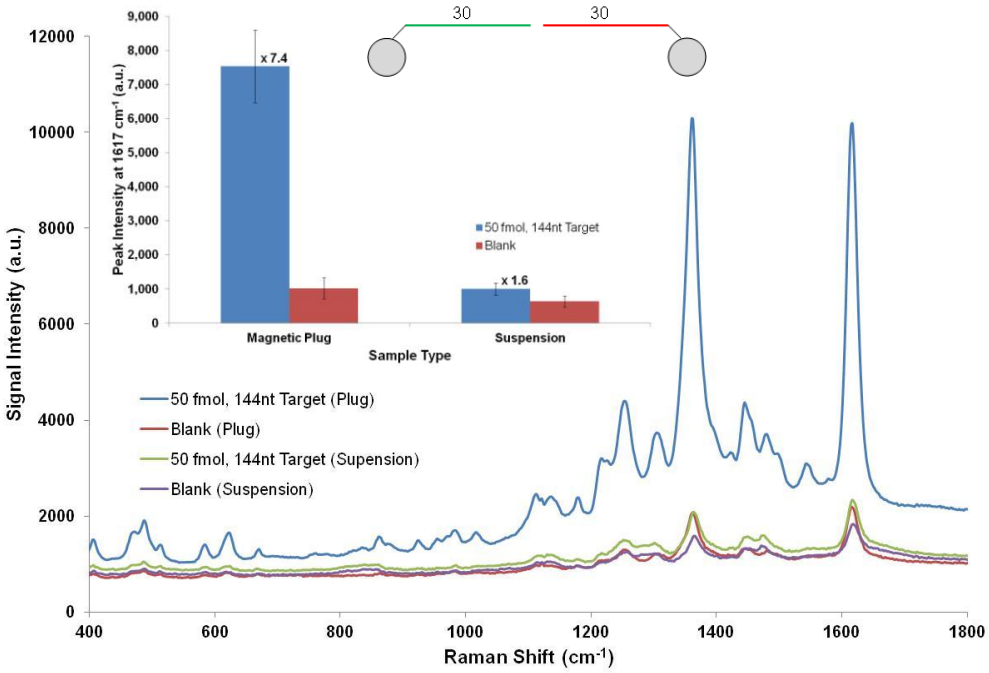

FIGURE 4.12: *Differences in RB1 signal intensity for samples of KRU$_{mir}$ conjugates in a 30-30 T-T combination with either target or no target DNA in 3% PEG/0.3 M PBS hybridisation buffer, showing results for samples in suspension vs. the magnetic plug of the same samples. Results for each sample type are the mean average from triplicate measurements from each of three different samples, and error bars represent ± one standard deviation. Numerical values above each target column refer to the level of discrimination vs. the corresponding blank sample.*

These results show that, for all of the probe combinations, the signal intensity for the 5 fmol target sample, and the level of discrimination between the target and blank sample, is much greater for the magnetic plug measurements than for measurement of the assemblies in suspension. There is always a slight increase in signal intensity for the blank sample when measured in the magnetic plug format rather than in suspension, however the increase in signal intensity for the target sample surpasses this resulting in a much greater level of discrimination for these magnetic plug samples. The greatest level of discrimination is achieved using the 24-24 T-T probes, which is likely due to the greatest level of hybridisation taking place between this probe combination and a long sequence of target DNA, as shown previously. The results also highlight, once again, that the increased nanoparticle separation inherent in the longer probes when in a tail-to-tail configuration does not appear to affect the SERS enhancement obtained from the nanoparticle assemblies. This may be a result

of the force exerted by the external magnet upon the assemblies, causing the nanoparticles to be pulled closer together than would be the case in suspension.

For the 24-24 T-T probe combination, magnetic plug measurements were obtained from samples containing 3 different concentrations of a 144nt target sequence, with the resultant average SERS spectra shown in Figure 4.13. Samples were prepared and analysed as described in the previous paragraphs. These results show that > 3:1 discrimination was achieved between a sample containing 5 fmol of 144nt length target DNA and a blank sample under the conditions described. It is also worth noting that, as with dextran sulfate, the use of PEG 10,000 in the hybridisation buffer has not caused interference in the SERS signal from the Raman reporter.

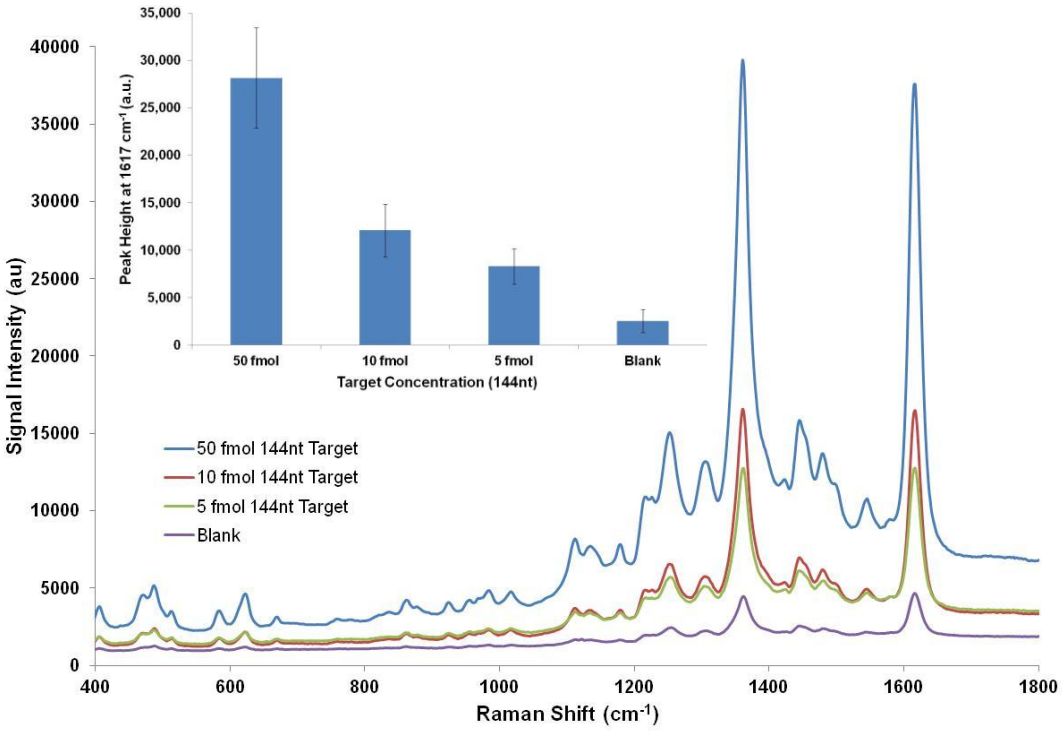

FIGURE 4.13: *Differences in RB1 signal intensity for samples of KRU_{mir} conjugates in a 24-24 T-T combination with different concentrations of 144nt target DNA (or blank) in 3% PEG/0.3 M PBS hybridisation buffer, showing results for magnetic plug measurements. Results for each concentration are the mean average from triplicate measurements from each of three different samples, and error bars represent ± one standard deviation.*

For the measurements of the nanoparticle assemblies in suspension, very poor discrimination between the 5 fmol target and blank samples is observed for all of the probe combinations, which may in part be due to the low concentration of target sequence used. Figure 4.14 shows some further suspension-based measurements using a higher concentration of target. Samples consisted of KRU_{mir}-P1-RB1 and KRU_{mir}-P2 conjugates (20 pM of each) combined with 20 nM of target DNA (24nt or 144nt) made to a total volume of 150 µL in 3% dextran sulfate/0.3 M PBS hybridisation buffer. Samples were prepared in a 96-well plate and allowed to hybridise for 60 min at room temperature, and then triplicate SERS measurements were taken of the solution within the well using a 514 nm excitation laser (5 x 1 s accumulations). Results are the average of triplicate SERS measurements from three individually hybridised samples of each type. Note that the 18-18 T-T probe combination was not used for this experiment due to problems with these conjugates at the time.

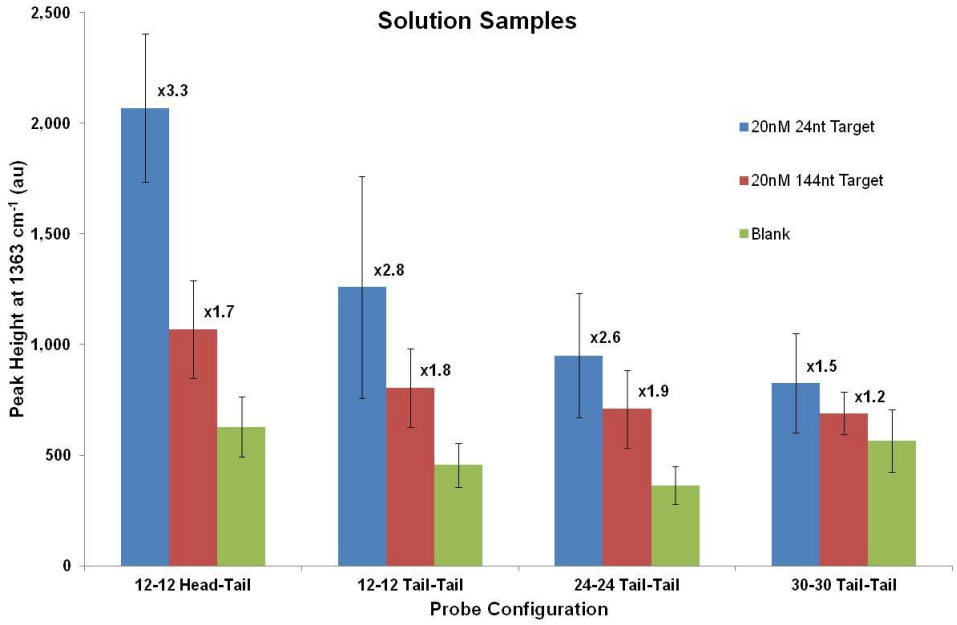

FIGURE 4.14: *Differences in RB1 signal intensity, measured as change in peak height at 1363 cm^{-1}, for samples of different combinations of KRU_{mir} conjugates with two lengths of 20 nM target DNA (or blanks) in 3% dextran sulfate/0.3 M PBS hybridisation buffer, showing results for samples in suspension. Results for each sample type are the mean average from triplicate measurements from each of three different samples, and error bars represent ± one standard deviation. Numerical values above each target column refer to the level of discrimination vs. the corresponding blank sample.*

For the 20 nM target concentration shown, poor discrimination between a 144nt target sample and a blank is again observed for all of the probe combinations. However, in the presence of the short 24nt target sequence, much better hybridisation is observed. In this case, the 12-12 H-T probe combination results in the best discrimination, followed by 12-12 T-T, then 24-24 T-T, with the 30-30 T-T combination providing the least level of discrimination. This pattern coincides with the degree of nanoparticle separation in the hybridised assemblies, and suggests that a larger nanoparticle separation leads to reduced signal intensity for the measurement of samples in suspension.

4.2.2 Detection of PCR DNA

The supplied PCR-amplified sequence of *C. krusei* consists of a 382 bp sequence, including the primer regions on each side. The full PCR sequence is shown in the Experimental section. Scheme 4.7 illustrates the relative location within the PCR sequence at which the 18-18 T-T probes hybridise.

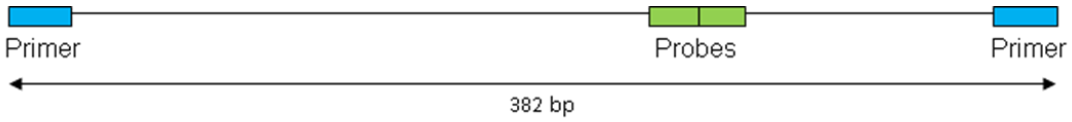

SCHEME 4.7: *Illustration of relative position of 18-18 T-T probes hybridising to section of PCR-amplified C. krusei plasmid DNA*

As described previously, the *C. krusei* PCR sequences were denatured and the two strands collected separately using streptavidin-coated magnetic beads and NaOH-denaturation. In the case of the *C. krusei* PCR DNA, the target region is on the opposite strand from that containing the primer sequences, i.e. the target is on the non-biotinylated strand, and therefore the ssDNA samples used in hybridisation experiments did not contain any magnetic beads. A negative control sample was prepared at the same time as the KRU PCR sample, which involved the collection

and denaturation of an aliquot of FUM PCR DNA in the same way as for the KRU PCR sample.

Hybridisation with a section of NaOH-separated KRU PCR DNA was attempted using the 18-18 T-T probe combination and 5% dextran sulfate in 0.3 M PBS hybridisation buffer. For extinction spectroscopy measurements, using 10 pM of each conjugate with 10 µL NaOH-separated PCR DNA and hybridisation at 40 °C, a very slight shift in the SPR peak was observed, with a small melting transition measured at 62.7 °C (Figure 4.15). The extent of nanoparticle assembly observed with this KRU PCR sample is less than for the FUM PCR DNA as detailed in the previous section, and may be due to the increased length of the former (382 bp cf. 252 bp). As described in the previous chapter, longer target DNA strands can result in greater steric and electrostatic hindrance, which can slow down the rate of hybridisation with probe strands. There may also be more secondary structures within the longer KRU PCR sequence, and indeed heating the sample to 40 °C was required to achieve even the minimal level of hybridisation as noted. Hybridisation with the 24-24 T-T probes was also attempted, although no improvement in the level of nanoparticle assembly was achieved.

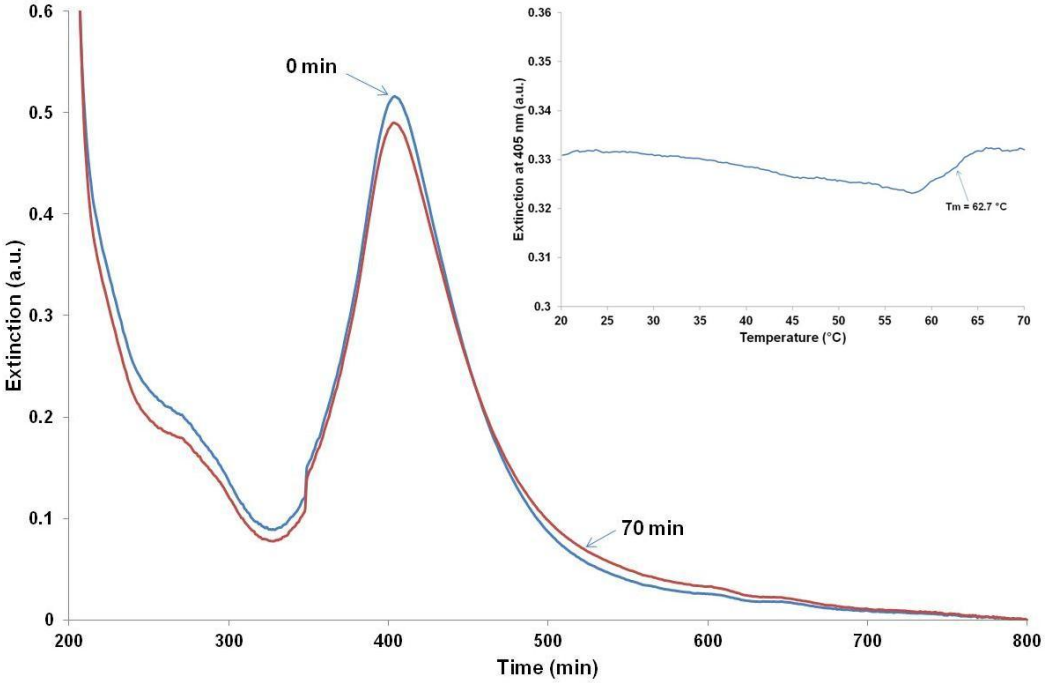

FIGURE 4.15: *Changes in extinction spectra 0 min and 70 min after addition of NaOH-separated KRU PCR sample (10 µL) to a mixture of KRU_{mir}-P1-RB1 and KRU_{mir}-P2 conjugates (10 pM of each) in 5% dextran sulfate/0.3 M PBS hybridisation buffer at 40 °C, and (inset) change in extinction at 405 nm of this sample upon heating from 25 to 70 °C at 1 °C/min, showing a small melting transition with T_m = 62.7 °C.*

SERS measurements were also carried out on mixtures of the KRU PCR and negative control samples with KRU_{mir} conjugates. For these experiments, 2 µL of the NaOH-separated PCR samples were mixed with KRU_{mir}-P1-RB1 and KRU_{mir}-P2 conjugates (1 µL of each) to a total of 12 µL in 5% dextran sulfate/0.3 M PBS buffer. Samples were allowed to hybridise for 60 min at 40 °C in Eppendorf tubes then transferred to glass capillary tubes, collected on top of a magnet, washed with 0.3 M PBS then directly interrogated with a 514 nm excitation laser (5 x 1 s accumulations). 3 separate samples were prepared for each of the PCR DNA and negative control, and triplicate SERS measurements were taken from each of these. Figure 4.16 shows the average SERS spectra for both types of sample, demonstrating that SERS enhancement is obtained with the PCR sample compared with a negative control. SERS is a much more sensitive technique than UV-Vis spectroscopy, hence even very low levels of hybridisation that show only slight changes in the extinction spectrum can lead to relatively large SERS enhancements.

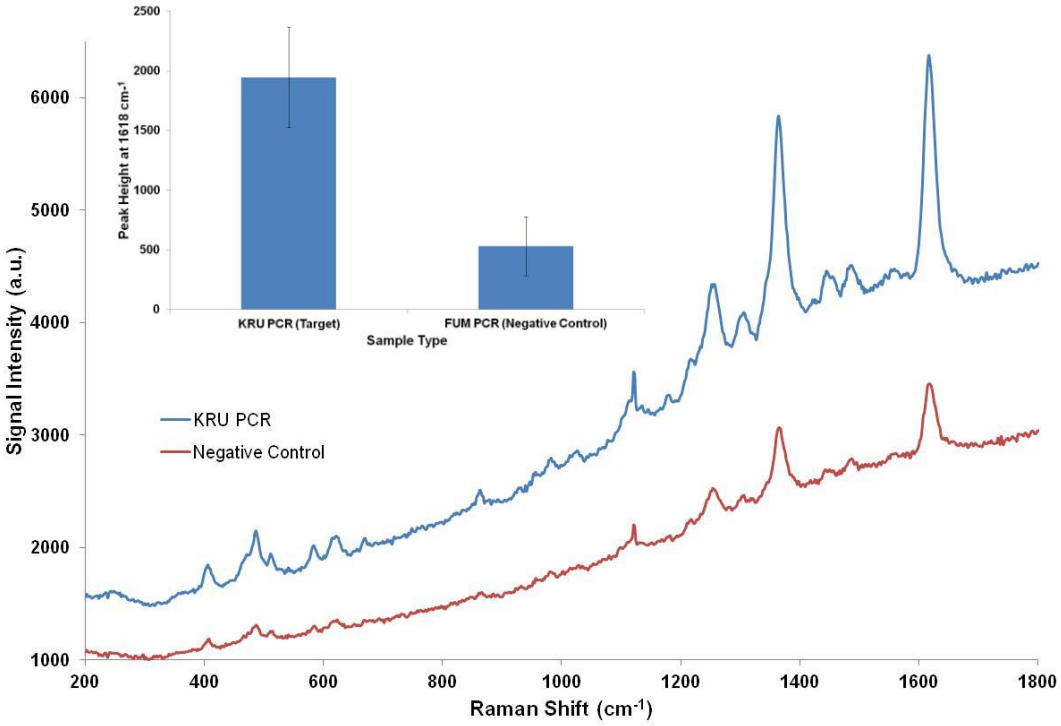

FIGURE 4.16: *Changes in RB1 signal intensity for samples of NaOH-separated KRU PCR DNA and a negative control sample hybridised with KRU_{mir}-P1-RB1 and KRU_{mir}-P2 conjugates in 5% dextran sulfate/0.3 M PBS buffer, showing stacked SERS spectra and (inset) change in peak height at 1618 cm^{-1}. Results are the average of triplicate measurements from each of 3 samples of each type.*

4.3 Summary of Assay for Detection of Long Target DNA

For the measurement of concentrated magnetic samples following nanoparticle assembly, good SERS enhancement was achieved for all probe combinations investigated. It appears that the level of enhancement is related to the extent of hybridisation with different probe combinations, as detailed in Chapter 3, rather than with the degree of nanoparticle separation within the assemblies. Conversely, for suspension-based measurements, hybridisation with a short target sequence indicated that the level of SERS enhancement reduced as the nanoparticles were spaced further apart in the assemblies. For hybridisation with long target sequences, poor discrimination (< 2:1) was observed for all probe combinations using suspension-based measurements. Measurement of magnetic plug samples consistently gave

much stronger SERS signals and greater levels of discrimination than measurement of the nanoparticle assemblies in suspension, allowing reliable detection of much lower target concentrations.

For measurements of the concentrated magnetic plug of nanoparticle assemblies, SERS discrimination of > 3:1 compared with blank samples has been demonstrated for just 4 fmol of a 150-base length of FUM target, and for 5 fmol of a 144-base length of KRU_{mir} target. The ability to detect such low concentrations of these long target sequences is due to a combination of the use of longer probe sequences in a tail-to-tail configuration and the use of a polymer as hybridisation accelerant in the buffer, as detailed in Chapter 3. Importantly, it has been shown that the SERS spectra of the Raman reporters is not affected by the presence of either PEG or dextran sulfate in the hybridisation buffer. The successful application of a nanoparticle assembly assay for the detection of low concentrations of long target DNA sequences represents an important step forwards in our capabilities, and creates opportunities for more progressive work in this area.

The developed assay was used to successfully detect two different types of PCR-amplified DNA sequence, specifically *A. fumigatus* and *C. krusei*. A limited amount of hybridisation was observed between the relevant probes and the single stranded DNA fragments, created using streptavidin-coated magnetic beads and alkaline treatment, and > 3:1 SERS enhancement was also obtained for each sequence. However, further improvements in the level of hybridisation will be required before this assay can be applied to the multiplexed detection of different PCR DNA targets.

The limited extent of hybridisation with PCR DNA is likely to be due in part to the very long PCR fragments that are used, given that hybridisation rate has been shown to decrease with increasing target length. It is also possible that the limited hybridisation is due to poor yield of ssDNA following the NaOH-separation method. Excess biotinylated primers present in the initial PCR solution will also bind to the streptavidin sites on the magnetic beads, and therefore not all of the dsDNA will necessarily bind to the beads and some may be removed in wash steps prior to

denaturation. Although a higher volume of beads can be used to counteract this, they had restricted availability and therefore only a limited number of tests could be run. The amount of dsDNA in the original PCR sample was not quantified, nor was the amount of ssDNA created from this, therefore it is possible that the quantity of ssDNA used in the experiments was insufficient to allow a good extent of hybridisation.

CHAPTER 5: Discussion and Conclusions

According to the aims of this project, a nanoparticle assembly assay was successfully developed for the detection of specific sequences of DNA, consisting of oligonucleotide-functionalised silver nanoparticle and silver-coated magnetic nanoparticle probes, with SERS analysis. Following some optimisation steps, a stable assay was developed that was capable of detecting ~ 20 fmol of multiple target sequences individually. The assay is adaptable and can be modified to suit a wide variety of targets simply by changing the probe sequence and by using different Raman reporters. The multiplexing capability of the assay was demonstrated by evidence of a successful duplex, although this aspect of the assay was not developed further as the choice was made to instead focus on achieving successful hybridisation with longer DNA sequences, as outlined below. This research represents the first combination of oligonucleotide-functionalised AgNPs and Ag@MNPs in a sandwich assay for DNA detection by SERS.

The use of magnetic nanoparticles, allowing for easy removal of the hybridised assemblies from the bulk of solution and concentration into a very small volume, resulted in significant improvements in sensitivity compared with nanoparticle assembly in solution. However, although it was hoped that the use of a magnetic collection step combined with rinsing of the hybridised nanoparticles would eliminate the presence of dye signal in blank samples, this issue continued to be a concern. There are three possible reasons for this effect: i) dye leaching from the AgNP surface and becoming attached to the Ag@MNP surface during the hybridisation and magnetic collection stages; ii) unwanted interactions between the AgNP and Ag@MNP conjugates that result in some of the dyed AgNPs being collected alongside the Ag@MNPs, even in the absence of target; and iii) physical trapping of the AgNPs during magnetic collection of the Ag@MNPs.

Many attempts were made to identify the cause and reduce the background dye levels throughout the project. Improvements were made by changing the method used to produce the Ag@MNPs, and also by the addition of polyacrylic acid to the

Ag@MNP-oligonucleotide conjugates to make these more stable. Careful control of the concentration of dye added to the AgNP probe was also necessary. In addition, an increased hybridisation temperature was at times found to help, indicating that there was some level of non-specific hybridisation taking place between the probe DNA strands on different nanoparticle conjugates. However, the background dye levels could not be eliminated completely and the decision was taken to accept these in order to move forward with other aspects of the project, such as the detection of long target sequences. Nonetheless, it may be useful to carry out further work in this area in order to improve the levels of discrimination between a target and blank sample. This could include investigating the use of silica or polymer-coatings on one or both of the nanoparticles in order to reduce their interactions, as well as careful consideration of the dye used and how it is attached to the AgNP surface in order to minimise the possibility of leaching from the surface. Interestingly, two magnetic nanoparticle assembly assays developed by other research groups that resulted in very good levels of detection with very low background dye levels used very different methods of attaching both the oligonucleotide sequences and the Raman reporters to the nanoparticles than the methods used here.[89, 93] It is possible that these attachment methodologies, such as EDC coupling, could result in an increased level of assay stability, although other disadvantages may result due to the complicated and time-consuming steps involved.

Improvements were made to the nanoparticle conjugation process during the project, allowing a much faster and streamlined process, a higher yield of good quality conjugates, and much less wastage of expensive oligonucleotide sequences. The stability of the dye-labelled AgNP-oligonucleotide conjugates and the Ag@MNP-oligonucleotide conjugates was also assessed over a period of 11 months from preparation when stored in 10 mM phosphate buffer in a refrigerator. Both sets of conjugates were stable throughout this period, although some detachment of oligonucleotide from the nanoparticle surfaces was observed. This resulted in some reduction in the extent of hybridisation, particularly with low target concentrations, most likely as a result of the dissociated oligonucleotide sequences hybridising preferentially with target DNA and hence reducing the effective target concentration

available to hybridise with nanoparticle-bound probe DNA. Despite this, a good level of hybridisation with higher target concentrations was observed 11 months after conjugate preparation. A reduction in SERS enhancement was observed over time, particularly for low target concentrations, which indicates that there is also some dissociation of the Raman reporter from the AgNP surface during storage. It is possible that this effect is worse for certain bonding groups, e.g. dyes bound through the isothiocyanate moiety may be more susceptible to dissociation than benzotriazole dyes, although further work would be required to verify this. These stability results tie in with the issue of background dye levels found in blank samples as discussed in the preceding paragraph, and again highlight the importance of careful consideration of the methodology used to attach ligands to nanoparticle surfaces.

One of the project aims was to develop a closed-tube assay, i.e. there was to be no additional sample handling or manual manipulation steps once the target was added to the testing vessel. The reason for this is that, if successful, the assay may be developed into a fully automated system that can be commercialised. In the work presented in this report, samples were generally prepared in Eppendorf tubes and then transferred to a capillary tube for magnetic collection, washing and SERS analysis following the hybridisation period. This was done to maximise the number of samples that could be prepared and analysed within a working day during the research phase. However, it was demonstrated during the project that samples can also be prepared inside the capillary tube without any change in the outcome, although the sample needs time to hybridise prior to application of the external magnet. The assay also used a simple flow cell composed of a glass capillary tube as it is simple, cheap and disposable. It should be possible to design instrumentation incorporating the key characteristics of these components, with automated wash steps and using an electromagnet to allow magnetic collection when required. The developed assay can therefore be considered as essentially a closed-tube assay. Furthermore, although most experiments allowed a 60 min hybridisation period with a 20 min magnetic collection, both of these times could be reduced providing the target concentration was sufficiently high and with automatic laser focussing during

sample analysis. It is expected that a period of one hour between addition of sample to the probes and the reporting of a result is a realistic estimate.

The development of the assay as discussed so far relates to the use of two 12-mer probes, hybridising to short (24-base) sequences of target DNA in a head-to-tail orientation. However, when the assay was applied to longer target sequences, a significant reduction in the rate and extent of hybridisation was observed, which worsened as the length of the target sequence was increased. This led to an investigation into the factors affecting the hybridisation and nanoparticle assembly processes, including probe length / orientation and buffer effects. It was hoped that longer probe sequences hybridised in a tail-to-tail orientation would lead to improved hybridisation with longer targets due to reduced steric hindrance, and this in fact proved to be the case, although the creation of longer duplexes was a strongly contributing factor too. Another amendment to the assay at this point involved the addition of polymers to the buffer to act as hybridisation accelerants, essentially by taking up space and thus forcing the probes and target into closer proximity and hence more likely to hybridise. Dextran sulfate and PEG 10,000 were both found to result in a significant improvement in the rate and extent of nanoparticle assembly upon hybridisation with long target sequences and, although both have previously been used in gold nanoparticle assays, to the best of knowledge this is the first time they have been used in a silver nanoparticle assay.

The changes to buffer, combined with the improvements made to the probe length and orientation, resulted in significant improvements in the rate and extent of hybridisation of the nanoparticle conjugates with long target sequences, based on the assessment of synthetic targets up to 144 bases in length. For the sequences investigated, two 24-mer probes hybridised in a tail-to-tail orientation were found to give the best level of hybridisation with long target sequences, through the creation of more base-pair interactions and reduced electrostatic and steric interactions within the system. This hybridisation was reduced when two 30-mer probes were used, which is likely due to slower diffusion of the conjugates and potential strand-strand interactions and secondary structure effects in the probe DNA. The surface coverage

of different lengths of probe DNA on the nanoparticles may also be a contributing factor, although further work would be required both to calculate the different loading values and to determine whether this was a contributing factor. For short target sequences, maximum hybridisation was achieved when the combined probe DNA length exactly matched the length of the target DNA, highlighting the range of complex interactions that take place in a nanoparticle assembly assay. This research appears to be the first to look in detail at the combined effects of probe length and configuration on the kinetics and thermodynamics of hybridisation with varying lengths of target within a nanoparticle assembly assay. The resultant information is an important contribution towards further development of nanoparticle assembly assays to allow detection of clinically relevant samples of target DNA.

Although the formation of nanoparticle assemblies between two 24-mer probes and long target sequences has now been clearly demonstrated, it was unclear whether this would translate into strong SERS enhancement since the distance between two nanoparticles with a 24-24 tail-to-tail probe combination is much greater than for a 12-12 head-to-tail combination. Indeed it has been shown that sub-nanometre separation between nanoparticles is crucial in order to achieve maximum SERS enhancement.[34, 36] Despite this, strong SERS enhancement was achieved with all of the probe combinations investigated, with differences in enhancement more likely to be a result of differences in the extent of hybridisation, rather than being related to nanoparticle separation. It is possible that when the nanoparticle assemblies are magnetically collected, the force of the external magnet is sufficient to disrupt the normal nanoparticle spacing within the assemblies, which could place the nanoparticles in sufficiently close proximity to allow strong SERS enhancement. Alternatively, it may simply be that the three-dimensional network of assemblies that form places a number of nanoparticles sufficiently close to one another to form enough hot spots to give good SERS enhancement, although for suspension-based measurements, reduced SERS enhancement was observed for increased nanoparticle separations.

The optimised assay conditions allowed very sensitive SERS detection of long target sequences with no spectral interference, with reliable detection of ~ 5 fmol of two different synthetic target sequences of 144-bases and 150-bases in length. The assay was also used to successfully detect PCR-amplified plasmid DNA specific to two different fungal species: a 252 bp sequence from *A. fumigatus* and a 382 bp sequence from *C. krusei*. In each case, > 3:1 SERS enhancement was achieved for each of these targets compared with a negative control sample. However, only a limited extent of hybridisation was observed and this will need to be improved before the assay can be used for robust detection of DNA from clinical samples, particularly in a multiplexed platform. The limited hybridisation is likely to be due in part to the very long sequences of PCR DNA used, with hybridisation appearing to be better with the shorter *A. fumigatus* amplicon than with the *C. krusei* amplicon. While shorter PCR fragments would be preferred, the sequences used were those supplied by RDL and could not be easily changed.

In order to further improve hybridisation with these very long DNA sequences, it may be necessary to use higher concentration of hybridisation accelerant in the buffer, as this has been shown in this report to increase the rate and extent of hybridisation. Unfortunately, the nanoparticle conjugates also become increasingly unstable, most likely due to increased non-specific hybridisation of oligonucleotide bases within the conjugates. Some evidence has been provided that the use of 'short internal complement' DNA may be useful as a way of preventing these non-specific hybridisations by acting as blocking sequences on the probe strands, which may then allow the use of higher polymer concentrations and hence higher rates of hybridisation with long target sequences. However, further work will be necessary to investigate this as only preliminary experimentation was carried out in this project due to time constraints. Factors that will need to be considered include the ratio of sicDNA to probe DNA; the optimal conditions to use for annealing and whether to centrifuge and re-disperse the annealed conjugates before use; the stability of the annealed probes; and the optimal length of sicDNA and its position relative to the probe DNA.

While nanoparticle-based SERS assays have been successfully applied to the detection of PCR DNA, this has so far not been achieved with a true nanoparticle assembly assay without using a microarray format. This is likely due to the effects of electrostatic and steric repulsion that result from the combination of large nanoparticles and long target sequences, which makes two-probe hybridisation with clinical targets very difficult. The work presented here therefore represents a step forward in capability within this area, and moves this technology closer to the point where it can be used in a multiplexed commercial platform.

CHAPTER 6: Experimental

6.1 Materials

6.1.1 Chemicals

All chemicals were supplied by Sigma-Aldrich, unless otherwise specified. 4-MP and RB.ITC provided by Sigma, MG.ITC provided by Life Technologies, and RB1 prepared in-house (previous student).[105] Double distilled and deionised water was used for all stages of sample preparation and analysis.

6.1.2 Buffer Preparation

60 mM phosphate buffer prepared by adding 60 mM aqueous sodium di-hydrogen phosphate (Fluka) to 100 mL of 60 mM aqueous di-sodium hydrogen phosphate (Fluka) until pH 7.3 reached. Phosphate buffered saline (PBS, 0.3 M, pH 7) prepared by combining 60 mM phosphate buffer with 2 M sodium chloride (BDH) to give a solution containing 10 mM phosphate and 0.3 M sodium chloride. Different concentrations of PBS prepared by altering the final concentration of sodium chloride in the buffer, with the final phosphate concentration remaining constant at 10 mM. PBS and phosphate buffers stored in a fridge and prepared fresh as required.

Dextran sulfate sodium salt from Leuconostoc spp. (average MW > 500,000) provided by Sigma-Aldrich. Polyethylene glycol (PEG) 10,000 provided by Fluka, PEG 2,000 provided by Alfa Aesar. Dextran sulfate and PEG buffers prepared by combining a mass of polymer to a volume of 0.3 M PBS to achieve the required percentage weight of polymer per unit volume of PBS; buffers containing polymers stored in a fridge and prepared fresh weekly.

20 x saline-sodium citrate (SSC) buffer consists of 3 M sodium chloride with 300 mM trisodium citrate. Buffer prepared by combining 50 mL of 6 M sodium chloride with 30 mL of 1 M sodium citrate, pH adjusted to 7.0 with hydrochloric acid and total volume adjusted to 100 mL with water. 1 x SSC prepared as a 1:20 dilution

of this. 10 x Tris-EDTA (TE) buffer consists of 100 mM Tris hydrochloride with 10 mM ethylenediaminetetraacetic acid (EDTA), prepared by combining 50 mL of each, adjusted to pH 7.5 with sodium hydroxide. 1 x TE buffer prepared as a 1:10 dilution of this.

6.2 Probe and Target Oligonucleotides

6.2.1 In-House Synthesis and Purification of Oligonucleotide Sequences

The model probe and target sequences referred to in Chapter 2 were synthesised and purified in-house. All reagents, phosphoramidites, linkers and spacers used for oligonucleotide synthesis were provided by Link Technologies, Bellshill.

i) Oligonucleotide Synthesis

Oligonucleotide synthesis was automated and was based on the use of DNA phosphoramidite nucleosides modified with a 4,4'-dimethoxytrityl protecting group on the 5'-OH, a β-cyanoethyl-protected 3'-phosphite, and appropriate protecting groups to protect the reactive primary amines in the heterocyclic nucleobases. The synthesis cycle consisted of four steps: deblocking (detritylation); activation/coupling; capping; and oxidation. Synthesis occurred in the 3' → 5' direction. Oligonucleotide sequences were synthesised on controlled pore glass (CPG) solid support columns; all columns had the first base already attached. 1 µmol columns were used for probe sequences and 1 µmol or 200 nmol columns were used for synthesis of the target or non-complementary sequences.

Once the automated synthesis was complete, the columns were removed from the instrument. Simultaneous cleavage of the sequences from the solid support and deprotection of the bases was carried out using ammonia: a syringe was attached at each end of the column and ammonia (1 mL) pushed through several times then left for at least an hour; the ammonia/ oligonucleotide mixture was transferred to a 2 mL plastic screw-cap vial, along with further ammonia (600-700 µL) used to wash out the syringe/column assembly; the vial was placed in a 45 °C heating block overnight

then the contents transferred to a 50 mL silanised round bottom flask and the ammonia removed by rotary evaporation; the remaining oligonucleotide was reconstituted in distilled water (1 mL) and transferred to an Eppendorf tube, ready for purification.

ii) Oligonucleotide Purification

Either two or three High Performance Liquid Chromatography (HPLC) steps were required for each synthesised DNA sequence. The first purification step used anion exchange HPLC with UV detection to separate the successful oligonucleotide sequences from failure sequences; the successful sequence was the final large peak. A gradient elution separation was carried out using 0.375 M sodium perchlorate, 0.25 M Tris buffer (pH 8) and water as eluents, at a total constant flow rate of 3 mL/min and a 27 min run-time. All HPLC buffers and eluents were filtered using Whatman nylon membrane filters (0.45 µm, 47 mm) immediately prior to using. A Resource Q 1 mL column was used for separation. Sequences were collected in a round bottom flask then the water removed using rotary evaporation and the sample re-suspended in distilled water (1.5 mL).

The above purification step introduced salt ions into the sample, which then had to be removed using size exclusion HPLC with UV and conductivity detection. This was an isocratic method using only water as the eluent at a flow rate of 3 mL/min and a 5 min run-time. A Sephadex Superfine desalting column was used and the target sequence was the first large peak. Samples were injected in 2 portions and the collections combined, then evaporated to dryness using rotary evaporation. For unmodified target and nonsense sequences, samples were reconstituted in distilled water (1 mL) and analysed by UV-Vis spectroscopy to determine concentration. For 5'-thiol modified sequences (i.e. both model probe sequences) samples were reconstituted in triethylammonium acetate, TEAA (0.1 M, 600 µL, pH 8) and then taken through a further step (see below).

5'-thiol modified sequences have a trityl group attached that needs to be removed through precipitation with silver nitrate in the presence of TEAA. Silver nitrate (1 M,

90 µL) was added to the oligonucleotide sequence, currently dissolved in 600 µL of TEAA (from previous step). The sample was vortexed briefly then left for 30 min at room temperature. Dithiothreitol (DTT, 1 M, 138 µL) was then added and the sample vortexed for 30 sec, left for 15 min, then centrifuged at 4,100 x g for 10 min and the supernatant collected. The remaining pellet was re-suspended in TEAA (500 µL), vortexed, centrifuged again, and the supernatant combined with the previous aliquot. This process was repeated twice more and all four supernatants combined. The sample was then purified by size exclusion HPLC with conductivity detection, using the exact same conditions as in the previous HPLC step, in order to remove the DTT and TEAA. Finally, the sample was evaporated to dryness using rotary evaporation then reconstituted in distilled water (1 mL) and analysed by UV-Vis spectroscopy to determine concentration.

iii) Determination of Oligonucleotide Concentrations

The concentration of the synthesised oligonucleotide sequences was determined using UV-Vis spectroscopy, based on the oligonucleotide maximum absorbance at ~ 260 nm. The purified sequence, currently dissolved in 1 mL distilled water, was added to a glass micro-cuvette, diluted with water, and its absorbance measured in the range 200-500 nm. The concentration was calculated using the Beer-Lambert equation:

$$A = \varepsilon l c$$

where: A = measured absorbance; ε = molar extinction coefficient ($M^{-1}cm^{-1}$); l = path length (cm, always 1 cm for the cuvettes used); and c = sample concentration (M). The dilution factor must also be taken into account in the calculation. The molar extinction coefficient (ε) for each of the oligonucleotide bases is as follows: A = 15,200 $M^{-1}cm^{-1}$; C = 7,050 $M^{-1}cm^{-1}$; G = 12,010 $M^{-1}cm^{-1}$; T = 8,400 $M^{-1}cm^{-1}$.

The molar extinction coefficient for the sequence of interest is determined by adding the total ε value for all bases in the sequence and multiplying by 0.9 (the hypochromicity factor, related to the different orientation of the bases). For example, the calculated ε value for the model probe 1 sequence [HS-$(HEG)_3$-CCTTAGTCCCTG] is 97,263 $M^{-1}cm^{-1}$. Most oligonucleotide modifications, such as

HEG spacer and thiol groups, do not have an associated ε value. The calculated concentration was used to determine the volume of probe sequence required to make nanoparticle conjugates, and the volume of target or non-complementary sequence required in hybridisation experiments.

6.2.2 Synthetic DNA Purchased Externally

Excepting those model sequences as detailed in the previous section, all synthetic oligonucleotide sequences used for probes and targets were purchased either from Integrated DNA Technologies, Inc. (IDT, USA), or from AtdBio (Southampton). Probe and target sequences were received in a lyophilised form; target sequences were reconstituted in buffer and used without further purification. Probe sequences were treated with DTT and purified by HPLC before use, to ensure that any disulfide bridges between the thiolated probe sequences were broken. In this procedure, the lyophilised oligonucleotide sequence was reconstituted in phosphate buffer (60 mM, 0.5 mL, pH 8.5) and added to a solution of dithiothreitol (15 mg in 0.5 mL water), mixed thoroughly and left for 1 h. The sample was then purified by size exclusion HPLC with conductivity detection, using the same conditions as detailed in the previous section, in order to remove the DTT. Finally, the sample was evaporated to near dryness using rotary evaporation then reconstituted in distilled water (1 mL) and analysed by UV-Vis spectroscopy to determine concentration.

6.2.3 PCR DNA

Aliquots of PCR-amplified plasmid DNA (50 µL) were supplied by Renishaw Diagnostics Ltd. Information on DNA concentration was not supplied, but based on 10^3 input copy number and 45 amplification cycles, an estimate of 1 mM target DNA per 50 µL aliquot was calculated (see section 4.1.2).

The target strands of 252 bp *A. fumigatus* and 382 bp *C. krusei* PCR sequences are shown below, where the primer regions are highlighted in blue and the sections that hybridise with the 18-18 tail-to-tail probes are underlined:

A. fumigatus PCR DNA:

5'- GCG TTC CTC GGT CCA GGC AGG CCG CAT TGC ACC CTC GGC TAT AAG ACA CCC CGA GAG GTG ATA CAT TCC GAG GGC CTT TGA CCG GCC GCC CAA ACC GAC GCT GGC CCG CCC ACG GGG AAG TAC ACC GGC ACG AAT GCC GGC TGA ACC CCG CGG GCG AGT CTG GTC GCA AAC GCT TCC CTT TCA ACA ATT TCA CGT GCT GTT TAA CTC TCT TTT CAA AGT GCT TTT CAT CTT TCG ATC ACT CTA CTT GTG CGC -3'

C. krusei PCR DNA:

5'- GAC AAT ATA TAA CGA TAC AGG GCC TTT GGT CTT GTA ATT GGA ATG AGT ACA ATG TAA ATA CCT TAA CGA GGA TCA ATT GGA GGG CAA GTC TGG TGC CAG CAG CCG CGG NAA TTC CAG CTC CAA TAG CGT ATA TTA AAG TTG TTG CAG TTA AAA AGC TCG TAG TTG AAC TTT GGG CCT GGG CGG ACG GTC TAC CTA TGG TAA GCA CTG TTG CGG CCG GGT CTT TCC TTC TGG CTA SCC TCG GGC GAA CCA GGA CGA TTA CTT TGA GGA AAT TAG AGT GTT CAA AGC AGG CCT TTG CTC GGA TAT ATT AGC ATG GAA TAA TAG AAT AGG ACG CAT GGT TCT ATT TTG TTN GTT TCT AGG ACC ATC GTA ATG ATT AAT AGG GAC G -3'

'S' and 'N' denote unknown bases: S effectively means G or C, but the actual base has not been determined for that particular accession code; N means no data could be obtained, therefore this base could be A, T, C or G. For this work, the underlined 'S' in the *C. krusei* sequence was taken to be G.

PCR dsDNA was converted to ssDNA according to the following procedure[d]: 200 µL streptavidin-coated magnetic beads (4 mg/mL, supplied by New England BioLabs Inc.) added to an Eppendorf tube, magnetically precipitated and redispersed in 1 x SSC buffer (100 µL). 20 µL of a 1:10 dilution of PCR DNA added and left on shaker for 1 h, then beads magnetically precipitated and re-dispersed in 1 x SSC

[d] Following a method detailed on the Life technologies website: http://www.lifetechnologies.com/uk/en/home/brands/product-brand/dynal/streptavidin-coupled-dynabeads/dynabeads-streptavidin.html#10 accessed 14th April 2015

buffer (100 µL). Beads magnetically precipitated twice more, with final re-dispersal in freshly prepared sodium hydroxide (0.15 M, 50 µL). Beads left in sodium hydroxide for 10 min only, then supernatant transferred to fresh Eppendorf tube and neutralised with 10 x TE buffer (pH 7.5, 9.5 µL) and acetic acid (1.25 M, 4.2 µL); this contains the non-biotinylated DNA strand. The remaining magnetic beads then washed once with sodium hydroxide (0.15 M, 100 µL), twice with 1 x TE buffer (100 µL), once with 1 x SSC (100 µL), then stored in 1 x SSC (100 µL); this contains the biotinylated DNA strand.

6.3 Nanoparticle Synthesis

6.3.1 Synthesis of Silver Colloid

i) Citrate-Reduction

Silver nanoparticle synthesis was carried out according to a modified Lee and Meisel method [31]. 500 mL water was added to a round bottom flask and heated to 45 °C using a Bunsen burner, then silver nitrate (90 mg in 10 mL water) was added and heated rapidly to boiling with vigorous stirring. Sodium citrate was then added (100 mg in 10 mL water) and the solution kept boiling for 30 min with vigorous stirring, then allowed to cool to room temperature. The nanoparticles were used without further purification. All glassware used for nanoparticle synthesis was first soaked in aqua regia (a 1:3 ratio mixture of concentrated nitric acid and hydrochloric acid) for at least 2 h and rinsed thoroughly with distilled water.

ii) Hydroxylamine Reduction

Production of AgNPs by hydroxylamine-reduction was carried out according to a procedure described by Leopold *et al.*[33] 89 mL of water was added to a conical flask along with freshly prepared aqueous sodium hydroxide (12.0 mg in 1 mL water) and hydroxylamine hydrochloride (10.7 mg). Silver nitrate (17.0 mg in 10 mL water) was added dropwise, with vigorous stirring of the solution throughout. The nanoparticles were used without further purification.

6.3.2 Synthesis of Magnetic Nanoparticles (MNPs)

Maghemite (γ-Fe_2O_3) MNPs were prepared by co-precipitation, following a method used by Kumar *et al.*[80]: iron(II) chloride tetrahydrate (1.98 g), iron(III) chloride hexahydrate (5.335 g) and concentrated hydrochloric acid (821 µL) were combined and made up to 25 mL with distilled water, giving an aqueous solution containing 0.4 M Fe^{2+}, 0.8 M Fe^{3+} and 0.4 M HCl. Sodium hydroxide (15.058 g) was added to a round-bottom flask along with 250 mL distilled water and heated to 50 °C on a heating mantle. The acidified iron salt solution was then added drop-wise with vigorous stirring and a black precipitate formed immediately. Stirring was continued for a further 20 min at 50 °C, then the solution left to settle and cool. The black precipitate (magnetite, Fe_3O_4) was washed twice with distilled water and once with 0.1 M nitric acid, then a further 125 mL of 0.1 M nitric acid added and the solution heated to 95 °C in a round bottom flask, with constant stirring, for 40 min. The resultant reddish-brown solution was centrifuged three times in total and the precipitate re-suspended in distilled water; this produced the stock maghemite MNPs.

6.3.3 Synthesis of Silver-Coated Magnetic Nanoparticles (Ag@MNPs)

i) Hydrazine Reduction

Stock maghemite (2 mL), distilled water (8 mL) and sodium citrate (1%, 250 µL) were added to a 4-dram vial. Silver nitrate (1% aqueous, 200 µL) was added after 15 min, followed by hydrazine hydrate (0.2 M, 25 µL, Fisher Scientific) after a further 5 min. A further 2 aliquots of hydrazine hydrate and silver nitrate were added in the same way, with 10 min between additions. The reactions were carried out under constant ultra-sonication. A final aliquot of sodium citrate (1%, 200 µL) was added and the vial sonicated for a further 20 min. The resultant sample was purified by two centrifugation steps followed by magnetic separation; these magnetically-collected nanoparticles were used for analysis and conjugate preparation[e].

[e] Note, when the reaction was carried out without any maghemite, silver nanoparticles were formed via hydrazine reduction. However, it seems that in the presence of maghemite the major product is Ag@MNPs since, following magnetic separation, the supernatant was almost clear.

ii) Glucose Reduction

In this procedure, Ag@MNPs were prepared using a glucose-reduction method, adapted from that used by Mandal *et al.*[100]: 1 mL stock MNPs were added to a screw-cap glass vial along with glucose (0.25 g), water (4 mL), and silver nitrate (1%, 1.5 mL). The mixture was sonicated for 10 min and then heated to 90 °C and held at this temperature for 90 min while rotating. The resultant Ag@MNPs were centrifuged three times and redispersed in sodium citrate (5 mM, 6 mL). Note that magnetic collection of a solution of the synthesised Ag@MNPs resulted in a clear supernatant, indicating that no non-magnetic silver nanoparticles were formed during reduction of the silver nitrate.

6.4 Conjugation of Nanoparticles with DNA and Raman Reporters

6.4.1 Slow Salt-ageing Method

Stock AgNPs (e.g. 0.6 nM, 1.5 mL) and distilled water (1.5 mL) were added to a 4-dram vial and 10 nmol of thiol-modified oligonucleotide sequence added, shaken gently then left in a dark cupboard overnight. A volume of phosphate buffer (60 mM, pH 7.3) was added to the sample such that the final buffer concentration was 10 mM, then the sample shaken gently and left in a cupboard overnight. A volume of 2 M sodium chloride was then added such that the final concentration in the vial was 0.05 M, and the sample left overnight. This same salt addition was repeated the next day such that the total concentration of salt in the sample was 0.1 M, and the sample again left in the dark overnight. The sample was then centrifuged at 3,400 x g for 20 min and re-suspended in PBS (0.3 M, pH 7, 500 µL). If required, a Raman reporter (e.g. RB.ITC, $1x10^{-6}$ M in PBS, 250 µL) was then added to the sample and shaken gently. The sample was stored in a dark cupboard overnight then centrifuged at 3,400 x g for 20 min and re-suspended in 1 mL PBS. The concentration of the final conjugate was determined using UV-Vis spectroscopy. Conjugation of Ag@MNPs with DNA was carried out in the same way except that no Raman reporter was added in the final step.

6.4.2 Fast, Low pH Method

The method used was adapted from that developed by Zhang *et al.*[101]: silver nanoparticles (e.g. 321 pM, 1 mL) and thiol-modified probe oligonucleotide sequence (e.g. 21.6 µM, 44.6 µL, 3000:1 ratio) were added to an Eppendorf tube, followed by 2 aliquots of 500 mM citrate.HCl buffer (20 µL each, 10 min gap between additions). Samples were left for 40 min then HEPES buffer (500 mM, 60 µL) and sodium chloride (2 M, 200 µL) were added, the samples left for a further 45 min then centrifuged and re-suspended in phosphate buffer (10 mM, 0.5 mL). If required, the Raman reporter was then added at, typically, a 1000:1 ratio (e.g. 10 µM, 60.8 µL), left overnight then the conjugate centrifuged twice more and stored in the fridge in phosphate buffer (10 mM, 0.5 mL). Conjugation of Ag@MNPs with DNA was carried out in the same way except that the conjugates were re-suspended in a combination of phosphate buffer (10 mM, 800 µL) and polyacrylic acid (10 mM, 200 µL), and also no Raman reporter was added in the final step.

6.5 Instrumentation

• A MerMade 6 instrument by BioAutomation Corporation was used for DNA Synthesis, and purification was carried out using a Dionex HPLC instrument with a P680 HPLC Pump, a UVD170U UV detector, and a CD20 Conductivity Detector.

• A Varian Cary 300Bio UV-Visible Spectrophotometer with Temperature Controller attached was used for all UV-Vis measurements, with Cary software used for data analysis.

• An inVia Raman Microscope by Renishaw, fitted with a 514 nm Flexible Laser Solutions Modu-Laser and a Leica DMLM microscope platform was used for all SERS measurements. All Raman data interpretation was carried out using GRAMS AI software.

• The dynamic light scattering (DLS) instrument used was a Zetasizer Nano series by Malvern.

• For fluorescence measurements, a Stratagene Mx3005P instrument from Agilent Technologies was used. A TAMRA filter set was used for Cy3 fluorescence measurements with an excitation wavelength of 556 nm and an emission wavelength of 580 nm.

• Scanning electron microscope (SEM) images were obtained using a FEI Sirion 200 ultra-high resolution Schottky field emission scanning electron microscope with FEI software.

6.6 Characterisation of Nanoparticles and Conjugates

6.6.1 Determination of Concentrations

The concentration of the synthesised nanoparticles and their conjugates was determined using UV-Vis spectroscopy and the Beer-Lambert equation as detailed previously (Section 6.2.1), based on the nanoparticle/conjugate maximum extinction at ~ 400 nm. In this case, the molar extinction coefficient (ε) value used was 2.87×10^{10} $M^{-1}cm^{-1}$, which is the molar extinction coefficient for 40 nm diameter silver nanoparticles with a λ_{max} of 400 nm.[95] This same calculation was used to determine the concentration of AgNPs and Ag@MNPs, in both the conjugated and non-conjugated form. The calculated concentrations were used to determine the quantity of oligonucleotide probe to add during conjugation, and also the volume of nanoparticle conjugates required in hybridisation experiments.

In order to confirm that the correct ε value has been applied and the correct nanoparticle concentration has been calculated, the number of Ag nanoparticles can be compared based on two different measurements: values calculated from concentration measurements and those calculated from the numbers of Ag atoms used during conjugate synthesis. These values are shown below for the two batches of AgNPs detailed in Chapter 2 (section 2.2.2), i.e. citrate-reduced AgNPs of 39 ± 9 nm diameter and a concentration of 608 pM, and hydroxylamine-reduced AgNPs of 48 ± 10 nm diameter and a concentration of 321 pM.

The number of Ag atoms per nanoparticle (N) is calculated as:

$$N = N_A(\pi\rho D^3/6M)$$

Where:

ρ = density of face centred cubic silver = 10.5 g cm^{-3} = 1.05 x10^{-20} g nm^{-3}

D = average diameter of NPs (nm)

M = atomic mass of Ag (= 107.87 g mol^{-1})

N_A = no. of atoms per mole (= 6.022 x10^{23} atoms/mol)

So for a 39 nm diameter AgNP, number of atoms per NP = 1.821 x10^6
Or for a 48 nm diameter AgNP, number of atoms per NP = 3.394 x10^6

For hydroxylamine-reduced AgNPs:

17.0 mg $AgNO_3$ used during AgNP synthesis, i.e. 10.7947 mg of Ag ions (63.49% by mass of $AgNO_3$ is Ag^+), i.e. 1.0007 x10^{-4} moles of Ag, i.e. = 6.026 x10^{19} atoms of Ag. If each AgNP contains 3.394 x10^6Ag atoms (as calculated above for 48 nm diameter AgNP), then there must be a total of 1.7755 x10^{13} AgNPs.

To determine the value based on the concentration of colloid produced: for 321 pM AgNPs, in 100 mL total volume have 3.21 x 10^{-11} moles of AgNPs in total, therefore the synthesised colloid contains 1.9331x10^{13} AgNPs in total, very similar to the value calculated based on quantity of $AgNO_3$ used during synthesis (< 10% difference).

For citrate-reduced AgNPs:

90.0 mg $AgNO_3$ used during AgNP synthesis, i.e. 0.057141g Ag ions, i.e. 5.2972 x10^{-4} moles of Ag, i.e. 3.190 x10^{20} atoms of Ag. If each AgNP contains 1.821 x10^6 Ag atoms (as calculated above for 39 nm diameter AgNP), then there must be a total of 1.752x10^{14} AgNPs.

To determine the value based on the concentration of colloid produced: for 608 pM AgNPs, in 520 mL total volume have 3.1616 x10^{-10} moles of AgNPs in total, therefore the synthesised colloid contains 1.9039 x10^{14} AgNPs in total, very similar

to the value calculated based on quantity of $AgNO_3$ used during synthesis (< 10% difference).

6.6.2 Calculation of Number of Oligonucleotides per Nanoparticle

A fluorescent dye-labelled thiol-modified 12-base probe sequence [HS-Cy3-$(HEG)_3$-TCTCAACTCGTA] was attached to hydroxylamine-reduced AgNPs following the standard fast, low-pH conjugation procedure. A 3000:1 probe:AgNP ratio was used, and the sample was centrifuged and re-dispersed in 10 mM phosphate buffer 3 times at the end of conjugation to ensure adequate removal of any unbound probe from the matrix. The concentration of the conjugate was determined by extinction spectroscopy.

To remove the dye-labelled oligonucleotide sequence from the conjugate, a 100 µL aliquot of conjugate was added to a 100 µL solution of 1.0 M dithiothreitol (DTT) in 0.18 M phosphate buffer (pH 8.0) and left on a shaker overnight. Three separate samples were prepared in the same way to ensure accuracy in the calculated value. By the next morning, all of the AgNPs had aggregated and dropped to the bottom of the Eppendorf tubes, indicating that the oligonucleotide probes had become detached from the nanoparticle surface. The samples were centrifuged for 20 min at 4,800 x g and the supernatants transferred to fresh vials; these samples contained the detached dye-labelled probe sequence. For fluorescence measurements, 50 µL aliquots of these supernatant solutions were analysed in triplicate and compared with control samples. Cy3 has an excitation wavelength of 550 nm and an emission wavelength of 580 nm.

A stock calibration solution was prepared by adding stock probe sequence (19.36 µM, 20 µL) to phosphate buffer (10 mM, 80 µL); this solution contains 387.2 pmol of probe sequence in 100 µL, i.e. 96.8 pmol per 25 µL aliquot. Further dilutions of this stock were prepared, all in 10 mM phosphate buffer, to provide a range of calibration solutions. For fluorescence measurements, 25 µL of each of the calibration solutions was mixed with 25 µL of a solution of 1.0 M DTT in 0.18 M phosphate buffer. Analysis of these control samples produced a plot of fluorescence

signal vs. quantity of probe sequence per 25 µL aliquot; the measured fluorescence level from the detached probe samples was then compared with this to determine the quantity of probe sequence in these aliquots. This was then compared with the concentration of nanoparticle-probe conjugate in the equivalent sample volume, as determined from extinction spectroscopy, to determine the number of DNA probes per individual silver nanoparticle.

6.7 SERS Analysis

Samples were typically prepared according to the following procedure, any deviations from this are as detailed in the main text: samples were made up to a total volume of 10 µL in hybridisation buffer, containing AgNP-P1-reporter conjugate, Ag@MNP-P2 conjugate, target or non-complementary sequence, and buffer. Samples were left to hybridise for one hour at room temperature then transferred to a glass capillary tube with a rare earth magnet fixed underneath. A magnetic plug was allowed to collect for a period of 20 min, with occasional mixing of the solution back and forth, then PBS buffer (0.3 M, 1 mL) was pumped through the capillary, using a length of silicon tubing attached to the end of the capillary and fixed to a peristaltic pump.

Samples were analysed through the capillary tube using x20 magnification lens and with a manually-adjusted laser focal point. 5 x 1 s accumulations were obtained at 100% laser power (unfocused laser power at sample = 22.5 mW), 514 nm laser, and 3 replicate measurements were obtained for each sample. The number of separately prepared samples (*n*) of each type varied, and is as detailed in the main text. All spectra shown are the average of 3 replicate measurements obtained from *n* different samples of the same type (e.g. same target concentration). Error bars represent ± one standard deviation. The reported SERS spectra have not been background-corrected, although they may have been stacked to allow a visual separation of overlapping peaks.

6.8 Reaction Kinetics Experiments

Experiments were carried out by combining AgNP-P1 and AgNP-P2 or Ag@MNP-P2 conjugates (e.g. 10 pM of each) with a certain concentration of target (e.g. 1 nM) and the correct hybridisation buffer to a total volume of 800 µL in a quartz cuvette. Spectra were collected every 10 min over a certain time period, typically 90 min, starting immediately after target addition. One spectrum consisted of a scan across the wavelength range 200-800 nm (or at times from 350-800 nm due to instrumentation problems) with extinction values monitored at 1 nm increments throughout this range. Hybridisation experiments were generally carried out at room temperature, unless otherwise stated; for the results detailed in Chapter 3, samples were maintained at 25 °C throughout each experiment. All spectra were converted to Excel for data analysis.

6.9 Melting Temperature (T_m) Measurements

Samples were prepared in the same way as for the reaction kinetics experiments and were left to hybridise for a period of time, typically 2 or 3 h, before analysis. Melting transition measurements were then carried out, and involved heating the samples from 25-70 °C (or 25-90 °C for samples with higher melting temperatures) at 1 °C/min while monitoring the extinction at either 405 nm (for samples containing AgNP-P1 and Ag@MNP-P2 conjugates) or 410 nm (for samples containing AgNP-P1 and AgNP-P2 conjugates). All spectra were converted to Excel for data analysis, and melting temperature values were taken as the maximum of the first derivative of the melting transition.

6.10 SEM Sample Preparation

The SEM samples were prepared on silicon wafers as follows: the wafers were first washed with a methanol-soaked swab and placed in an oxygen plasma cleaner for 90 seconds. A positive surface charge was then created by applying a few drops of a

solution of poly (diallyldimethylammonium chloride) (PDDA, 10 μL, Sigma Aldrich) in sodium chloride (1 mL, 1 mM) to cover the wafer surface for 20 min, before rinsing with water and drying under a stream of nitrogen. A few drops of colloid were then applied to the wafer and left for 30 min, then removed and fresh colloid reapplied, before rinsing the wafer with water and drying under a stream of nitrogen. In the case of the hydroxylamine-reduced AgNPs shown in Figure 2.3, the PDDA-treated wafer was placed overnight in an Eppendorf tube containing 50 pM of AgNP-oligonucleotide conjugate then rinsed with water and dried under a stream of nitrogen. The diameter of the nanoparticles was measured from the SEM image using ImageJ software.

REFERENCES

1. C. R. Calladine, H. R. Drew, B. F. Luisi and A. A. Travers, *Understanding DNA: the molecule and how it works*, Elsevier Academic Press, Third edn., 2004.
2. L. Pray, *Nature Education*, 2008, **1**, 100.
3. *Nucleic Acids in Chemistry and Biology, Third Edition*, 2006.
4. Human Genome Project Information, http://www.ornl.gov/sci/techresources/Human_Genome/home.shtml, (accessed 4th July 2012).
5. G. D. Brown, D. W. Denning, N. A. R. Gow, S. M. Levitz, M. G. Netea and T. C. White, *Science Translational Medicine*, 2012, **4**.
6. G. D. Brown, D. W. Denning and S. M. Levitz, *Science*, 2012, **336**, 647-647.
7. E. M. Southern, *Journal of Molecular Biology*, 1975, **98**, 503-&.
8. K. Mullis, F. Faloona, S. Scharf, R. Saiki, G. Horn and H. Erlich, *Cold Spring Harbor Symposia on Quantitative Biology*, 1986, **51**, 263-273.
9. K. L. Muldrew, *Current Opinion in Pediatrics*, 2009, **21**, 102-111.
10. P. M. Holland, R. D. Abramson, R. Watson and D. H. Gelfand, *Proceedings of the National Academy of Sciences of the United States of America*, 1991, **88**, 7276-7280.
11. S. Tyagi and F. R. Kramer, *Nature Biotechnology*, 1996, **14**, 303-308.
12. N. Thelwell, S. Millington, A. Solinas, J. Booth and T. Brown, *Nucleic Acids Research*, 2000, **28**, 3752-3761.
13. D. Whitcombe, S. Kelly, J. Mann, J. Theaker, C. Jones and S. Little, *American Journal of Human Genetics*, 1999, **65**, A412-A412.
14. X. Jin, S. Yue, K. S. Wells and V. L. Singer, *Biophysical Journal*, 1994, **66**, A159-A159.
15. Y. Sun, F. Xu, Y. Zhang, Y. Shi, Z. Wen and Z. Li, *Journal of Materials Chemistry*, 2011, **21**, 16675-16685.
16. M. Harper, K. McKeating and K. Faulds, *Physical Chemistry Chemical Physics*, 2013, **15**, 5312-5328.
17. C. V. Raman and K. S. Krishnan, *Nature*, 1928, **121**, 501-502.
18. W. Smith, *Chemical Society Reviews*, 2008, **37**, 955-964.
19. M. Fleischmann, P. J. Hendra and A. J. McQuilla, *Chemical Physics Letters*, 1974, **26**, 163-166.

20. D. L. Jeanmaire and R. P. Vanduyne, *Journal of Electroanalytical Chemistry*, 1977, **84**, 1-20.
21. M. G. Albrecht and J. A. Creighton, *Journal of the American Chemical Society*, 1977, **99**, 5215-5217.
22. J. J. Laserna, *Analytica Chimica Acta*, 1993, **283**, 607-622.
23. J. A. Creighton, C. G. Blatchford and M. G. Albrecht, *Journal of the Chemical Society-Faraday Transactions Ii*, 1979, **75**, 790-798.
24. P. L. Stiles, J. A. Dieringer, N. C. Shah and R. R. Van Duyne, *Annual Review of Analytical Chemistry*, 2008, **1**, 601-626.
25. N. E. Motl, A. F. Smith, C. J. DeSantis and S. E. Skrabalak, *Chemical Society Reviews*, 2014, **43**, 3823-3834.
26. S. Schluecker, *Angewandte Chemie-International Edition*, 2014, **53**, 4756-4795.
27. S. Nie and S. Emory, *Science*, 1997, **275**, 1102-1106.
28. K. Kneipp, Y. Wang, H. Kneipp, L. Perelman, I. Itzkan, R. Dasari and M. Feld, *Physical Review Letters*, 1997, **78**, 1667-1670.
29. G. McNay, D. Eustace, W. E. Smith, K. Faulds and D. Graham, *Applied Spectroscopy*, 2011, **65**, 825-837.
30. M. Rycenga, C. M. Cobley, J. Zeng, W. Li, C. H. Moran, Q. Zhang, D. Qin and Y. Xia, *Chemical Reviews*, 2011, **111**, 3669-3712.
31. P. C. Lee and D. Meisel, *Journal of Physical Chemistry*, 1982, **86**, 3391-3395.
32. C. H. Munro, W. E. Smith, M. Garner, J. Clarkson and P. C. White, *Langmuir*, 1995, **11**, 3712-3720.
33. N. Leopold and B. Lendl, *Journal of Physical Chemistry B*, 2003, **107**, 5723-5727.
34. J. M. McMahon, A.-I. Henry, K. L. Wustholz, M. J. Natan, R. G. Freeman, R. P. Van Duyne and G. C. Schatz, *Analytical and Bioanalytical Chemistry*, 2009, **394**, 1819-1825.
35. I. Khan, D. Cunningham, R. E. Littleford, D. Graham, W. E. Smith and D. W. McComb, *Analytical Chemistry*, 2006, **78**, 224-230.
36. K. L. Wustholz, A.-I. Henry, J. M. McMahon, R. G. Freeman, N. Valley, M. E. Piotti, M. J. Natan, G. C. Schatz and R. P. Van Duyne, *Journal of the American Chemical Society*, 2010, **132**.
37. C. A. Mirkin, R. L. Letsinger, R. C. Mucic and J. J. Storhoff, *Nature*, 1996, **382**, 607-609.

38. A. Alivisatos, K. Johnsson, X. Peng, T. Wilson, C. Loweth, M. Bruchez and P. Schultz, *Nature*, 1996, **382**, 609-611.

39. R. Elghanian, J. J. Storhoff, R. C. Mucic, R. L. Letsinger and C. A. Mirkin, *Science*, 1997, **277**, 1078-1081.

40. J.-S. Lee, A. K. R. Lytton-Jean, S. J. Hurst and C. A. Mirkin, *Nano Letters*, 2007, **7**, 2112-2115.

41. J. J. Storhoff, R. Elghanian, R. C. Mucic, C. A. Mirkin and R. L. Letsinger, *Journal of the American Chemical Society*, 1998, **120**, 1959-1964.

42. R. Jin, G. Wu, Z. Li, C. Mirkin and G. Schatz, *Journal of the American Chemical Society*, 2003, **125**, 1643-1654.

43. J. Storhoff, A. Lazarides, R. Mucic, C. Mirkin, R. Letsinger and G. Schatz, *Journal of the American Chemical Society*, 2000, **122**, 4640-4650.

44. P. S. Randeria, M. R. Jones, K. L. Kohlstedt, R. J. Banga, M. O. de la Cruz, G. C. Schatz and C. A. Mirkin, *Journal of the American Chemical Society*, 2015, **137**, 3486-3489.

45. L. M. Demers, C. A. Mirkin, R. C. Mucic, R. A. Reynolds, R. L. Letsinger, R. Elghanian and G. Viswanadham, *Analytical Chemistry*, 2000, **72**, 5535-5541.

46. S. J. Hurst, A. K. R. Lytton-Jean and C. A. Mirkin, *Analytical Chemistry*, 2006, **78**, 8313-8318.

47. T. A. Taton, G. Lu and C. A. Mirkin, *Journal of the American Chemical Society*, 2001, **123**, 5164-5165.

48. Y. C. Cao, R. C. Jin, S. Thaxton and C. A. Mirkin, *Talanta*, 2005, **67**, 449-455.

49. J. J. Storhoff, A. D. Lucas, V. Garimella, Y. P. Bao and U. R. Muller, *Nature Biotechnology*, 2004, **22**, 883-887.

50. J. J. Storhoff, S. S. Marla, P. Bao, S. Hagenow, H. Mehta, A. Lucas, V. Garimella, T. Patno, W. Buckingham, W. Cork and U. R. Muller, *Biosensors & Bioelectronics*, 2004, **19**, 875-883.

51. Y. P. Bao, M. Huber, T. F. Wei, S. S. Marla, J. J. Storhoff and U. R. Muller, *Nucleic Acids Research*, 2005, **33**.

52. B. M. Reinhard, M. Siu, H. Agarwal, A. P. Alivisatos and J. Liphardt, *Nano Letters*, 2005, **5**, 2246-2252.

53. C. Sonnichsen, B. M. Reinhard, J. Liphardt and A. P. Alivisatos, *Nature Biotechnology*, 2005, **23**, 741-745.

54. N. Liu, M. Hentschel, T. Weiss, A. P. Alivisatos and H. Giessen, *Science*, 2011, **332**, 1407-1410.
55. D. Thompson, A. Enright, K. Faulds, W. Smith and D. Graham, *Analytical Chemistry*, 2008, **80**, 2805-2810.
56. J. Dougan, C. Karlsson, W. Smith and D. Graham, *Nucleic Acids Research*, 2007, **35**, 3668-3675.
57. L. Barrett, J. Dougan, K. Faulds and D. Graham, *Nanoscale*, 2011, **3**, 3221-3227.
58. L. Guerrini, L. Barrett, J. A. Dougan, K. Faulds and D. Graham, *Nanoscale*, 2013, **5**, 4166-4170.
59. D. G. Thompson, R. J. Stokes, R. W. Martin, R. J. Lundahl, K. Faulds and D. Graham, *Small*, 2008, **4**.
60. H. J. Parab, C. Jung, J.-H. Lee and H. G. Park, *Biosensors & Bioelectronics*, 2010, **26**, 667-673.
61. I. Larmour, K. Faulds and D. Graham, *Chemical Science*, 2010, **1**, 151-160.
62. D. Graham, D. Thompson, W. Smith and K. Faulds, *Nature Nanotechnology*, 2008, **3**, 548-551.
63. X. Qian, X. Zhou and S. Nie, *Journal of the American Chemical Society*, 2008, **130**, 14934-14935.
64. F. McKenzie and D. Graham, *Chemical Communications*, 2009, 5757-5759.
65. J. Wrzesien and D. Graham, *Tetrahedron*, 2012, **68**, 1230-1240.
66. F. McKenzie, K. Faulds and D. Graham, *Nanoscale*, 2010, **2**, 78-80.
67. D. Thompson, K. Faulds, W. Smith and D. Graham, *Journal of Physical Chemistry C*, 2010, **114**, 7384-7389.
68. L. Guerrini, F. McKenzie, A. W. Wark, K. Faulds and D. Graham, *Chemical Science*, 2012, **3**, 2262-2269.
69. Z. Zhang, Y. Wen, Y. Ma, J. Luo, L. Jiang and Y. Song, *Chemical Communications*, 2011, **47**, 7407-7409.
70. J. Hu, P. Zheng, J. Jiang, G. Shen, R. Yu and G. Liu, *Analyst*, 2010, **135**, 1084-1089.
71. Y. W. C. Cao, R. C. Jin and C. A. Mirkin, *Science*, 2002, **297**, 1536-1540.
72. R. C. Jin, Y. C. Cao, C. S. Thaxton and C. A. Mirkin, *Small*, 2006, **2**, 375-380.
73. A.-H. Lu, E. L. Salabas and F. Schueth, *Angewandte Chemie-International Edition*, 2007, **46**, 1222-1244.

74. S. Laurent, D. Forge, M. Port, A. Roch, C. Robic, L. V. Elst and R. N. Muller, *Chemical Reviews*, 2008, **108**, 2064-2110.

75. B. Jun, G. Kim, J. Baek, H. Kang, T. Kim, T. Hyeon, D. Jeong and Y. Lee, *Physical Chemistry Chemical Physics*, 2011, **13**, 7298-7303.

76. A. Espinosa, A. Serrano, A. Llavona, J. Jimenez de la Morena, M. Abuin, A. Figuerola, T. Pellegrino, J. F. Fernandez, M. Garcia-Hernandez, G. R. Castro and M. A. Garcia, *Measurement Science & Technology*, 2012, **23**.

77. J. Lee, Y. Lee, J. K. Youn, H. Bin Na, T. Yu, H. Kim, S.-M. Lee, Y.-M. Koo, J. H. Kwak, H. G. Park, H. N. Chang, M. Hwang, J.-G. Park, J. Kim and T. Hyeon, *Small*, 2008, **4**, 143-152.

78. J. Du and C. Jing, *Journal of Colloid and Interface Science*, 2011, **358**, 54-61.

79. J. Du and C. Jing, *Journal of Physical Chemistry C*, 2011, **115**, 17829-17835.

80. G. Kumar, N. Rangarajan, B. Sonia, P. Deepika, N. Rohman and C. Narayana, *Bulletin of Materials Science*, 2011, **34**, 207-216.

81. I. Robinson, L. D. Tung, S. Maenosono, C. Waelti and N. T. K. Thanh, *Nanoscale*, 2010, **2**, 2624-2630.

82. T. R. Sarkar and J. Irudayaraj, *Analytical Biochemistry*, 2008, **379**, 130-132.

83. S. I. Stoeva, F. W. Huo, J. S. Lee and C. A. Mirkin, *Journal of the American Chemical Society*, 2005, **127**, 15362-15363.

84. X. Xu, D. G. Georganopoulou, H. D. Hill and C. A. Mirkin, *Analytical Chemistry*, 2007, **79**, 6650-6654.

85. J. M. Nam, S. I. Stoeva and C. A. Mirkin, *Journal of the American Chemical Society*, 2004, **126**, 5932-5933.

86. J. M. Nam, C. S. Thaxton and C. A. Mirkin, *Science*, 2003, **301**, 1884-1886.

87. H. Zhou, J. Lee, T. J. Park, S. J. Lee, J. Y. Park and J. Lee, *Sensors and Actuators B-Chemical*, 2012, **163**, 224-232.

88. Y. Liang, J.-L. Gong, Y. Huang, Y. Zheng, J.-H. Jiang, G.-L. Shen and R.-Q. Yu, *Talanta*, 2007, **72**, 443-449.

89. H. Zhang, M. Harpster, H. Park and P. Johnson, *Analytical Chemistry*, 2011, **83**, 254-260.

90. H. Zhang, M. H. Harpster, W. C. Wilson and P. A. Johnson, *Langmuir*, 2012, **28**, 4030-4037.

91. B. Guven, I. H. Boyaci, U. Tamer and P. Calik, *Analyst*, 2012, **137**, 202-208.

92. K. Strelau, A. Brinker, C. Schnee, K. Weber, R. Moller and J. Popp, *Journal of Raman Spectroscopy*, 2011, **42**, 243-250.

93. J.-M. Li, W.-F. Ma, L.-J. You, J. Guo, J. Hu and C.-C. Wang, *Langmuir*, 2013, **29**, 6147-6155.

94. L. Lin, E. Crew, H. Yan, S. Shan, Z. Skeete, D. Mott, T. Krentsel, J. Yin, N. A. Chernova, J. Luo, M. H. Engelhard, C. Wang, Q. Li and C.-J. Zhong, *Journal of Materials Chemistry B*, 2013, **1**, 4320-4330.

95. J. Yguerabide and E. E. Yguerabide, *Analytical Biochemistry*, 1998, **262**, 137-156.

96. T. Donnelly, W. E. Smith, K. Faulds and D. Graham, *Chemical Communications*, 2014, **50**, 12907-12910.

97. National Center for Biotechnology Information, http://blast.ncbi.nlm.nih.gov/Blast.cgi, (accessed 27th June 2012).

98. A. K. R. Lytton-Jean and C. A. Mirkin, *Journal of the American Chemical Society*, 2005, **127**, 12754-12755.

99. R. Keir, D. Sadler and W. Smith, *Applied Spectroscopy*, 2002, **56**, 551-559.

100. M. Mandal, S. Kundu, S. Ghosh, S. Panigrahi, T. Sau, S. Yusuf and T. Pal, *Journal of Colloid and Interface Science*, 2005, **286**, 187-194.

101. X. Zhang, M. R. Servos and J. Liu, *Chemical Communications*, 2012, **48**, 10114-10116.

102. A. Hajdu, M. Szekeres, I. Y. Toth, R. A. Bauer, J. Mihaly, I. Zupko and E. Tombacz, *Colloids and Surfaces B-Biointerfaces*, 2012, **94**, 242-249.

103. C. H. Sun, M. L. Wang, Q. Feng, W. Liu and C. X. Xu, *Russian Journal of Physical Chemistry A*, 2015, **89**, 291-296.

104. W. Leng and P. J. Vikesland, *Langmuir*, 2014, **30**, 8342-8349.

105. G. McAnally, C. McLaughlin, R. Brown, D. Rodson, K. Faulds, D. Tackley, E. Smith and D. Graham, *The Analyst*, 2002, **127**, 838-841.

106. J. W. Hu, B. Zhao, W. Q. Xu, B. F. Li and Y. G. Fan, *Spectrochimica Acta Part a-Molecular and Biomolecular Spectroscopy*, 2002, **58**, 2827-2834.

107. W. E. Doering and S. M. Nie, *Analytical Chemistry*, 2003, **75**, 6171-6176.

108. K. Kim, H. B. Lee, Y. M. Lee and K. S. Shin, *Biosensors & Bioelectronics*, 2009, **24**, 1864-1869.

109. D. Graham, C. McLaughlin, G. McAnally, J. C. Jones, P. C. White and W. E. Smith, *Chemical Communications*, 1998, 1187-1188.

110. B. D. Smith, N. Dave, P.-J. J. Huang and J. Liu, *Journal of Physical Chemistry C*, 2011, **115**, 7851-7857.
111. A. Driscoll, M. Harpster and P. Johnson, *Physical Chemistry Chemical Physics*, 2013, **15**, 20415-20433.
112. N. Bhatt, P.-J. J. Huang, N. Dave and J. Liu, *Langmuir*, 2011, **27**, 6132-6137.
113. T. Donnelly, K. Faulds and D. Graham, *Particle and Particle Systems Characterization*, 2016.
114. Y. Takeda, T. Kondow and F. Mafune, *Journal of Physical Chemistry C*, 2008, **112**, 89-94.
115. A. E. Prigodich, O.-S. Lee, W. L. Daniel, D. S. Seferos, G. C. Schatz and C. A. Mirkin, *Journal of the American Chemical Society*, 2010, **132**, 16296-16296.
116. X. Zhang, P.-J. J. Huang, M. R. Servos and J. Liu, *Langmuir*, 2012, **28**, 14330-14337.
117. K. H. Su, Q. H. Wei, X. Zhang, J. J. Mock, D. R. Smith and S. Schultz, *Nano Letters*, 2003, **3**, 1087-1090.
118. J. G. Wetmur, *Biopolymers*, 1975, **14**, 2517-2524.
119. L. Di Michele, B. M. Mognetti, T. Yanagishima, P. Varilly, Z. Ruff, D. Frenkel and E. Eiser, *Journal of the American Chemical Society*, 2014, **136**, 6538-6541.
120. C. J. Loweth, W. B. Caldwell, X. G. Peng, A. P. Alivisatos and P. G. Schultz, *Angewandte Chemie-International Edition*, 1999, **38**, 1808-1812.
121. Polyethylene glycol (PEG) and pegylation of proteins, https://www.lifetechnologies.com/uk/en/home/life-science/protein-biology/protein-biology-learning-center/protein-biology-resource-library/pierce-protein-methods/polyethylene-glycol-peg-pegylation-proteins.html, (accessed 27th April 2015, 2015).
122. R. Wilson, *Nucleic Acid Therapeutics*, 2011, **21**, 437-440.